Master's Thesis of Engineering

Experimental Study on the Composite Beam Using U-shaped Steel Beam and Angle Shear Connectors

전단연결 앵글과 U 자형 강재보를 활용한 합성보의 실험적 연구

Feburary 2021

Graduate School of Engineering

Seoul National University

Architecture and Architectural Engineering

Hyoung Seok Oh

Experimental Study on the Composite Beam Using U-shaped Steel Beam and Angle Shear Connectors

Advisor: Thomas Kang

Submitting a Master's thesis of
Architecture and Architectural Engineering

October 2020

Graduate School of Engineering
Seoul National University
Architecture and Architectural Engineering

Hyoung Seok Oh

Confirming the Master's thesis written by
Hyoung Seok Oh

December 2020

Chair	Sung-Gul Hong	(Seal)
Vice Chair	Thomas Kang	(Seal)
Examiner	Cheol-Ho Lee	(Seal)

Abstract

Experimental Study on the Composite Beam Using U-shaped Steel Beam and Angle Shear Connectors

Hyoung Seok Oh
Department of Architecture and Architectural Engineering
College of Engineering
Seoul National University

Recently in Korea, because of the development of industry and demand for high floor area ratio associated with land price rise, buildings are becoming larger, higher, and adopting long-span. In response to this situation, applications of composite beam construction are increasing, and one of the beams used in Korea is the composite beam using a U-shaped steel beam and angle shear connectors. Conversely, despite the advantages of reducing construction duration and floor height, there is a lack of relevant studies and criteria. Therefore, in this study, flexural tests were conducted for the composite beam using U-shaped steel beam and angle shear connectors with the presence of transverse reinforcement in concrete slab, and the orientation and interval of angles were chosen as the main variables. Push-out tests were also conducted with the variables of orientation and interval of shear

connectors, sectional shape of shear connector, and presence of shear connector as the main variables.

The whole test program was conducted in two phases at an interval of one year. In material tests, concrete compressive strength was measured to be much lower than the specified strength of 24 MPa. It appears that the quality of the concrete was low and not reliable. In flexural test results, higher flexural strength was measured as angles were placed in the inverse direction and/or the interval of angles decreased. In push-out test results, the higher shear strength of push-out specimens was measured in the order of the right direction channel, the right direction angle, and the inverse direction angle. In previous studies, the shear connectors attached to the U-shaped steel beam showed the behavior of an angle member with fixed ends under uniformly distributed lateral loads. But in this study result, the deformation of angle shear connectors was predominantly either folding inward or outward. In all push-out tests, the web-to-web clear distance of the U-shaped steel beam was fixed to 384 mm, and in this condition, such a folding deformation was valid. This study results can be useful data for the development and update of relevant criteria, and basic research data for flexural performance of composite beams using a U-shaped steel beam and angle shear connectors and shear performance of shear connectors.

Keywords: Angle shear connector, shear connector, U-shaped steel beam, composite beam, flexural test, push-out test
Student Number: 2019-24377

Contents

List of Tables

List of Figures

Chapter 1. Introduction

1.1 Introduction

Recently, buildings are becoming larger, higher, and adopting long-span in Korea because of the development of industries and demand for high floor area ratio caused by land price rising. In response to this situation, steel frame structures and steel framed reinforced concrete structures, which are suitable for high-rise buildings and long-span structures, have been adopted. However, the steel structure and steel framed reinforced concrete structure have a disadvantage of elevating the overall height of the building compared to the reinforced concrete structure, reducing efficiency in terms of floor area ratio and increasing the building's exterior materials, which leads to rising of building finishing cost and labor cost. In order to solve these problems, a variety of floor height reducing composite beams which can achieve high economic efficiency and reduction of construction duration have been developed and applied to the construction sites.

The composite beam using U-shaped steel beam and angle shear connectors is one of the various floor height reducing composite beams (**Figure 1-1**). In this composite beam system, angles are attached to the top of the U-shaped steel beam as shear connectors. The method using angle as shear connector is already being used in Europe (**Figure 1-2**), and criteria for the method are specified in the Eurocode 4 (2001). This structural system can achieve both composite effect and web-to-web spacing maintenance effect, which is essential for the U-shaped section. And this system is much more economical than a method in which spacing maintainers and shear connectors are constructed separately.

Also, this system can obtain a higher moment of inertia than the existing steel beam system, because the inside of the U-shaped steel beam is filled with concrete. The U-shaped beam serves as both the form of concrete and tensile reinforcement, which can reduce the depth of the beam by 30% compared to the existing wide flange section steel beam (Ahn et al., 2015). Unlike the existing steel structure system with shear studs attached to the top of the wide flange section of steel beams at the construction site, this composite beam system has the advantage of construction duration reduced by welding angle shear connectors to U-shaped steel beams at the factory. Due to these various advantages, applications of the composite beam using U-shaped steel beam and angle shear connectors are increasing in Korea. The comparison between the composite beam using U-shaped steel beam and angle shear connectors and the existing beams is summarized in **Table 1-1.**

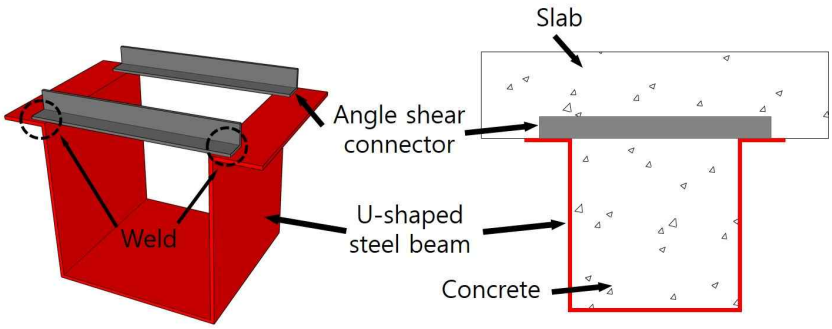

Figure 1-1 Composite beam using U-shaped steel beam and angle shear connectors (Ahn et al., 2015)

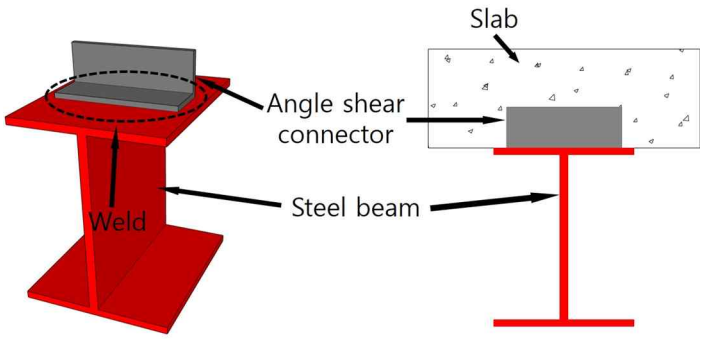

Figure 1-2 Method using angle as shear connector in Europe (Eurocode 4, 2001)

Table 1-1 Characteristic of each structure type (Kim, 2015)

	Reinforced concrete structure	**Steel frame structure**	**Composite beam structure**
Section	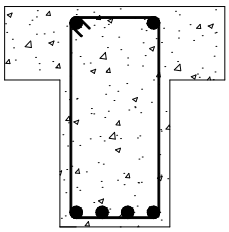	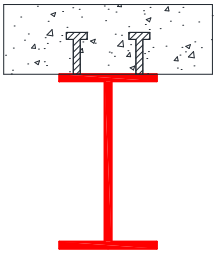	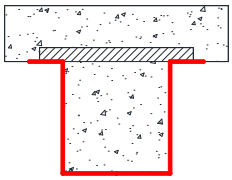
Advantage	• Economic • No fire protection required	• Available for long-span structure • Eco-friendly • High constructability • Advantageous for construction site management • Reduction of construction duration	• Economic • Available for floor height reduction • Available for long-span structure • Eco-friendly • High constructability • Advantageous for construction site management • Reduction of construction duration
Disadvantage	• Not suitable for long-span structure • Increase of construction duration • Crack occurrence • Disadvantageous for construction site management • Increase of floor height	• Increase of material cost • Fire protection required	• Fire protection required

Even though applications of the composite beam using U-shaped steel beam and angle shear connectors are on the rise, there is a lack of relevant studies and guidelines. The previous studies on the interface shear performance of the composite beam were focused on the length of angle, size of angle section, and welding length of the angle as the main variables. However, prior studies

had problems with the experimental method and were conducted under different conditions from the actual composite beam condition, which is considered to have insufficient reliability. Also, the data on interface shear strength of the composite beam according to the interval of angle shear connectors is insufficient. Furthermore, studies on the flexural performance of composite beam using U-shaped steel beam and angle shear connectors are almost nonexistent. Therefore, it is necessary to research the flexural behavior of the composite beam and study the interface shear performance of the composite beam more reliably.

1.2 Scope and objectives

The main purpose of this study is to research the flexural and interface shear performance of composite beam using U-shaped steel beam and angle shear connectors by performing flexural and push-out tests. Six composite beam specimens for the flexural tests and sixteen push-out specimens for the push-out tests were constructed. The specimens were designed according to AC495 (2018), which is the criteria for conducting a test of the composite beam using U-shaped steel beam and angle shear connectors, approved by the International Code Council Evaluation Service (ICC-ES). The whole test was conducted in two phases, phase 1 and phase 2, at an interval of one year. In the flexural test, the interval and direction of angle shear connectors and the presence of transverse reinforcement in concrete slab were considered as the main variables. In the push-out test, the interval and direction of shear connectors, the sectional shape of shear connectors, and the presence of shear connectors were considered as the main variables. By conducting the tests, the following various features were investigated and analyzed: 1) flexural strength and interface shear strength; 2) behavior and deformation of shear connectors; 3) composite behavior between the concrete slab and U-shaped steel beam; 4) deformation progress of specimens; 5) comparison between measured maximum shear strengths of shear connectors and nominal shear

strengths calculated by various design equations; and 6) comparison between measured maximum flexural strengths and nominal flexural strengths calculated by plastic stress distribution method.

1.3 Organization

This thesis is composed of six main chapters. The introduction, research background, purpose of the study, and scope are shown briefly in **Chapter 1**. In **Chapter 2**, the previous studies on composite beam using U-shaped steel beam and angle shear connectors are reviewed and discussed. Also, current codes about the composite beam and design equations of angle and channel shear connectors are reviewed. The design process, detailed plan of specimens, material properties, and construction process are described in **Chapter 3**. The results of flexural test and push-out test of phase 1 are presented and discussed in **Chapter 4**. The results of flexural and push-out tests of phase 2 are examined and discussed in **Chapter 5**. Finally, conclusions are given in **Chapter 6**.

Chapter 2. Literature Review

2.1 Codes and guidelines

2.1.1 AC495 (2018)

AC495 (2018) is a guideline for evaluation of cold-formed-steel (CFS) structural beams with steel angle anchors acting compositely with cast-in-place concrete slabs, which is accepted by ICC-ES. It contains specimen design, testing methods, and evaluation criteria for composite beam using U-shaped steel beam and angle shear connectors. In this study, the criteria for specimen design and testing methods were based on AC495 (2018).

In Section 3.2.5, the nominal shear strength and the design shear strength provided by the steel angle anchors are given in **Eqs. (2-1)** and **(2-2)**.

$$Q_n = 0.6(100\,\text{mm})^{3/2}(t_f + 0.5t_w)\sqrt{f_c' E_c} \,/\, \sqrt{l_a} \tag{2-1}$$

$$V' = \sum \Phi_v Q_n = n\ \Phi_v Q_n \geq \text{Min}\,[F_c, F_t] \tag{2-2}$$

Where,

V' : sum of adjusted shear strengths provided by steel angle anchors, N
n : number of steel angle anchors between the point of maximum positive moment point and the point of zero moment
Q_n : nominal shear strength of each steel angle anchor, N
F_c : compressive strength of the concrete slab above top flange of CFS, N
F_t : tensile yield strength of the CFS structural beam, N
Φ_v : adjustment factor (= 0.75)
t_f : thickness of horizontal leg of steel angle anchor, mm
t_w : thickness of vertical leg of steel angle anchor, mm
f_c' : specified concrete compressive strength, MPa
E_c : modulus of elasticity of concrete, MPa
l_a : CFS structural beam web-to-web clear distance, mm

Eq. (2-1) is a developed version of the nominal shear strength equation of one steel channel anchor embedded in a concrete slab from AISC 360-10 (2010), suggested by Kang et al. (2017). Kang et al. (2017) proposed the formula by analyzing previous test results of Kim et al. (2014) and Ahn et al. (2015), which indicate that the failure mode of the steel angle anchor showed a similar pattern to a beam with fixed ends under uniformly distributed loads. Considering the moment of a beam subjected to distributed load is inversely proportional to the square of U-shaped steel beam web-to-web distance, Kang et al. (2017) modified the AISC 360-10 (2010) design equation by making it divided by the square of the web-to-web distance. In addition, a constant was modified to $0.6(100\ \text{mm})^{3/2}$ through calibration with data, and the equation was revised to being inversely proportional to $(l_a)^{1/2}$ due to little adverse effect with small deflection.

In Section 3.3, performance requirements for the specimens are specified. For the push-out test, the performance requirement for measured peak shear strength of each steel angle anchor is specified. For the flexural test, flexural strength and ductility are the main performance requirements. More details about performance requirements are presented in **Eqs. (2-3)** to **(2-5)**.

$$V_p / V_a \geq 1.0 \tag{2-3}$$

$$M_p / M_a \geq 1.0 \tag{2-4}$$

$$R_{cap} = \theta_u / \theta_y \geq 3.0 \tag{2-5}$$

Where,

V_p : tested peak shear strength of each steel angle anchor for each specimen
V_a : nominal shear strength of each steel angle anchor for each specimen configuration determined in **Eq. (2-1)**
M_p : tested peak flexural strength of each beam specimen
M_a : nominal flexural strength of each beam specimen
θ_u : ultimate beam-end rotation (beam-end rotation at 20 percent drop from peak point)
θ_y : yield beam-end rotation

In Section 3.3.4.3, the definition and calculation method of composite beam ductility are specified. The composite beam end rotation measurement method and calculation of ultimate beam-end rotation (θ_u) and yield beam-end rotation (θ_y) are presented in **Figure 2-1**.

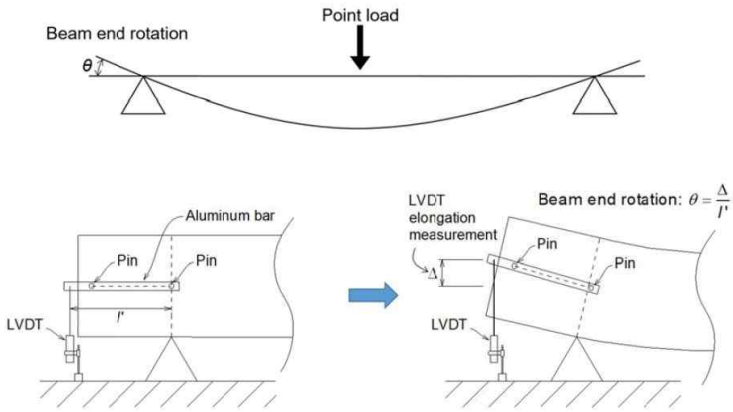

(a) Beam end rotation measurements

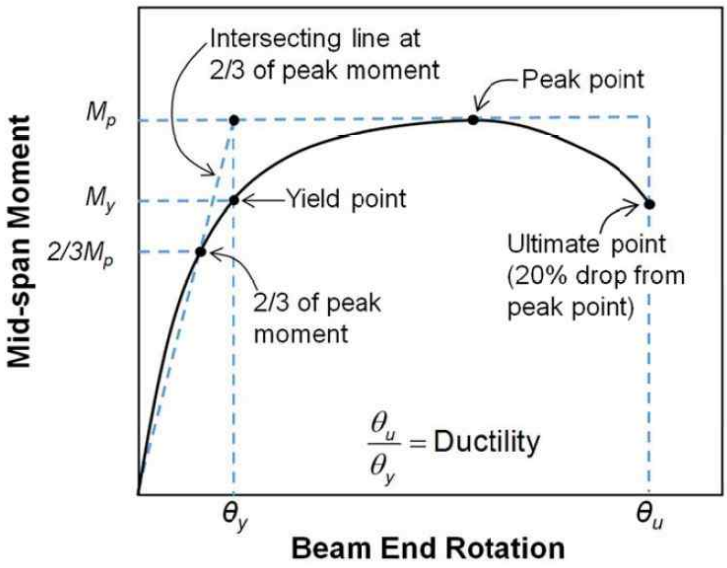

(b) Beam end moment to rotation curve

Figure 2-1 Beam end rotation measurements and beam end moment to rotation curve including ductility calculation method (AC495, 2018)

2.1.2 Eurocode 4 (2001)

Eurocode 4 (2001) suggests the design equation for the steel angle connectors in solid slabs and the ductility performance requirement of the shear connectors. The suggested design shear strength equation of a steel angle shear connector welded to the steel beam is given in **Eq. (2-6)**, and **Figure 2-2** illustrates the steel angle shear connector.

$$P_{Rd} = 10bh^{3/4} f_{ck}^{2/3} / \gamma_v \qquad (2\text{-}6)$$

Where,

P_{Rd} : the design resistance of an angle connector, N
b : length of the angle, mm
h : width of the upstanding leg of the angle, mm
f_{ck} : characteristic strength of concrete, N/mm^2
γ_v : the partial safety factor, 1.25

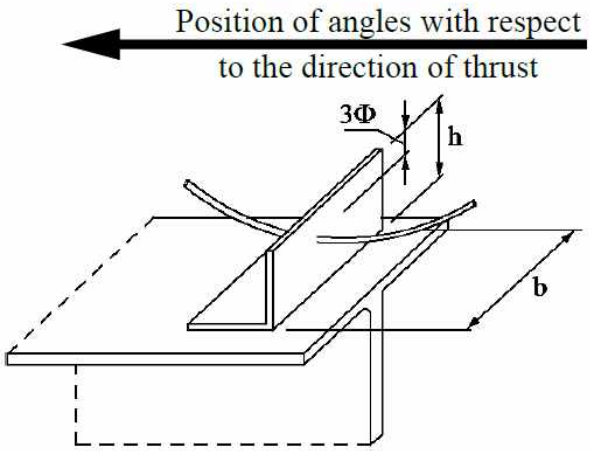

Figure 2-2 Angle sheer connector welded to the steel beam (Eurocode 4, 2001)

In **Eq. (2-6)**, the shear strength of the steel angle connector is proportional to the length of angle (b) and width of the upstanding leg of the angle (h). It means that the shear strength of the steel anchor is also proportional to the area of angle which is in contact with the concrete slab. The design equation is suggested for the steel angle connector welded to the steel beam, which means the whole flange area of the steel angle is connected with the steel beam. However, in the composite beam using U-shaped steel beam and angle shear connectors, the steel angles are welded on the flange of the composite beam at both ends, but not connected with the middle part of the steel angle. Therefore, it seems that **Eq. (2-6)** is not suitable for the composite beam using U-shaped steel beam and angle shear connectors.

Eurocode 4 (2001) also suggests the ductility performance requirement of the shear connectors. In Eurocode 4 (2001), if the characteristic slip capacity (δ_u) of the push-out test specimen is not less than 6 mm, the shear connector is evaluated to be ductile. The characteristic slip capacity (δ_u) is determined in accordance with the maximum shear strength reduced by 10% (P_{Rk}) as presented in **Figure 2-3**.

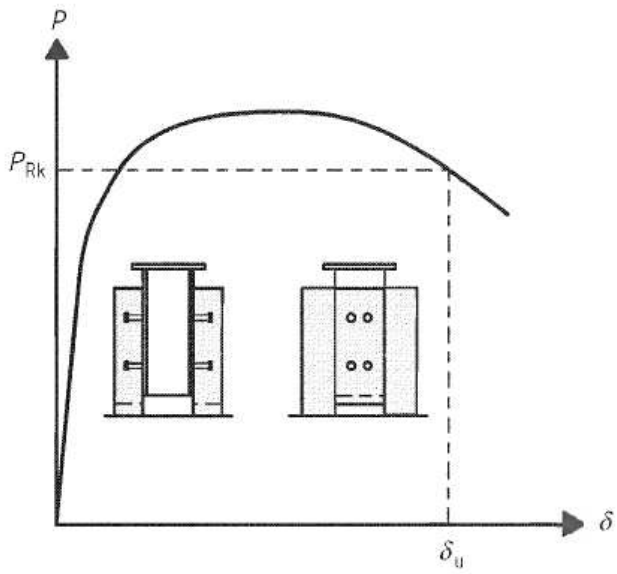

Figure 2-3 Determination of slip capacity δ_u (Eurocode 4, 2001)

2.1.3 AISC 360-16 (2016)

AISC 360-16 (2016) suggests the equation for the nominal shear strength of one hot-rolled channel anchor embedded in a solid concrete slab in Section I8-2b, as presented in **Eq. (2-7)**. In **Eq. (2-7)**, the nominal shear strength of the channel connector is proportional to the thickness of the channel flange and web (t_f and t_w) and length of the channel (l_a). This equation is a modified form of the formula for the strength of channel anchors presented in Slutter and Driscoll (1965), which was based on the results of pushout tests and a few simply supported beam tests with solid slabs by Viest et al. (1952). In Slutter and Driscoll (1965), the formula for the ultimate strength of one channel connector is specified as **Eq. (2-8)**.

$$Q_n = 0.3(t_f + 0.5t_w)l_a\sqrt{f_c'E_c} \tag{2-7}$$

$$q_u = 550(h + 0.5t)w\sqrt{f_c'} \tag{2-8}$$

Where,

Q_n : the nominal shear strength of one hot-rolled channel anchor embedded in a solid concrete slab, N
t_f : thickness of channel anchor flange, mm
t_w : thickness of channel anchor web, mm
l_a : length of channel anchor, mm
f_c' : compressive strength of concrete, MPa (ksi)
E_c : modulus of elasticity of concrete, MPa
q_u : ultimate strength of one channel connector, kip
h : average flange thickness, in.
t : web thickness, in.
w : length of channel, in.

In commentary section I8-2b, the criteria for considering eccentricity on channel connector is given in **Eqs. (2-9)** to **(2-12)**. Eccentricities need not be considered in the welded design for cases where the welds at the toe and heel of the channel are greater than 5 mm and the channel connector meets the following requirements:

$$1.0 \le \frac{t_f}{t_w} \le 5.5 \quad (2\text{-}9)$$

$$\frac{H}{t_w} \ge 8.0 \quad (2\text{-}10)$$

$$\frac{L_c}{t_f} \ge 6.0 \quad (2\text{-}11)$$

$$0.5 \le \frac{R}{t_w} \le 1.6 \quad (2\text{-}12)$$

Where,

H : height of anchor, mm
L_c : length of anchor, mm
R : radius of the fillet between the flange and the web of the channel anchor, mm
t_f : thickness of channel anchor flange, mm
t_w : thickness of channel anchor web, mm

2.1.4 CAN/CSA -S16-01 (2001)

CAN/CSA-S16-01 (2001) suggests the design shear resistance of the channel shear connectors in solid slabs of normal-density concrete as presented in **Eq. (2-13)**. This equation is based on the results of push-out tests by Slutter and Driscoll (1965). However, most of the push-out specimens in Slutter and Driscoll (1965) have channel connectors with 102 mm height and 152 mm length. Therefore, **Eq. (2-13)** is only valid within a limited range of channel connectors.

$$q_{rs} = 36.5\phi_{sc}(t + 0.5w)L_c\sqrt{f_c'} \quad (2\text{-}13)$$

Where,

q_{rs} : design shear resistance of the channel shear connector, N
ϕ_{sc} : the resistance factor, 0.80
t : average flange thickness of channel shear connector, mm
w : web thickness of channel shear connector, mm
L_c : length of channel shear connector, mm
f_c' : compressive strength of concrete at 28 days, MPa

2.2 Previous studies

2.2.1 Kim (2018)

Kim (2018) measured and analyzed the flexural performance of the composite beam using U-shaped steel beam and angle shear connectors by conducting flexural tests with seven specimens. One of the specimens only consists of the U-shaped steel beam and angle shear connectors except for concrete. Two of the specimens are the composite beams with hollow-core precast concrete (PC) slab, the others are the composite beams with truss deck. **Table 2-1** shows the features of flexural test specimens.

Table 2-1 Test specimens list (Kim, 2018)

Specimen	Composite	U-section [mm]	Angle Size [mm]	Angle pitch [mm]	Slab thickness [mm]	Composite ratio [%]
S01-L4OS300	No	U-460×400×6	L-40×5	300	-	-
C01-L30S300	Yes		L-30×3	300	150	40
C02-L40S300	Yes		L-40×5	300	150	54
C03-L50S200	Yes		L-50×6	200	150	100
C04-L50S300	Yes		L-50×6	300	150	70
PC01-L50S200	Yes		L-50×6	200	210 (PC: 160, Topping: 50)	100
PC02-L50S300	Yes		L-50×6	300		70

The flexural test was conducted using a 3,000 kN actuator, and the test load was applied at a rate of 0.05 mm/sec until the load decreased to 80% of peak load. The flexural test was carried out with a four-point bending test to apply the distributed load similarly as possible (**Figure 2-4(a)**). To measure the deflection of the center of the specimen, the displacement meters were installed at the center of the specimen, and 25 strain gauges were attached to the specimen for strain measurement (**Figure 2-4(b)**).

(a) Test set up (b) Measuring plan

Figure 2-4 Flexural test specimen set up (Kim, 2018)

Figure 2-5 shows the load-displacement relation curve of flexural specimens. Theoretically expected nominal peak load (P_e) was marked as the red dotted line in load-displacement relation graphs. The peak loads of all specimens were measured larger than theoretically expected nominal peak loads. All specimens showed that the load-displacement curve tends to increase rapidly at the beginning, but its stiffness begins to decrease after the specimens yield. In the specimens C01 ~ C04, the test loads of the specimens decreased rapidly after the peak load. The test loads of PC01 and PC02 decreased slowly after the peak load. The test load of S01-L40S300 decreased rapidly after the peak load because of local buckling, and it began to decrease slowly accompanied by the lateral torsional buckling. Also, the local buckling was observed in both web and flange of the beam.

In the specimens with concrete slab, there were no local buckling and lateral torsional buckling. Instead, the failures of specimens with concrete slab were dominated by concrete crushing which was observed in the concrete slab. In case of specimens with hollow-core PC slab, not only the concrete crushing but also shear fracture was observed.

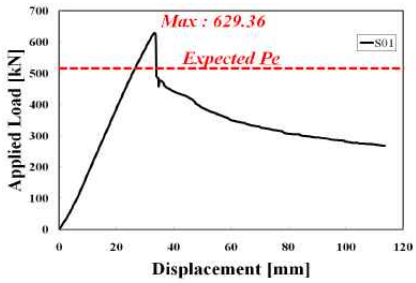

(a) S01-L40S300

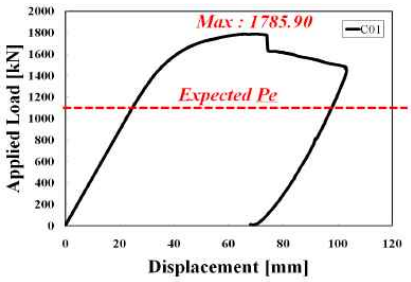

(b) C01-L30S300

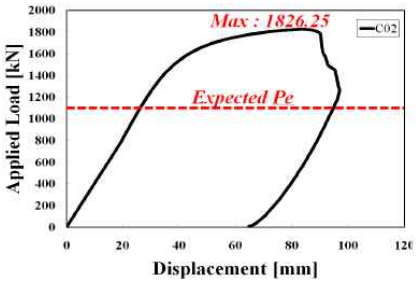

(c) C02-L40S300

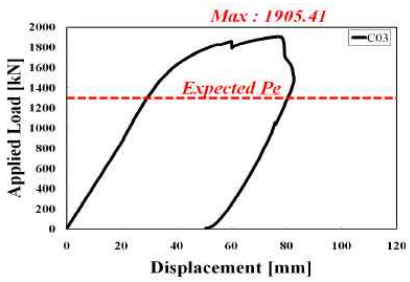

(d) C03-L50S200

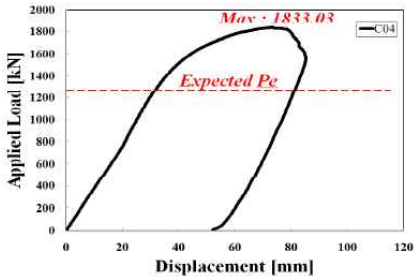

(e) C04-L50S300

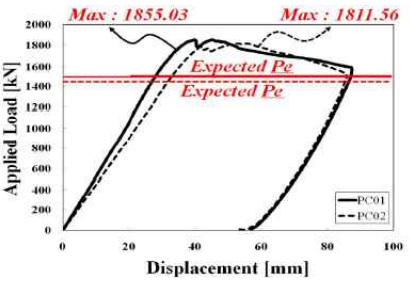

(f) PC01-L50S200, PC02-L50S300

Figure 2-5 Load-displacement relation curve (Kim, 2018)

Table 2-2 shows the flexural test results summary. The test results show that the ratio of measured peak load to theoretically expected nominal peak load (P_u / P_e) is 1.22 to 1.55, which means the specimens have sufficient flexural performance. In the pure steel beam (S01-L40S300), the angle connectors provided a restraint condition on the flange of the U-shaped steel beam, with the test peak load measured higher than the theoretically expected nominal peak load. By comparing the pure steel beam (S01-L40S300) and the composite beam (C01- L40S300), the measured peak load of the composite beam is about 2.9 times that of the steel beam. The specimens with hollow-core PC slab showed a lower ratio of measured peak load to theoretically expected nominal peak load than the specimens with concrete truss deck slab because of shear fracture. In terms of the interval of angles and angle section variable, as the size of the angle section increased and interval of angles decreased, the higher flexural performance of the composite beam was measured.

Table 2-2 Test result summary (Kim, 2018)

Specimen	Ultimate load (P_u) [kN]	Expected load (P_e) [kN]	P_u / P_e
S01-L4OS300	629	513	1.23
C01-L30S300	1,786	1,150	1.55
C02-L40S300	1,826	1,189	1.54
C03-L50S200	1,905	1,318	1.45
C04-L50S300	1,833	1,232	1.49
PC01-L50S200	1,855	1,514	1.22
PC02-L50S300	1,812	1,428	1.27

2.2.2 Kim et al. (2014)

Kim et al. (2014) measured and analyzed the shear strengths of angle shear connectors which are attached to the U-shape steel beam by conducting push-out tests with 22 specimens. All specimens consist of four series, one of them is the series of specimens with shear studs. The main variables are the size of angle (L-30×30×3, L-40×40×5, L-50×50×6), the length of welding (20 mm, 30 mm, 40 mm), and the angle pitch (200 mm, 300 mm). The push-out test was conducted using a 3,000 kN Universal Testing Machine (UTM) to apply the compressive load to the specimen statically. To measure the slip between the concrete slab and the U-shaped steel beam, two displacement meters were attached to both sides of the specimen. The 3D model of the push-out test specimen and test set up is presented in **Figure 2-6**. **Table 2-3** summarizes the push-out test specimens and variables.

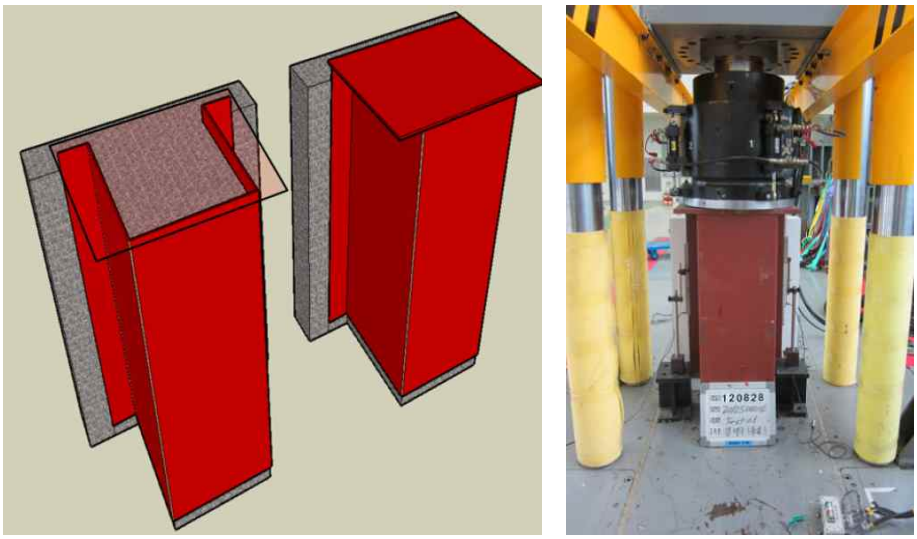

(a) 3D view of push-out test specimen (b) Test set up

Figure 2-6 3D view of specimen and test set up (Kim et al., 2014)

Table 2-3 Test specimen (Kim et al., 2014)

Specimen			**Shear Connector**	**Height [mm]**	**Thickness [mm]**	**Diameter [mm]**	**No. SCs [ea]**	**Pitch [mm]**
Series I (Stud)	1	S-100-19-300	Headed Welding Stud	100	-	19	6	@300
	2	S-100-19-200		100	-	19	8	@200
	3	S-100-19-150		100	-	19	10	@150
Specimen			**Shear Connector**	**Depth [mm]**	**Thickness [mm]**	**Welding [mm]**	**No. SCs [ea]**	**Pitch [mm]**
Baseline	4	EA-00	-	-	-	-	-	-
Series II (L-30)	5	EA-30-20-200	Equal Angle	30	3	20	4	@200
	6	EA-30-30-200		30	3	30	4	@200
	7	EA-30-40-200		30	3	40	4	@200
	8	EA-30-20-300		30	3	20	3	@300
	9	EA-30-30-300		30	3	30	3	@300
	10	EA-30-40-300		30	3	40	3	@300
Series III (L-40)	11	EA-40-20-200		40	5	20	4	@200
	12	EA-40-30-200		40	5	30	4	@200
	13	EA-40-40-200		40	5	40	4	@200
	14	EA-40-20-300		40	5	20	3	@300
	15	EA-40-30-300		40	5	30	3	@300
	16	EA-40-40-300		40	5	40	3	@300
Series IV (L-50)	17	EA-50-20-200		50	6	20	4	@200
	18	EA-50-30-200		50	6	30	4	@200
	19	EA-50-40-200		50	6	40	4	@200
	20	EA-50-20-300		50	6	20	3	@300
	21	EA-50-30-300		50	6	30	3	@300
	22	EA-50-40-300		50	6	40	3	@300

Figure 2-7 shows the load-displacement curves of the specimens. Through the load-displacement curves, it was revealed that angle shear connectors have an equivalent shear performance with shear stud connectors when the size and welding length of the angle are properly secured.

As for the shear performance according to the welding length of the angle, the shear strength of specimens with 30 mm welding length increased by 13% ~ 49% compared to the specimens with 20 mm welding length, and the shear strength of specimens with 40 mm welding length increased by 1% ~ 9% compared to the specimens with 30 mm welding length. In case of the size of the angle, the shear strength of specimens with 40 mm depth increased by 19% ~ 56% compared to the specimens with 30 mm depth, and the shear strength of specimens with 50 mm depth increased by 38% ~ 56% compared to the specimens with 40 mm depth. In the case of the angle pitch variable, the shear strength of specimens with 200 mm pitch increased 1.2 times that of the specimens with 300 mm pitch.

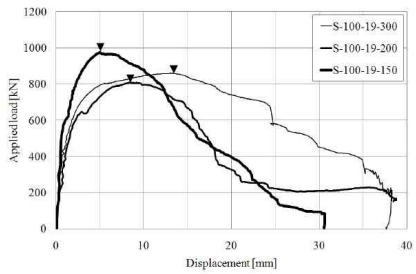

(a) Load – displacement curve (Series I)

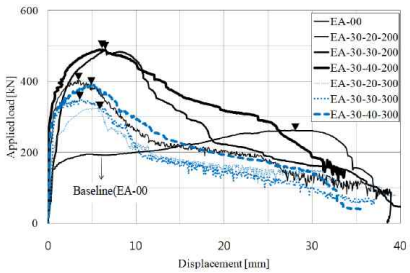

(b) Load – displacement curve (Series II)

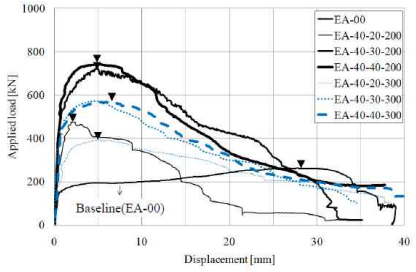

(c) Load – displacement curve (Series III)

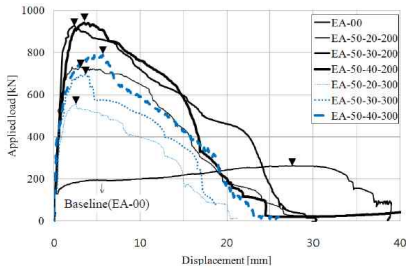

(d) Load – displacement curve (Series IV)

Figure 2-7 Load – displacement curves of the specimens (Kim et al., 2014)

The failure mode of the angle shear connector showed a similar pattern to a beam with fixed ends under uniformly distributed loads. The welded end parts of the angle shear connector serve as fixed ends when the load is applied, and plastification was proceeded by increased moment at the ends, which led to increase of flexural deformation at the center of the angle shear connector. The failure mode of the angle shear connector is presented in **Figure 2-8**.

(a) Failure mode of EA-40-40-200

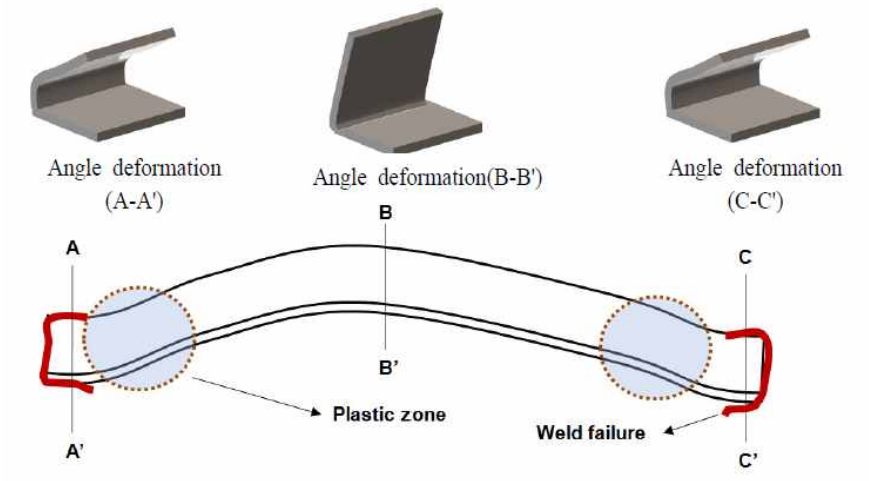

(b) Angle deformation after test

Figure 2-8 Failure mode of the angle shear connector (Kim et al., 2014)

Based on the push-out test results, Kim et al. (2014) suggested the design equation of the steel angle shear connector which is applied safety factor (γ_v = 1.25) from Eurocode 4 (2001) as presented in **Eq. (2-14)**. The suggested design equation showed a good response to the test results.

$$Q_{\text{Pro}} = \frac{\left\{ \frac{10 h^{\frac{2}{3}} f_{ck}^{\frac{2}{3}}}{\left(0.0012 l_w^2 - 0.057 l_w + 1.9\right)^{\frac{2}{3}}} \right\}}{\gamma_v} \tag{2-14}$$

Where,

Q_{Pro} : the shear strength of a steel angle shear connector, kN
h : height of the angle, mm
f_{ck} : concrete strength, MPa
l_w : length of welding, mm
γ_v : the safety factor, 1.25

2.2.3 Ahn et al. (2015)

Ahn et al. (2015) measured and analyzed the shear strengths of angle shear connectors which are attached to the U-shape steel beam by conducting push-out tests with 18 specimens. To minimize the frictional force between the concrete and the steel, the depth of the U-shaped steel beam was designed as 30 mm and not filled with concrete. The main variables are the U-shaped steel beam web-to-web distance (250 mm, 300 mm, 350mm, 400 mm) and the concrete compressive strength (24 MPa, 30 MPa). Three specimens were produced with each same variable, and total 18 push-out test specimens were constructed. Three of the specimens are the specimens with the steel stud shear connectors. The push-out test was conducted with 3,000 kN UTM, and the displacement of the specimen was measured by Linear Variable Displacement Transducers (LVDT). **Table 2-4** summarizes the push-out test specimens and test results, and **Figure 2-9** describes details of the push-out test specimen.

Table 2-4 Specimens and test results (Ahn et al., 2015)

No.	Specimen	The web-to-web distance [mm]	Concrete strength [MPa]	Shear strength [kN]	Characteristic resistance (P_{Rk}) [kN]	Ductility (δ_u) [mm]
1	Be01-250-24	250	24	323.6	265.5	10.7
2	Be02-250-24	250	24	295.0		10.1
3	Be03-250-24	250	24	319.0		10.8
4	Be04-300-24	300	24	272.1	244.9	11.7
5	Be05-300-24	300	24	279.0		13.5
6	Be06-300-24	300	24	290.6		12.5
7	Be07-350-24	350	24	279.8	220.7	10.0
8	Be08-350-24	350	24	259.2		8.0
9	Be09-350-24	350	24	245.2		10.0
10	Be10-400-24	400	24	244.6	206.3	18.9
11	Be11-400-24	400	24	232.8		21.3
12	Be12-400-24	400	24	229.3		19.0
13	Be13-400-30	400	30	274.0	231.6	15.6
14	Be14-400-30	400	30	257.4		16.7
15	Be15-400-30	400	30	261.3		15.0
16	St01-200-24	300	24	76.1	61.5	19.7
17	St02-200-24	300	24	68.3		17.3
18	St03-200-24	300	24	69.4		17.6

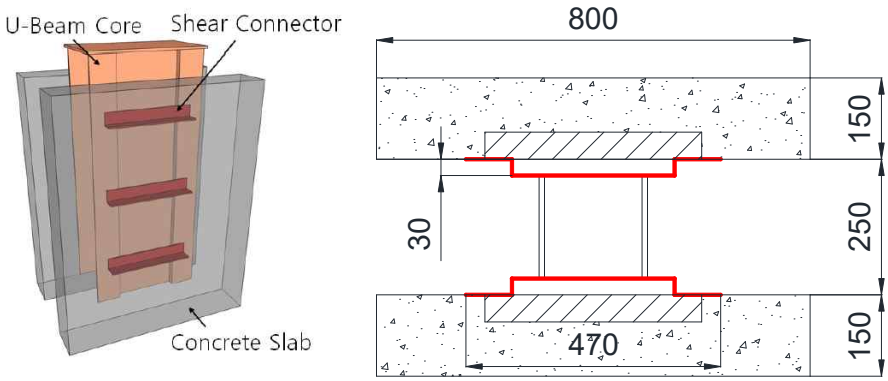

(a) 3D view of the specimen (b) Plan of the specimen

Figure 2-9 Specimen detail (Ahn et al., 2015) (Unit: mm)

Figure 2-10 shows the load-displacement curves of the specimens. In this study, the behavior of the angle shear connector was the same as the behavior in Kim et al. (2014) in which the angle behaves similarly to a beam with fixed ends under uniformly distributed loads. Therefore, as the U-shaped steel beam web-to-web distance increased, the shear strength of the specimen decreased. The shear strength of the angle shear connector decreased by 8% each time the web-to-web distance increased by 50 mm. The ductility (δ_u) of the specimen was calculated by criteria from Eurocode 4 (2001), which was already mentioned in **Section 2.1.2**. The ductility showed a tendency to increase as the web-to-web distance increased. However, the specimens with 350 mm web-to-web distance exceptionally showed the opposite behavior. As concrete strength increased from 24 MPa to 30 MPa, the shear strength of the specimens increased by 12% and the ductility decreased by 21%. In the specimens with the shear studs, the shear strength was a quarter of the shear strength of specimens with the angle shear connectors, but ductility performance was similar.

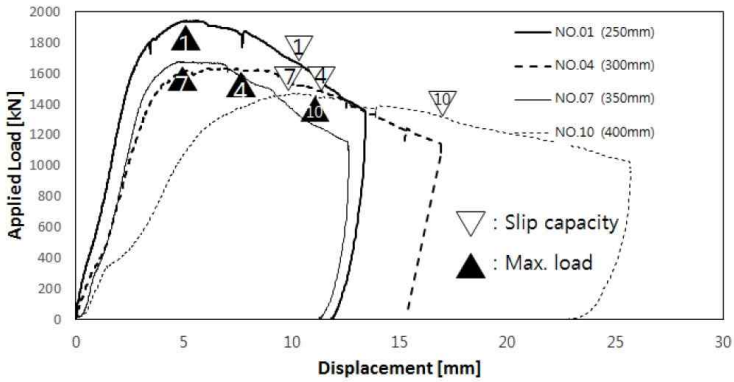

(a) Web-to-web distance

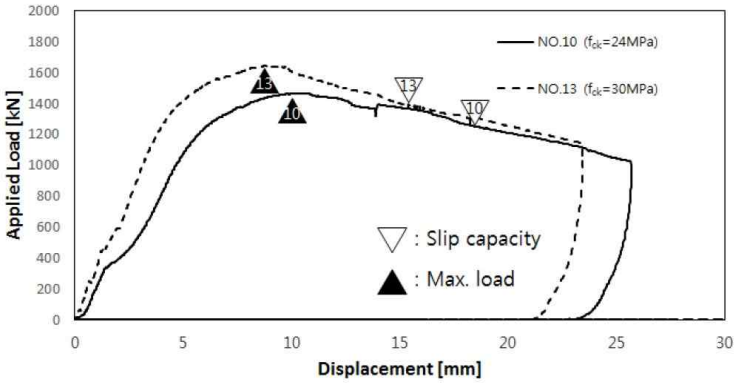

(b) Concrete stregnth

Figure 2-10 Load-displacement curves of the specimens (Ahn et al., 2015)

Ahn et al. (2015) suggest the design equation of the angle shear connector which is based on the formula of Eurocode 4 (2001) and test results. By considering that the angle showed similar behavior to a beam with fixed ends under uniformly distributed loads, the design equation was suggested as **Eq. (2-15)**.

$$R_{BESTO} = \frac{31000 h^{\frac{3}{4}} f_{ck}^{\frac{2}{3}}}{\sqrt{b}} \tag{2-15}$$

Where,

R_{BESTO} : the shear strength of an angle shear connector, N
h : height of the angle, mm
f_{ck} : concrete strength, MPa
b : web-to-web distance, mm

2.3 Discussion

In this chapter, codes and guidelines which suggest design equation for steel angle and channel connector were reviewed. Researches on previous studies that measured and analyzed the shear strength of angle shear connectors and flexural performance of the composite beam using U-shaped steel beam and angle shear connectors were also conducted.

In AC495 (2018), the design equation of the angle shear connector which is attached to the U-shaped steel beam is suggested. AC495 (2018) angle design equation is based on the test result that angles behave like beams with fixed ends subjected to distributed loads. Eurocode 4 (2001) also proposes an angle design equation, but it is valid for the angle of which the whole flange is welded to the steel beam. Therefore, the nominal shear strength of the angles calculated by AC495 (2018) design equation is expected to be more accurate than which is calculated by the Eurocode 4 (2001) equation. In CAN/CSA-S16-01 (2001) and AISC 360-16 (2016), the design equations of a channel shear connector are specified. However, the equation of CAN/CSA-S16-01 (2001) is based on a limited range of test results, which does not seem to be reliable.

Kim (2018) conducted the flexural test with seven specimens. In this study, the measured peak load was 1.22 to 1.55 times the theoretically expected nominal peak load, which means the specimens have sufficient flexural performance. As the angle size increased and the interval of angles decreased, the flexural strength of the specimens increased. However, because the number of specimens according to the variables was not sufficient, it is hard to determine the tendency by referring to the test results. In Kim et al. (2014), 22 specimens were analyzed by push-out tests. The angle shear connector showed a similar failure mode of the beam with fixed ends under uniformly distributed loads (**Figure 2-8**). As the welding length and angle size increased and angle pitch decreased, the shear strength of the specimen increased. But in

the study, it is expected that the specimens were subjected to eccentric loads because the cross-section of the specimens was designed as asymmetric (**Figure 2-6**). Therefore, the results of Kim et al. (2014) are not reliable. Ahn et al. (2015) also conducted push-out tests with 18 specimens. In the study, the measured shear strength of the specimens increased when the web-to-web distance decreased and concrete strength increased. The specimens of Ahn et al. (2015) were likely to show different results from the actual composite beam behavior because the depth of the steel beam was designed as 30 mm and not filled with concrete (**Figure 2-9**). In other words, the effect of the concrete filled in steel beam on angle shear connector was completely excluded. Thus, it seems that the test results of Ahn et al. (2015) have not enough reliability.

Chapter 3. Specimen Construction and Test Setup

In this chapter, the design and manufacturing process of specimens and test setup are described. The specimens were designed based on criteria from AC495 (2018). The test procedure and evaluation also followed the guideline. The whole experiment was conducted in two phases: phase 1 and phase 2. The two phases of tests were carried out at an interval of one year. In phase 1, three flexural specimens and six push-out specimens were measured and analyzed. In phase 2, three flexural specimens and ten push-out specimens were measured and analyzed.

3.1 Phase 1

3.1.1 Flexural specimens

The flexural specimens were designed according to AC495 (2018) Sections 3.2 and 4.4. The specimen was designed to be simply-supported with pinned-pinned supports and subjected to a concentrated load at mid-span. The concrete slab width of the test specimen was designed to be 1,536 mm which is four times the web-to-web clear distance of the steel structural beam (= 384 mm). The composite beam span length was designed to be 9,400 mm, which is 15.7 times the overall composite beam depth (= 600 mm). The depth of concrete slab was 200 mm and the depth of steel structural beam was 400 mm. In all specimens, the concrete slabs had the longitudinal reinforcements. The composite beam was extended 300 mm beyond the center of each support so that the total length of flexural beam specimen was 10,000 mm. The drawings of flexural beam specimens are shown in **Figure 3-1** and **Appendix A**.

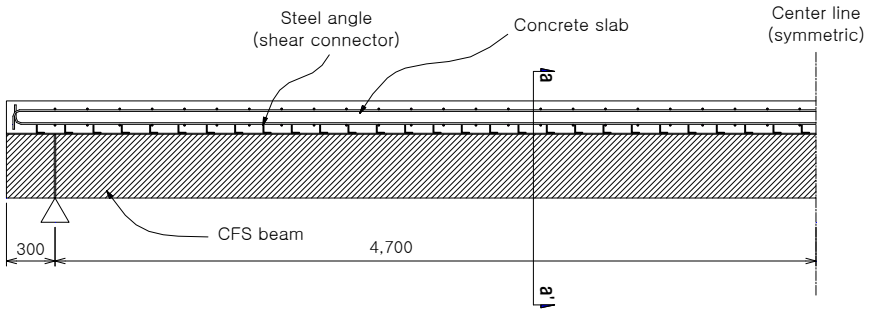

(a) Elevation view

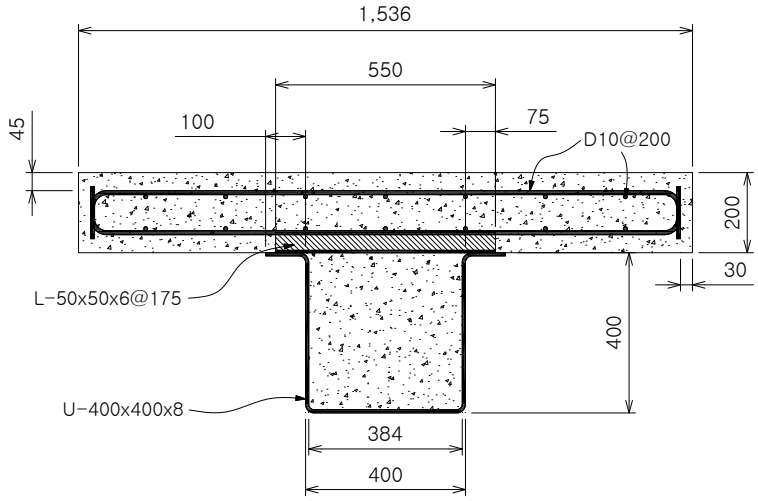

(b) Section view (section a-a')

Figure 3-1 Flexural test specimen (FT01-R175) (Unit: mm)

The nominal flexural strength (M_n) of specimens was calculated based on AC495 (2018) Section 3.2.2, referring to AISC 360-16 (2016) Section I3. The nominal flexural strength was determined from the plastic stress distribution on the composite section for the limit state of yielding, as shown in **Figure 3-2**. The nominal flexural strength based on the specified material strength [concrete compressive strength (f_c') = 24 MPa and steel yield strength (f_y) = 345 MPa] was M_n = 1,394.68 kN-m. The calculation procedures are shown in **Eqs. (3-1)** to (**3-6)**. In the strength calculation procedure, mild steel reinforcements in the concrete slab were neglected.

< Nominal flexural strength calculation procedure based on AISC 360 plastic stress distribution method (PSDM) >

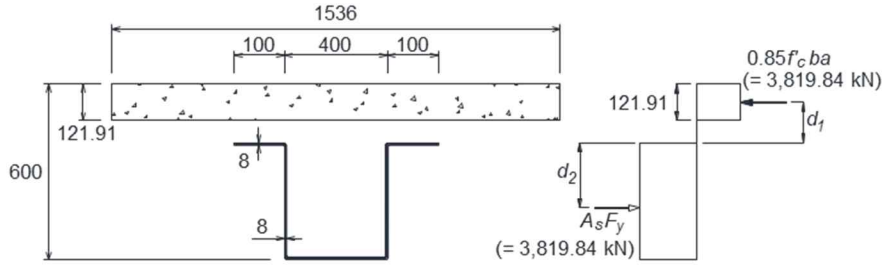

Figure 3-2 Flexural strength calculation based on PSDM (Unit: mm)

$$F_c = 0.85 A_c f'_c = 0.85(1{,}536 \text{ mm})(200 \text{ mm})(24 \text{ MPa}) = 6{,}266.88 \text{ kN} \tag{3-1}$$

$$\begin{aligned} F_t &= A_s f_y = (A_{tf} + A_w + A_{bf}) f_y \\ &= (1{,}728 \text{ mm}^2 + 6{,}144 \text{ mm}^2 + 3{,}200 \text{ mm}^2)(345 \text{ MPa}) = 3{,}819.84 \text{ kN} \end{aligned} \tag{3-2}$$

Since $F_c > F_t$, plastic neutral axis (PNA) is in the concrete slab. The depth of the equivalent compression stress block is calculated to be a = 121.91 mm. Since fully composite behavior is assumed, $\sum Q_n$ is ensured to be larger than F_c and F_t.

$$a = \frac{\text{Min}[F_t, F_c, \sum Q_n]}{0.85 f'_c b} = \frac{F_t}{0.85 f'_c b} = \frac{(A_{tf} + A_w + A_{bf}) f_y}{0.85 f'_c b} = 121.91 \text{ mm} \tag{3-3}$$

Distances from the centroid of compression and tensile forces to the top flange, d_1 and d_2, can be calculated using the following **Eqs. (3-4)** and **(3-5)**, respectively.

$$d_1 = h_s - \frac{a}{2} = 139.05 \text{ mm} \tag{3-4}$$

$$d_2 = \frac{A_{tf}\dfrac{t}{2} + A_w\left(\dfrac{h - h_s}{2}\right) + A_{bf}\left(h - h_s - \dfrac{t}{2}\right)}{A_{tf} + A_w + A_{bf}} = 226.06 \text{ mm} \tag{3-5}$$

The nominal flexural strength (M_n, plastic moment) of the flexural specimen is:

$$M_n = 0.85 f'_c b a d_1 + A_s f_y d_2 = 1{,}394.68 \text{ kN-m} \tag{3-6}$$

Note: f_c' is concrete compressive strength; f_y is steel yield strength; F_c is compressive force; F_t is tensile force; A_s is U-shaped steel beam section area; A_{tf} is top flange section area; A_w is web section area; A_{bf} is bottom flange section area; A_c is concrete slab section area; $\sum Q_n$ is sum of nominal strengths of steel anchors; b is width of concrete slab; a is depth of the equivalent compression stress block; t is thickness of U-shaped steel beam; h is overall composite beam depth; h_s is depth of concrete slab; d_1 is distance from the centroid of compression force to the top flange; and d_2 is distance from the centroid of tensile force to the top flange.

The arrangement of steel angle shear connectors was designed in accordance with AC495 (2018) Section 3.2.5. The nominal shear strength provided by the steel angle anchor (Q_n) is given in **Eq. (3-7)** and the design shear strength provided by the steel angle anchors, which is defined as the sum of adjusted shear strength provided by steel angle anchors (V') (i.e. the load transfer of the positive moment at the interface between the concrete slab and U-shaped steel structural beam) is calculated from **Eq. (3-8)**. By **Eq. (3-8)**, the sum of design shear strength (V') should be larger than the smaller of F_c = 6,266.88 kN and F_t = 3,819.84 kN. The number of steel angle anchors (n) attached on the half span (= 4,700 mm) should be larger than 24.86. In phase 1, 27 steel angle anchors were attached in the spacing of s = 175 mm.

$$Q_n = \left(0.6(100\text{ mm})^{3/2}(t_f + 0.5t_w)\sqrt{f_c' E_c}\right) / \sqrt{l_a} = 204.85\text{ kN} \quad (3\text{-}7)$$

$$V' = \sum \phi_v Q_n = n\phi_v Q_n \geq \text{Min}\left[F_c,\ F_t\right] \quad (3\text{-}8)$$

$$n \geq \frac{\text{Min}\left[F_c,\ F_t\right]}{\phi_v Q_n} = 24.86 \quad (3\text{-}9)$$

Q_n : nominal shear strength of each steel angle anchor, N
t_f : thickness of horizontal leg of steel angle anchor, mm
t_w : thickness of vertical leg of steel angle anchor, mm
f_c' : specified concrete compressive strength, MPa
E_c : modulus of elasticity of concrete, MPa
l_a : CFS structural beam web-to-web clear distance, mm
V' : sum of adjusted shear strengths provided by steel angle anchors, N
n : number of steel angle anchors
ϕ_v : adjustment factor (= 0.75)
F_c : compressive strength of the concrete slab above top flange of CFS, N
F_t : tensile yield strength of the CFS structural beam, N

Three specimens were designed with the main variables of steel angle direction and slab transverse reinforcements. For all specimens, the interval of steel angle connectors was designed as 175 mm, which is minimal spacing calculated by **Eqs. (3-7)** to **(3-9)**. Specimen FT01-R175 was designed to evaluate performance of the beam with slab transverse reinforcements and the right angle direction. Specimen FT01-R175-N was constructed to investigate the effect of presence of transverse reinforcement on longitudinal shear capacity of concrete slab. Specimen FT01-I175 was designed with slab transverse reinforcement and inverse angle direction. All other parameters, such as material properties, geometrical shape, longitudinal reinforcement, and spacing of shear connector, were designed the same. The test variables of flexural specimens are summarized in **Table 3-1**.

Table 3-1 Test variables of flexural test specimens (phase 1)

Test specimen	Shear connector (Steel angle)		Slab transverse reinforcements (Top and bottom)
	Spacing (mm)	Angle direction	
FT01-R175	175	ㄴ ㄱ (The right direction)	D10@200
FT01-R175-N	175	ㄴ ㄱ (The right direction)	No transverse reinforcements
FT01-I175	175	ㄱ ㄴ (The inverse direction)	D10@200

3.1.2 Push-out specimens

The push-out test specimens were designed per AC495 (2018) Sections 3.2 and 4.3. Six specimens were designed with main experiment parameters of the direction and interval of angle shear connectors. The U-shaped steel beam core was designed to be composed of two hat-shaped U-170×400×8 steel beams welded back-to-back. The steel angle shear connectors had L-50×50×6 section and welded to the top flanges of each side of the steel beam core, and a reinforced concrete slab was attached to each side of the steel beam core. The steel beam core was made of ASTM A572 Grade 50 steel, and the steel

angle shear connector was made of ASTM A36 steel. In the concrete slabs, 24 MPa compressive strength concrete and SD400 D10 reinforcing bars were used.

Each specimen had four shear connectors (two steel angles on each side). As the main variables, two directions of steel angle were considered, which were the right direction and inverse direction. Three intervals of shear connectors were considered, which were 175 mm, 225 mm, and 300 mm. For all specimens, the clear distance between two slabs was designed to be 1.7 times the slab thickness (= 340 mm). For each specimen, the length and width of slab were determined depending on the spacing of shear connectors. For all specimens, all material properties were the same. The drawings of push-out specimens are shown in **Figure 3-3** and **Appendix A**. The test variables of push-out specimens are summarized in **Table 3-2**.

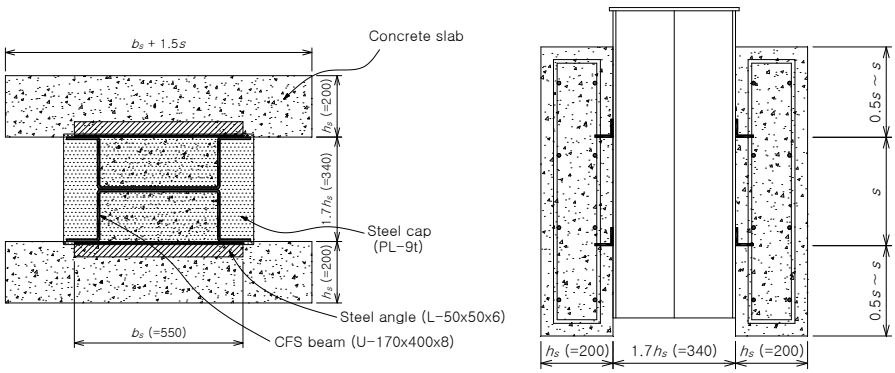

(a) Top view (b) Side view

Figure 3-3 Push-out specimens (phase 1) (Unit: mm)

Table 3-2 Test variables of push-out test specimens (phase 1)

Test specimen	CFS beam		Concrete slab		Shear connector (Steel angle)	
	Section	**Length (mm)**	**Width (mm)**	**Length (mm)**	**Spacing (mm)**	**Angle direction**
PT01-I300	U-170×400×8	850	1,000	800	300	⌟ ⌞ (The inverse direction)
PT01-I225	U-170×400×8	655	888	605	225	⌟ ⌞ (The inverse direction)
PT01-I175	U-170×400×8	525	813	475	175	⌟ ⌞ (The inverse direction)
PT01-R300	U-170×400×8	850	1,000	800	300	⌝ ⌜ (The right direction)
PT01-R225	U-170×400×8	655	888	605	225	⌝ ⌜ (The right direction)
PT01-R175	U-170×400×8	525	813	475	175	⌝ ⌜ (The right direction)

3.1.3 Material properties

For both the flexural test and push-out test specimens, concrete having the specified compressive strength of 24 MPa was used, and SD400 D10 reinforcing bars were used for reinforcement. In all test specimens, reinforcing bars were placed at the top and bottom of concrete slab at a 200 mm spacing. In the flexural test specimens, the CFS structural beam had a U-shaped U-400×400×8 section, which is made of ASTM A572 Grade 50 steel. In the push-out test specimens, the CFS beam core had a U-shaped U-170×400×8 section, which was also made of ASTM A572 Grade 50 steel. For the angle shear connectors, L-50×50×6 section with 550 mm length, which was made of ASTM A36 steel, was used. All the materials to be used for the test specimens are summarized in **Tables 3-3** and **3-4**.

Table 3-3 Steel material property of test specimens (phase 1)

Type	Section	Material
Angle shear connector	L-50×50×6	ASTM A36 (f_y=250 MPa)
CFS structural beam	U-400×400×8	ASTM A572 Grade 50 (f_y=345 MPa)
CFS beam core	U-170×400×8	ASTM A572 Grade 50 (f_y=345 MPa)
Reinforcement bar	d = 10 mm	SD400 D10 (f_y=400 MPa)

Note: f_y is yield strength; d is diameter of reinforcement.

Table 3-4 Concrete material property of test specimens (phase 1)

Type	Specified concrete compressive strength	Elastic modulus
Concrete	24 MPa	23,187 MPa

Note: The elastic modulus of concrete is calculated using ACI 318-19 Equation 19.2.2.1.b.

3.1.4 Flexural test setup

The flexural test was performed using a 10,000 kN UTM, and the test was carried out with a three-point loading. The load was applied to the mid-span of beam using a 1,950 mm length, 500 mm width steel frame (**Figure 3-4**). The lateral supports were installed at 1/4 and 3/4 span of beam to prevent the buckling of the beam. The test load was applied monotonically at a rate of 0.01 mm/sec under displacement control, according to the AC495 (2018) Section 4.4.2 requirements. The test load was applied until the UTM load decreased to 80% of peak load. To measure the deflection of beam, three LVDTs were installed at the 1/4, 1/2, and 3/4 span of beam. For both ends, horizontal slip between steel beam and concrete slab was measured with an LVDT, and beam-end rotation was measured using the pre-installed aluminum bar and an LVDT (**Figure 3-5**).

Also, strain of steel beam and concrete slab was measured at the mid-span. The strain gauges were attached to the top of concrete slab (5 concrete strain gauges), the side of concrete slab and steel beam (2 concrete strain gauges and 4 steel strain gauges), and the bottom of steel beam (5 steel strain gauges). The details of LVDT and strain gauge setup are presented in **Appendix B**.

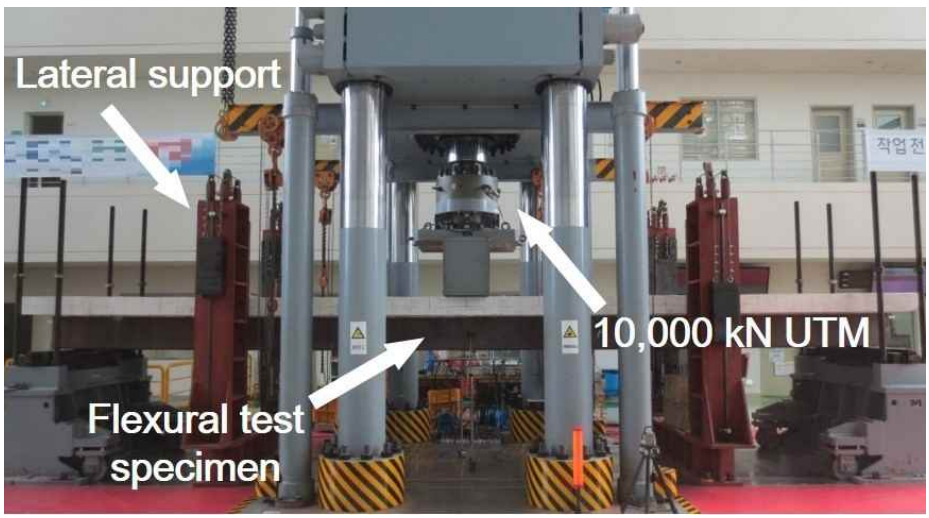

Figure 3-4 Flexural test set up (phase 1)

Figure 3-5 Horizontal slip and beam-end rotation measurement (phase 1)

3.1.5 Push-out test setup

The push-out test was performed using a 10,000 kN UTM. The load was applied to the loading plate at the top of test specimen (**Figure 3-6**). The test load was applied monotonically at a rate of 0.01 mm/sec under displacement control, according to the AC495 (2018) Section 4.3.2 requirements. The test load was applied until the UTM load decreased to 75% of peak load. To measure load-horizontal slip relation, two LVDTs were installed on both sides of specimens. Additionally, ten steel strain gauges were installed in longitudinal direction to measure strain of steel angle shear connectors (five steel strain gauges for each of the top and bottom angle shear connectors). The LVDT and strain gauge set up of push-out test specimens are provided in **Appendix B**.

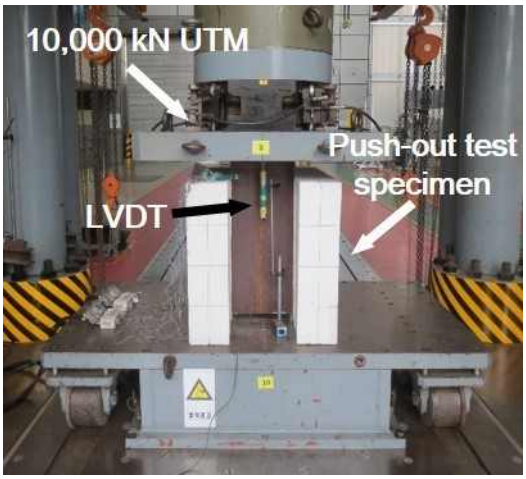

Figure 3-6 Push-out test set up (phase 1)

3.2 Phase 2

3.2.1 Flexural specimens

The flexural test specimens in phase 2 were designed according to AC495 (2018) Sections 3.2 and 4.4, as in phase 1. Three specimens were constructed for phase 2 and designed the same as the specimens in phase 1 except for the arrangement of the angle shear connectors. The interval of the angle shear connectors was considered as the main variable (175 mm, 400 mm, and 550 mm). The reinforcements in concrete slabs were arranged in both longitudinal and transverse directions in all specimens. The drawings of flexural test specimens are shown in **Appendix A**, and test variables are summarized in **Table 3-5**.

Table 3-5 Test variables of flexural test specimens (phase 2)

Test specimen	Shear connector (Steel angle)		Transverse and longitudinal slab reinforcements (Top and bottom)
	Spacing (mm)	Angle direction	
FT02-I175	175	⌟ ⌞ (The inverse direction)	D10@200
FT02-I400	400		
FT02-I550	550		

3.2.2 Push-out specimens

Phase 2 push-out test specimens were designed per AC495 (2018) Sections 3.2 and 4.3. Ten specimens were designed with main experiment parameters of shear connector direction, the sectional shape of shear connector, the presence of the shear connector, and the interval of shear connector. Phase 2 push-out test specimens were designed similar to phase 1 push-out test specimens, and there were some differences in regard to variables. Two specimens were designed without steel shear connectors to investigate the effects of concrete slabs on the shear strength of push-out test specimens (PT02-0-1, PT02-0-2). In phase 2, the specimens with channel shear connectors were constructed to investigate the performance of channel (PT02-C175, PT02-C400, and PT02-C550). Specimens PT02-I175 and PT02-C175 were designed with six shear connectors, the others with shear connectors were designed with four shear connectors. The drawings of push-out test specimens are presented in **Appendix A**, and test variables are summarized in **Table 3-6**.

Table 3-6 Test variables of push-out test specimens (phase 2)

Test specimen	CFS beam		Concrete slab		Shear connector (Steel angle)	
	Section	Length (mm)	Width (mm)	Length (mm)	Spacing (mm)	Shear connector direction
PT02-0-1	U-170×400×8	700	813	650	-	-
PT02-0-2	U-170×400×8	1,050	1,150	1,000	-	-
PT02-I175	U-170×400×8	700	813	650	175	⌟ ⌞ (The inverse direction)
PT02-I400	U-170×400×8	1,050	1,150	1,000	400	⌟ ⌞ (The inverse direction)
PT02-I550	U-170×400×8	1,300	1,375	1,250	550	⌟ ⌞ (The inverse direction)
PT02-R400	U-170×400×8	1,050	1,150	1,000	400	⌝ ⌜ (The right direction)
PT02-R550	U-170×400×8	1,300	1,375	1,250	550	⌝ ⌜ (The right direction)
PT02-C175	U-170×400×8	700	813	650	175	⊓ ⊓ (The right direction)
PT02-C400	U-170×400×8	1,050	1,150	1,000	400	⊓ ⊓ (The right direction)
PT02-C550	U-170×400×8	1,300	1,375	1,250	550	⊓ ⊓ (The right direction)

3.2.3 Material properties

In phase 2, the same steel and concrete materials used in phase 1 were applied for the specimens. For the steel channel shear connectors, C-75×40×5×7 section with 550 mm length, which is made of ASTM A36 steel, was used. The other specified material properties were the same as phase 1 material properties presented in **Tables 3-3** and **3-4**. The specified material property of the steel channel shear connector used for the push-out test specimens is presented in **Tables 3-7**.

Table 3-7 Material property of steel channel shear connector

Type	Section	Material
Channel shear connector	C-75×40×5×7	ASTM A36 (f_y=250 MPa)

Note: f_y is yield strength.

3.2.4 Flexural test setup

The flexural test was conducted under the same condition as phase 1, except for lateral supports. The lateral supports were not installed in phase 2 because they were considered unnecessary. The test load was applied monotonically at a rate of 0.01 mm/sec under a displacement control using a 10,000 kN UTM, and the test load was applied until the UTM load decreased to 80% of peak load. To measure the deflection of beam, two LVDTs were installed at the 1/4 and 3/4 span of beam, and a wire potentiometer was installed at the beam mid-span. For both ends, horizontal slip between steel beam and the concrete slab was measured with an LVDT, and beam-end rotation was measured using an LVDT and an aluminum rectangular pipe embedded in concrete, as shown in **Figure 3-7**.

The strain gauge setting was the same as phase 1 except for angle shear connectors. In order to investigate the deformation of angle shear connectors, six strain gauges were attached to two angle shear connectors which were

located in the middle of the beam. Three of them were attached in transverse direction, while the others were attached in longitudinal direction. The setting of LVDT and strain gauge for the flexural specimens is presented in **Appendix B**.

Figure 3-7 Horizontal slip and beam-end rotation measurement (phase 2)

3.2.5 Push-out test setup

The push-out test was conducted under the same condition as phase 1. The test load was applied monotonically at a rate of 0.01 mm/sec under a displacement control using a 10,000 kN UTM, and the test load was applied until the UTM load decreased to 75% of peak load. To measure the load-horizontal slip relation, two LVDTs were installed on both sides of specimens. Additionally, the other two LVDTs were installed at the top and bottom of steel beam core top flange, to measure the vertical separation between the steel beam core and concrete slabs. Also, ten strain gauges were installed on shear connectors to measure deformation of shear connectors. Five of them were attached in transverse direction, while the others were attached in longitudinal direction. In specimens with four shear connectors, strain gauges were attached to the bottom of shear connectors. In specimens with six shear connectors, strain gauges were attached to middle shear connectors. The

LVDT and strain gauge set up of push-out test is shown in **Appendix B**.

3.3 Specimen construction

Figure 3-8 summarizes the manufacturing process of the flexural and push-out test specimens. There was no difference in the manufacturing process between phase 1 and phase 2 except for several variables. For the push-out test specimens, strain gauges were installed on shear connectors for each specimen, and then the formwork and reinforcement work was conducted. For the flexural test specimens, strain gauges were attached to shear connectors, and then formwork and reinforcement work proceeded. To measure beam-end rotation, the aluminum bars were installed by drilling holes in the forms (**Figure 3-8(e)**). The steam curing was conducted for all specimens to derive the strength of the concrete. After the concrete curing, the painting and gird work was conducted for all specimens to figure out the concrete cracks more precisely.

(a) Grinding work for
strain gauge installment

(b) Strain gauge installment
(shear connector, push-out specimen)

(c) Strain gauge installment
(shear connector, flexural specimen)

(d) Form and reinforcement installment

(e) Aluminum bar installment

(f) Concrete pouring

(g) Steam curing

(h) Painting and grid work

Figure 3-8 Specimen construction process

3.4 Testing for component materials

3.4.1 Steel

For the steel components (CFS structural beam and steel shear connector), uniaxial tensile tests were conducted in accordance with AC495 (2018) Section 4.2.1, referring to ASTM A370 test method. ASTM A572 Grade 50 (f_y = 345 MPa) steel was used for CFS structural beam, and ASTM A36 (f_y = 250 MPa) steel was used for steel shear connector. For each material, three replicate specimens were manufactured and tested. The material tests of phase 1 and phase 2 were carried out in different facilities, and the elastic modulus of steel component was assumed to 200 GPa. The measured yield strength and tensile strength of each specimen are summarized in **Table 3-8**.

Table 3-8 Steel material test results

Type		**Yield strength (f_y)**	**Tensile strength (f_u)**
Phase 1	ASTM A572 Grade 50	443.4 MPa	560.5 MPa
	ASTM A36	364.7 MPa	489.6 MPa
Phase 2	ASTM A572 Grade 50	470 MPa	594.8 MPa
	ASTM A36	335.7 MPa	427 MPa

3.4.2 Concrete

The manufacturing and uniaxial compression tests of concrete cylinder specimens were conducted in accordance with AC495 (2018) Section 4.2.2. The concrete cylinder specimens were prepared by ASTM C31 and tested per ASTM C39. For the concrete used in the specimens, 150 × 300 mm concrete cylinder specimens were prepared for the test, eight and twenty concrete cylinders were used in phase 1 and phase 2, respectively.

As in the steel component test, the concrete tests of phase 1 and phase 2 were carried out in different facilities, the elastic modulus of concrete in phase 2

was not measured and calculated by ACI 318-19 (2019) Equation 19.2.2.1.b. The measured concrete compressive strengths are shown in **Tables 3-9** and **3-10**.

Table 3-9 Concrete material test results (phase 1)

Type	**Compressive strength (f_c')**	**Material strength (E_c)**
Phase 1	20.84 MPa	21,800 MPa

Table 3-10 Concrete material test results (phase 2)

Batch	**Compressive strength (f_c')**	**Specimens**
1	20.1 MPa	FT02-I550
2	18.7 MPa	FT02-I400
3	17.7 MPa	FT02-I175
4	20.7 MPa	PT02-I175 PT02-0-1 PT02-I400 PT02-I550 PT02-C175
5	21.4 MPa	PT02-0-2 PT02-R400 PT02-R550 PT02-C400 PT02-C550

3.5 Discussion

In this chapter, the design of specimens, the construction process of the specimens, and the test setup were described. Also, material properties and material tests were conducted. The main summaries are as follows:

In phase 1, three flexural test specimens and six push-out test specimens were designed and constructed. The main variables of flexural test were the direction of the angle shear connector and the presence of slab transverse reinforcements. In push-out tests, direction and interval of the angle shear connectors were considered as the main variables.

In phase 2, three flexural test specimens and ten push-out test specimens were prepared for the test. The interval of the angle shear connectors was considered as the main variable of flexural test, and the angles were arranged in inverse direction for all flexural test specimens. The main variables of push-out test were the interval, direction, sectional shape, and presence of steel shear connectors.

The material tests were conducted for the concrete and steel components to measure the actual strength of the materials. The measured concrete compressive strengths were much lower than specified concrete strength, 24 MPa. However, the steel yield strengths were measured much higher than the specified steel yield strength. This phenomenon may have an adverse impact on the flexural and push-out behaviors.

Chapter 4. Phase 1 Test Results

In this chapter, results of phase 1 test are presented. Flexural tests with three specimens and push-out tests with six specimens were conducted in phase 1. Through the tests, flexural and interface shear performance of the composite beam were evaluated.

4.1 Flexural test

4.1.1 Flexural strength and ductility

Tables 4-1 and **4-2** summarize the test results of flexural strength and ductility. Measured peak load (P_p) is the peak load measured at UTM load cell, and measured peak moment (M_p) is obtained from measured peak load and self-weight of the specimen. The nominal flexural strength (M_n) is calculated according to plastic stress distribution method which is demonstrated in **Section 3.1.1**. The nominal peak load (P_n) is derived from the nominal flexural strength and self-weight of the specimen. The ductility of the specimen is calculated from criteria in AC495 (2018) Section 3.3.4.3, which is presented in **Figure 2-1**. In **Table 4-2**, the words north end and south end signify cardinal directions in laboratory where the experiment was conducted.

Table 4-1 Flexural test results of specimen flexural strength (phase 1)

Specimen	Measured peak load, P_p (kN)	Measured peak moment, M_p (kN-m)	Nominal peak load, P_n (kN)	Nominal flexural strength, M_n (kN-m)
FT01-R175	639.88	1,633.72	646.28	1,648.76
FT01-R175-N	605.98	1,554.05		
FT01-I175	676.87	1,720.65		

Table 4-2 Flexural test results of specimen ductility (phase 1)

Specimen	Yield beam-end rotation, θ_y (rad)		Ultimate beam-end rotation, θ_u (rad)		Ductility	
	North end	South end	North end	South end	North end	South end
FT01-R175	0.01235	0.01647	0.0382	0.04233	3.09	2.57
FT01-R175-N	0.00746	0.01113	0.02078	0.02681	2.79	2.41
FT01-I175	0.01084	0.01673	0.0469	0.06	4.33	3.59

The larger measured peak load and higher ductility were measured in the order of FT01-I175, FT01-R175, and FT01-R175-N. Furthermore, FT01-I175 was the only specimen that measured peak moment exceeded the nominal flexural strength. It means that it is more advantageous to place the angle shear connectors in the inverse direction in terms of flexural strength and ductility.

The load-deflection curves and beam-end rotation curves of the flexural test specimens are presented in **Figures 4-1** and **4-2**, respectively. In all specimens, load-deflection curves maintained linear behavior until the 2/3 of measured peak load, and after that point the stiffness started to decrease. After reaching the measured peak load, the load gradually decreased except for FT01-R175-N. In FT01-R175-N, the load decreased rapidly after the peak load. Two main reasons for this behavior of FT01-R175-N can be inferred. The first reason is that the absence of transverse reinforcement could cause longitudinal shear failure between section with angle (section A) and section without angle (section B) as presented in **Figure 4-3**. However, no evidence of longitudinal shear failure of concrete slab was observed including longitudinal shear cracks. The second reason is that lateral supports were installed so close to the concrete slab in FT01-R175-N. As a result, severe cracks in the concrete slab occurred by friction between the concrete slab and lateral support, and it led to reduction of the flexural strength and ductility of the beam. **Figure 4-4** shows the failure of concrete slab caused by frictional force. Also, lateral supports

tightly installed to the concrete slab acted as additional support of the composite beam, which may reduce the flexural strength and ductility of the beam by shortening the beam span. Therefore, the main reason for rapid strength degradation after peak load and lower performance of flexural strength and ductility than other specimens is tight adhesion with lateral supports.

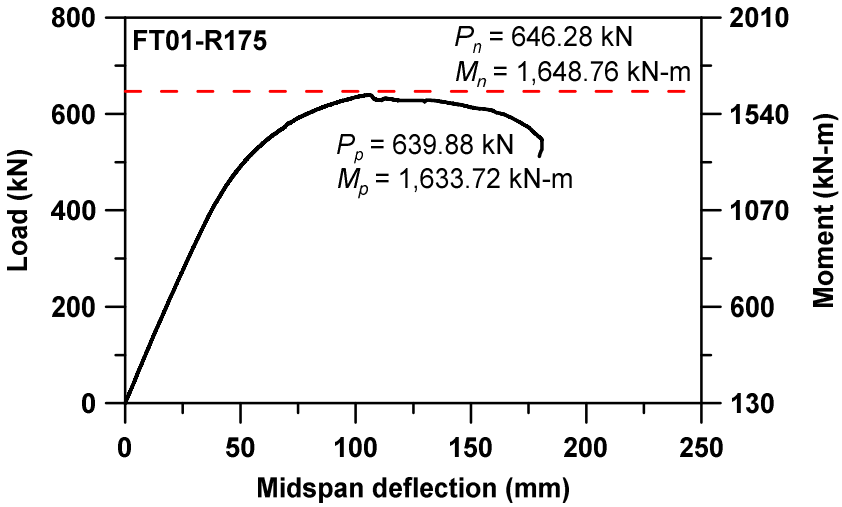

(a) FT01-R175

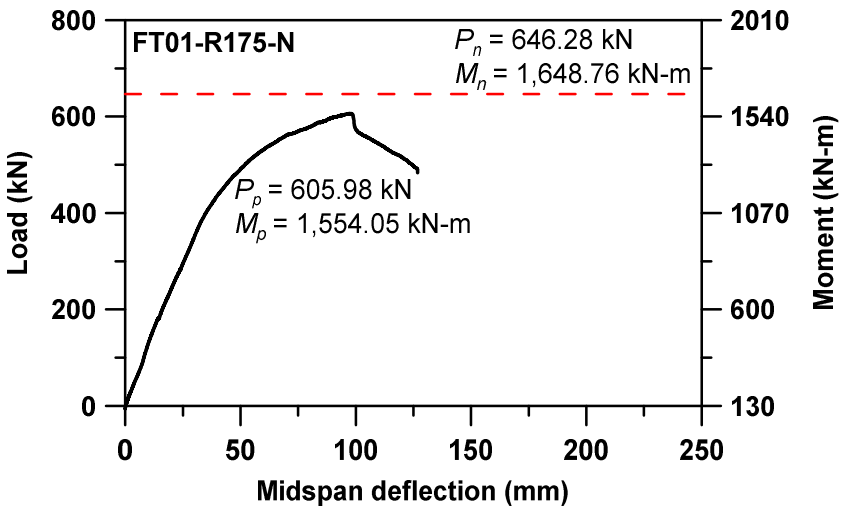

(b) FT01-R175-N

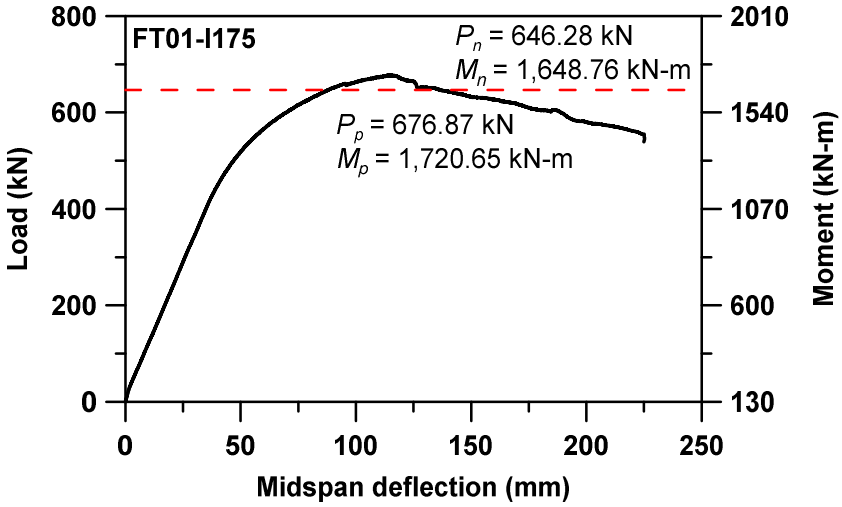

(c) FT01-I175

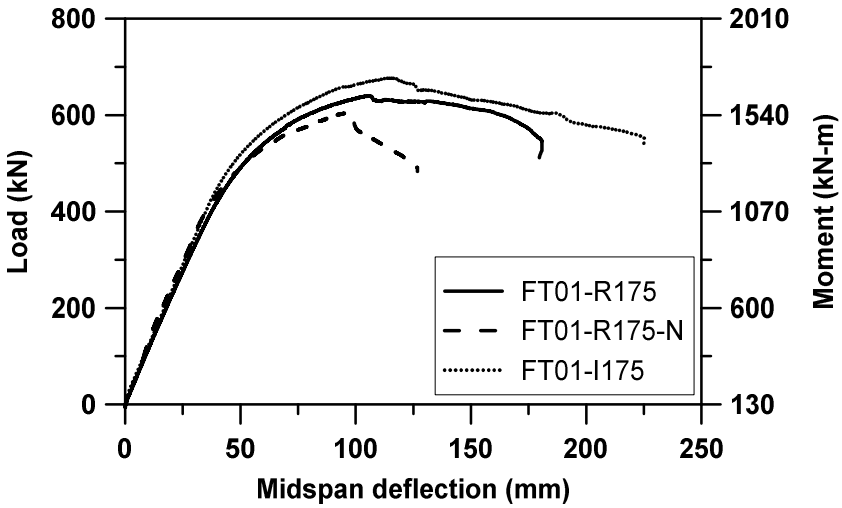

(d) All flexural test specimens

Figure 4-1 Load-deflection curves in flexural test (phase 1)

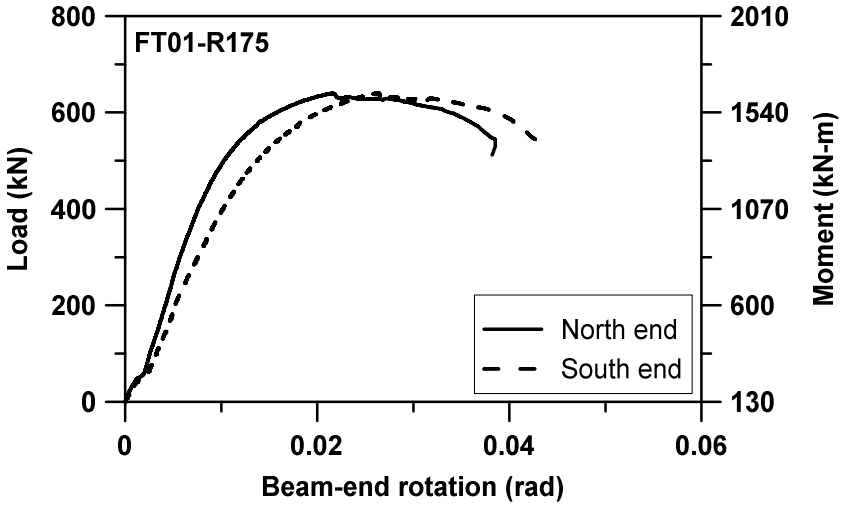

(a) FT01-R175

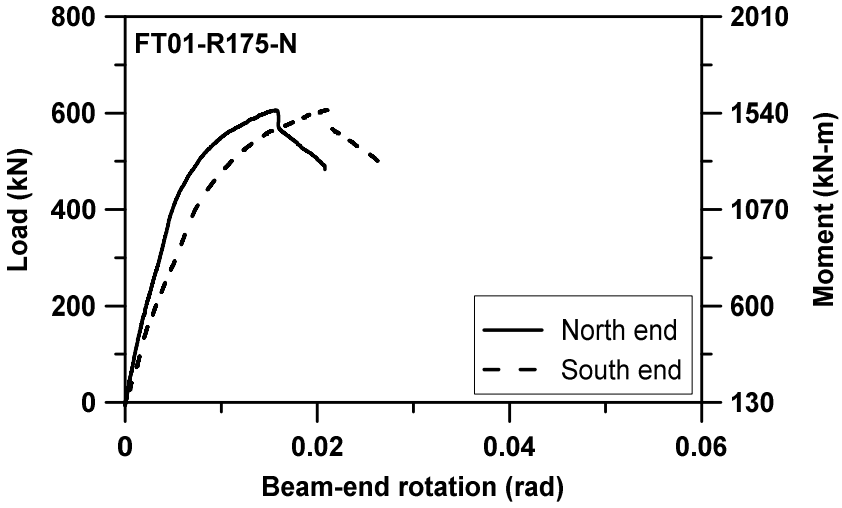

(b) FT01-R175-N

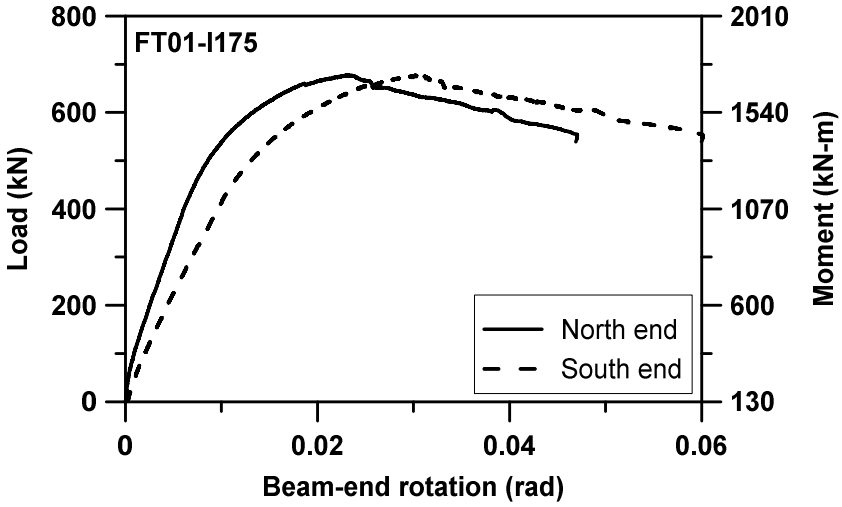

(c) FT01-I175

Figure 4-2 Beam-end rotation curves in flexural test (phase 1)

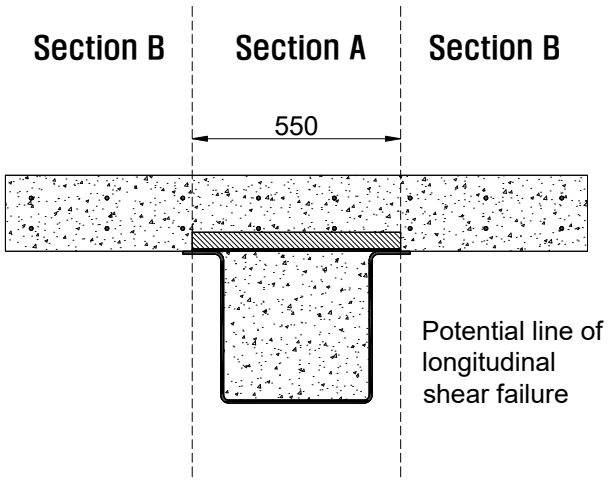

Figure 4-3 Potential line of longitudinal shear failure (Unit: mm)

Figure 4-4 Concrete failure due to friction between concrete slab and lateral support (FT01-R175-N)

In beam-end rotation curves, all specimens showed a difference in the beam-end rotations between two ends, which is suspected to have a slight eccentric loading during the test. The beam-end rotation curves showed similar behavior to the load-deflection curves in all specimens.

4.1.2 Concrete slab and U-shaped steel beam strain measurement

Figures 4-5 to **4-7** show strain measurement results of the flexural test specimens. In strain measurement results of the composite beam side (**Figure 4-5**), the strains measured at the loading stages of $0.2P_p$, $0.4P_p$, $0.6P_p$, P_y, and P_p are shown. The strains of U-shaped steel beam (SG6 to SG9) showed elastic behavior before the specimen reaching yield load (P_y) in all specimens. After the yield load, strains of U-shaped steel beam reached plastic behavior region and the strains in bottom part of the steel beam increased rapidly. However, in FT01-R175-N, only SG6 and SG7 strain gauges exceeded yield strain and the other strains in steel beam did not show plastic behavior until the end of test. It seems because the applied UTM load in FT01-R175-N sharply declined after peak load (P_p), and the test ended earlier compared to other specimens. It means that load rapidly reached the endpoint which is 80% of the peak load before the U-shaped steel beam enters plastic behavior region.

The distributions of beam side strains showed that the location of neutral axis gradually moved upward until reaching the peak load. In all specimens, the neutral axis was located in the concrete slab after reaching yield load. The neutral axis location of FT01-I175 was in the concrete slab from loading stage $0.2P_p$ to P_p, and movement of the neutral axis was almost nonexistent after loading stage $0.4P_p$.

The strains of the steel beam lower flange bottom surface (SG1 to SG5) remained linear before yield load, and they increased rapidly right after that point in FT01-R175 and FT01-I175. In FT01-R175-N, strains increased linearly until the yield load, and then strains almost maintained their value from the yield load stage to when the beam deflection reached about 100 mm. After around 100 mm deflection, the strains increased sharply. The strains of the lower flange of steel beam were also measured in five different loading stages. In FT01-R175 and FT01-I175, the lower flange surface of steel beam entered the plastic behavior region. However, in FT01-R175-N, only the edge part of lower flange (SG1 and SG5) exceeded the yield strain even in the loading stage of peak load (P_p). The strain measurements of SG1 to SG5 are shown in **Figure 4-6**.

The strain measurements of the top surface of the concrete slab (CG1 to CG5) are illustrated in **Figure 4-7**. The strains of concrete slab increased until reaching around 0.2% compressive strain. And the compressive strains declined while the load of the composite beam decreased. For results in which strains are measured at loading stages, the compressive strains at loading stage of yield load (P_y) showed about 0.1% strain. At the loading stage of peak load (P_p), the 0.2% compressive strain was observed on average. There was no particular correlation of the compressive strain according to the location of the strain gauges.

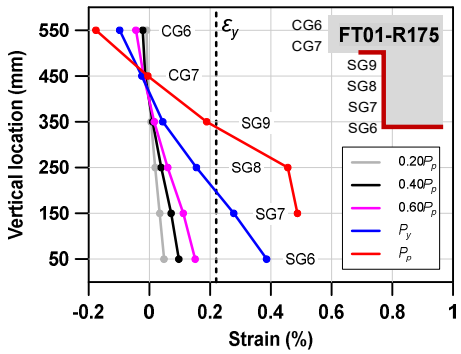

(a) Strains according to loading stage (FT01-R175)

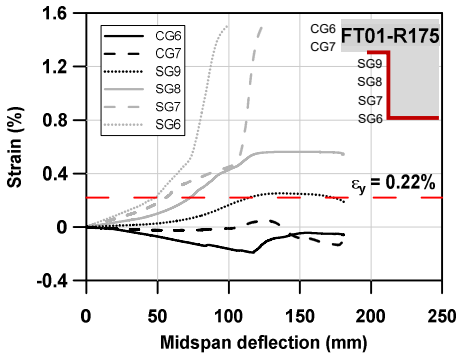

(b) Strain-deflection curve (FT01-R175)

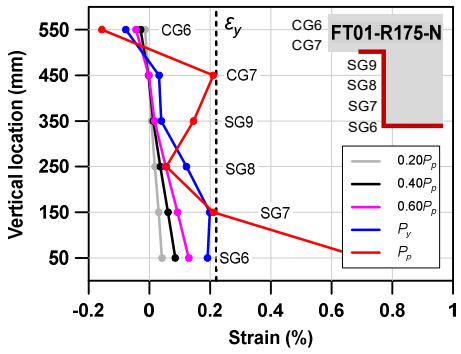

(c) Strains according to loading stage (FT01-R175-N)

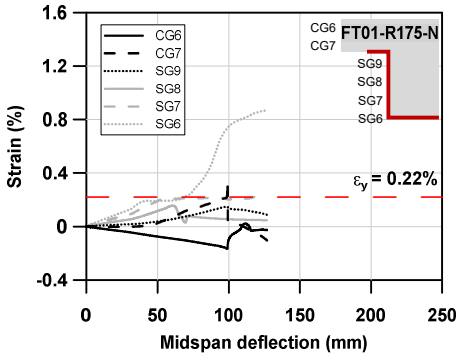

(d) Strain-deflection curve (FT01-R175-N)

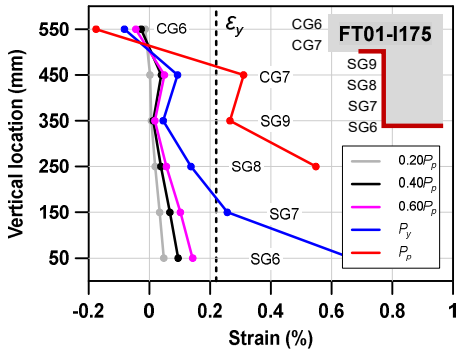

(e) Strains according to loading stage (FT01-I175)

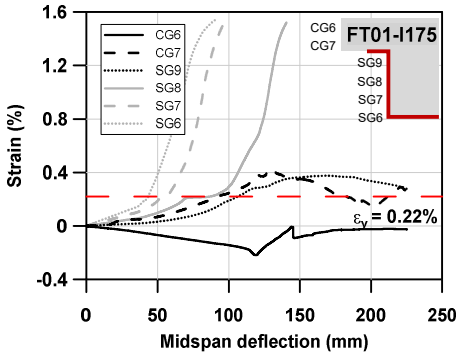

(f) Strain-deflection curve (FT01-I175)

Figure 4-5 Strain measurements of the composite beam side surface (phase 1)

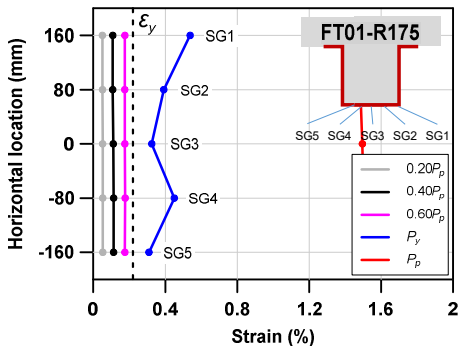

(a) Strains according to loading stage (FT01-R175)

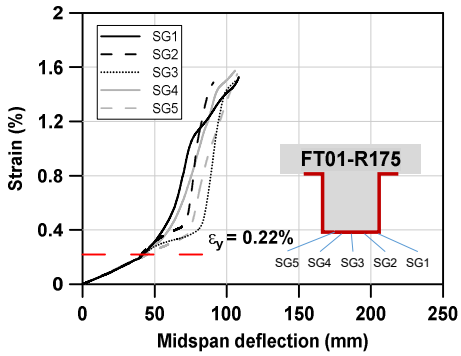

(b) Strain-deflection curve (FT01-R175)

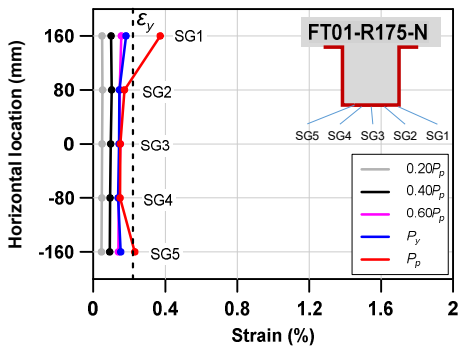

(c) Strains according to loading stage (FT01-R175-N)

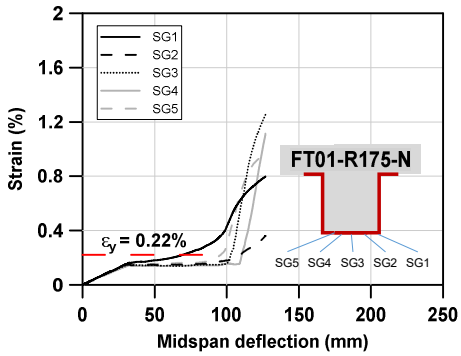

(d) Strain-deflection curve (FT01-R175-N)

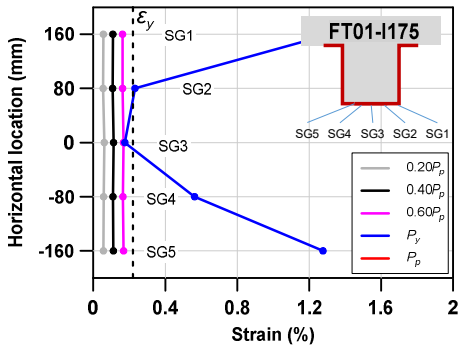

(e) Strains according to loading stage (FT01-I175)

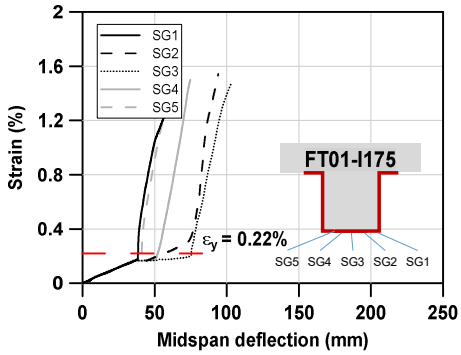

(f) Strain-deflection curve (FT01-I175)

Figure 4-6 Strain measurements of steel beam lower flange bottom surface (phase 1)

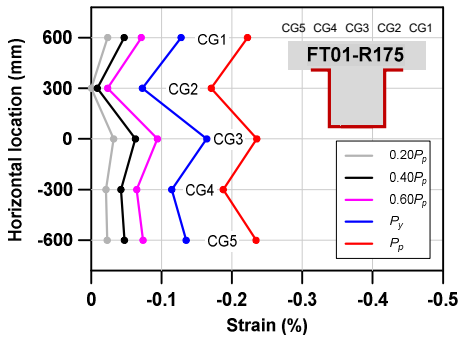

(a) Strains according to loading stage (FT01-R175)

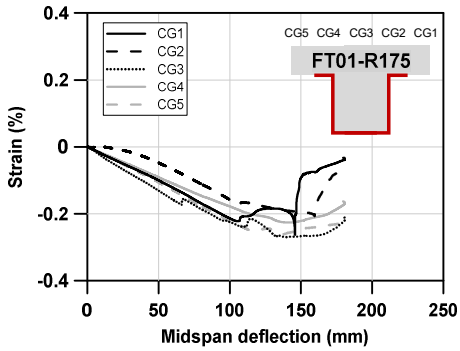

(b) Strain-deflection curve (FT01-R175)

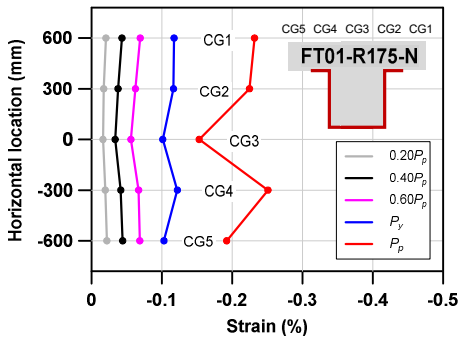

(c) Strains according to loading stage (FT01-R175-N)

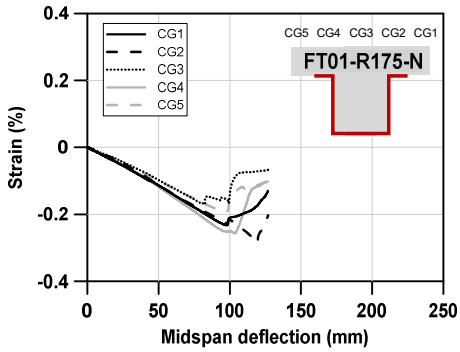

(d) Strain-deflection curve (FT01-R175-N)

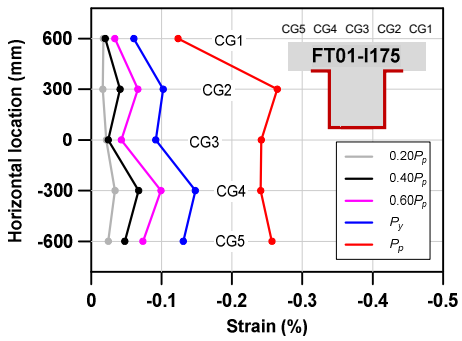

(e) Strains according to loading stage (FT01-I175)

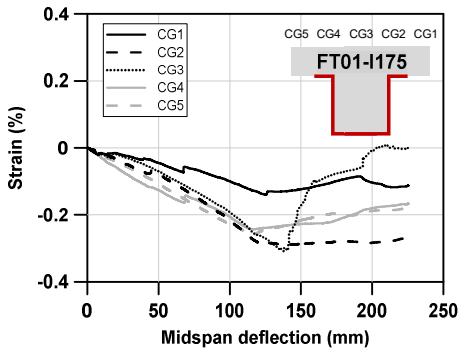

(f) Strain-deflection curve (FT01-I175)

Figure 4-7 Strain measurements of the top surface of concrete slab (phase 1)

4.1.3 Failure mode and deformation

The concrete cracks and failure modes of each flexural test specimen were observed in the test and summarized in **Figures 4-8** to **4-10**. Before reaching peak load, no cracks occurred in the concrete slabs. The concrete slab was mostly in compression. It is presumed that considerable tensile cracks occurred in the concrete enclosed by the U-shaped steel beam. Near the peak load, longitudinal fine cracks were observed in the concrete slab, suggesting the concrete slab was under severe compressive stress. At the ultimate stage, severe longitudinal cracks and spalling of side concrete were observed, and the failures of flexural test specimens were dominated by concrete crushing. In the bottom surface of concrete slab at the middle of the beam, concrete cracks were generated by compressive stress in the concrete slab. In FT01-I175, there was a large concrete spalling on the west side of concrete slab bottom surface. After the test, no relative slip between steel beam and concrete slab was observed, and there was no sign of longitudinal cracks due to shear connector failures. It means that the composite behavior of flexural test specimens performed very properly. As mentioned in **Section 4.1.1**, concrete failure occurred due to friction between the concrete slab and lateral supports in FT01-R175-N.

After the flexural tests, the concrete slabs were demolished and angle shear connector deformation was investigated. **Figure 4-11** shows the deformation of the angle shear connectors of flexural test specimens. In all specimens, negligible deformation of shear connectors and no weld-zone failures were observed. It indicates that the angle shear connectors had enough shear resistance in flexural tests. Also, local buckling did not occur in all steel beams.

(a) Concrete cracks on concrete slab east side

(b) Concrete cracks on concrete slab west side

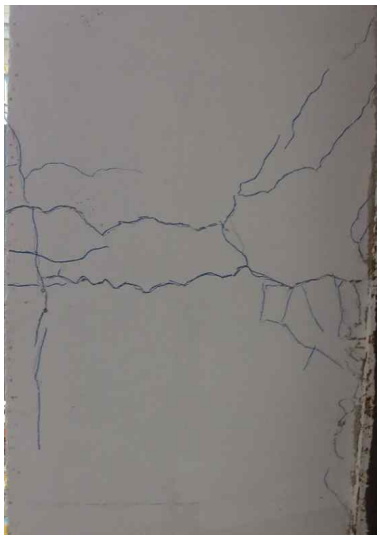

(c) Concrete cracks on concrete slab bottom surface (east)

(d) Concrete cracks on concrete slab bottom surface (west)

(e) North end of the specimen

(f) South end of the specimen

Figure 4-8 Concrete cracks and failure mode of FT01-R175 after the test

(a) Concrete cracks on concrete slab east side

(b) Concrete cracks on concrete slab west side

(c) Concrete cracks on concrete slab bottom surface (east)

(d) Concrete cracks and spalling on concrete slab bottom surface (west)

(e) North end of the specimen

(f) South end of the specimen

Figure 4-9 Concrete cracks and failure mode of FT01-I175 after the test

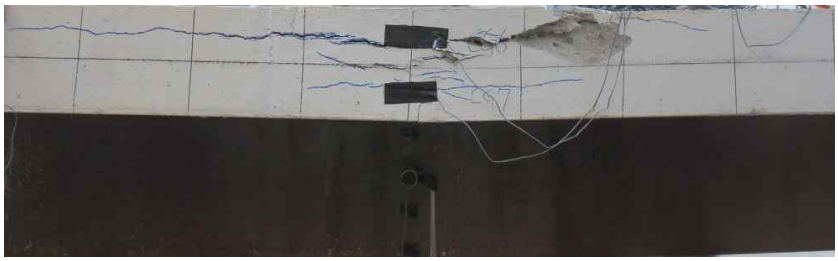

(a) Concrete cracks on concrete slab east side

(b) Concrete cracks on concrete slab west side

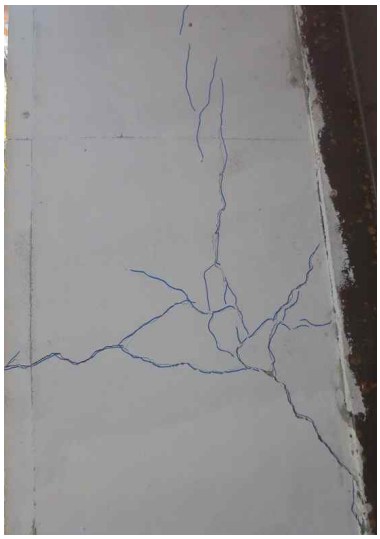

(c) Concrete cracks on concrete slab bottom surface (east)

(d) Concrete cracks on concrete slab bottom surface (west)

(e) North end of the specimen

(f) South end of the specimen

(g) Concrete failure due to frictional force between concrete slab and lateral supports

Figure 4-10 Concrete cracks and failure mode of FT01-R175-N after the test

(a) Angle deformation at mid span – top view (FT01-R175)

(b) Angle deformation at mid span – elevation view (FT01-R175)

(c) Angle deformation at mid span – top view (FT01-R175-N)

(d) Angle deformation at mid span – elevation view (FT01-R175-N)

(e) Angle deformation at mid span – top view (FT01-I175)

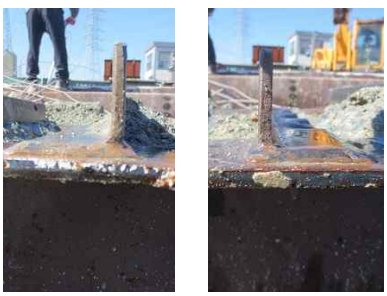

(f) Angle deformation at mid span – elevation view (FT01-I175)

Figure 4-11 Deformation of angle shear connectors in flexural test (phase 1)

4.2 Push-out test

4.2.1 Shear strength and load-horizontal slip curve

Figure 4-12 illustrates the load-horizontal slip curves of push-out test specimens and **Table 4-3** summarizes the result of push-out test. Measured peak strength (V_p) is the peak shear strength measured at UTM load cell, and measured peak strength per shear connector (V_{pc}) is obtained from dividing measured peak strength by the number of angles. Horizontal slip is the relative displacement between steel beam and concrete slabs. Measured ultimate horizontal slip (Δ_u) is the horizontal slip when the UTM load was reached 75% of measured peak strength.

The interval of angle shear connectors was proportional to the maximum shear strength of push-out test specimens. Specimen PT01-R225 was only the exception of this proportional relation. Considering that the push-out test of PT01-R225 was conducted 3 weeks later than the others for certification, it seems that increase of concrete strength in 3 weeks led to the increase of PT01-R225 shear strength. According to AC495 (2018) push-out test specimen design criteria, as the interval of the angles increases, the cross section area of concrete slabs contacted with concrete enclosed by the U-shaped steel beam increases. In other words, the area of concrete resisting shear force also increases when the interval of the angles gets wider. Considering the proportional relation between the measured peak strength and interval of the angles, it means that concrete contributes to the shear strength of push-out test specimen. Also, the specimen with the right direction angles had higher shear capacity than specimen with the inverse direction angles. Thus, it is more advantageous to place the angle shear connectors in the right direction in terms of shear resistance. The load-horizontal curves showed elastic behavior at the beginning, and then stiffness degradation was maintained until the peak load. After the peak load, it was observed that measured load started to decline by yielding and deformation of the angle shear connectors.

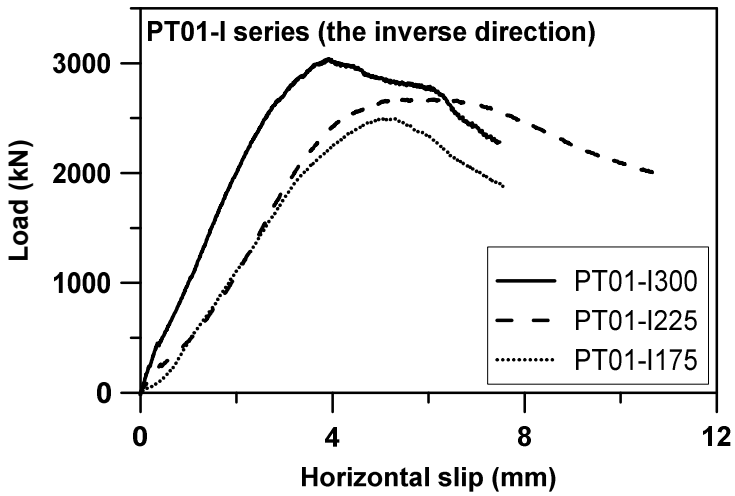

(a) Push-out test specimens with the inverse direction angles

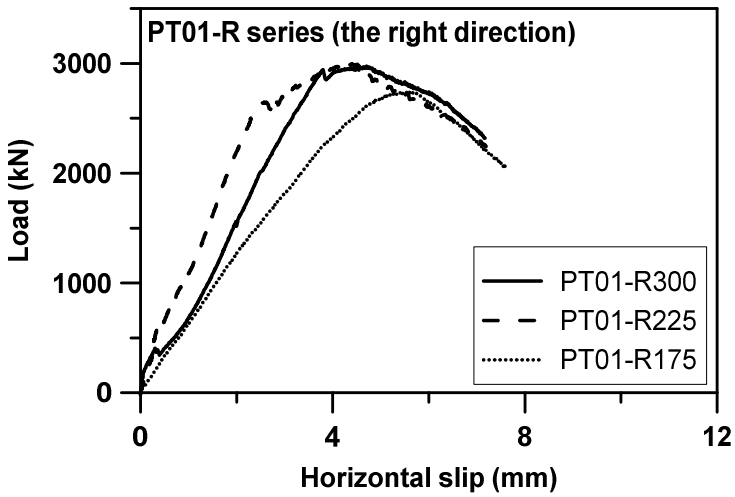

(b) Push-out test specimens with the right direction angles

Figure 4-12 Load-horizontal slip curves of the push-out test (phase 1)

Table 4-3 Push-out test results of specimen shear strength (phase 1)

Specimen	Angle direction	Measured peak strength, V_p (kN)	Measured peak strength per shear connector, V_{pc} (kN)	Measured ultimate horizontal slip, Δ_u (mm)
PT01-I175	⌟ ⌞ (The inverse direction)	2,497.88	624.47	7.59
PT01-I225		2,674.8	668.7	10.68
PT01-I300		3,039.12	759.78	7.48
PT01-R175	⌝ ⌜ (The right direction)	2,739.53	684.88	7.61
PT01-R225		3,002.75	750.69	7.19
PT01-R300		2,976.24	744.06	7.17

4.2.2 Comparison with shear connector design equations

Table 4-4 shows the comparison between measured peak strength per shear connector of the push-out test specimens and nominal shear strength calculated by four shear connector design equations; AC495 (2018) angle anchor design equation (**Eq. (2-1)**), Eurocode 4 (2001) angle anchor design equation (**Eq. (2-6)**), AISC 360-16 (2016) channel anchor design equation (**Eq. (2-7)**), and CAN/CSA-S16-01 (2001) channel anchor design equation (**Eq. (2-13)**). The average values of measured peak strength per shear connector divided by nominal shear strength of shear connector were low in the order of AISC 360-16 (2016), CAN/CSA-S16-01 (2001), Eurocode 4 (2001), and AC495 (2018). AISC 360-16 (2016) design equation estimated the shear strength of an angle shear connector almost the same although it is a design formula for a channel shear connector. However, the measured peak strength per shear connector was 3 to 4 times the nominal shear strength calculated by AC495 (2018) angle shear connector design equation. In the other design equations, the values were 1 to 1.6 on average. It indicates that AC495 (2018) equation may be overly conservative. The AC495 (2018) equation was proposed based on the failure mode that an angle shear connector acts like a beam with fixed ends under uniformly distributed loads.

Considering that nominal shear strength calculated by AC495 (2018) design equation is much lower than measured peak strength per shear connector, it could be assumed that failure mode of an angle of the push-out test specimen is different from the failure mode of AC495 (2018) design equation. In addition, the channel shear connector equations estimated the shear strength of an angle attached to the push-out test specimen more precisely than the angle shear connector equations.

Table 4-4 Comparison with shear connector design equations (phase 1)

Specimen	V_{pc} (kN)	V_{AC495} (kN)	V_{Euro4} (kN)	V_{AISC} (kN)	V_{CAN} (kN)	V_{pc} / V_{AC495}	V_{pc} / V_{Euro4}	V_{pc} / V_{AISC}	V_{pc} / V_{CAN}
PT01-I175	624.5	185.7	437.4	698.8	460.7	3.36	1.43	0.89	1.36
PT01-I225	668.7					3.6	1.53	0.96	1.45
PT01-I300	759.8					4.09	1.74	1.09	1.65
PT01-R175	684.9					3.69	1.57	0.98	1.49
PT01-R225	750.7					4.04	1.72	1.07	1.63
PT01-R300	744.1					4.01	1.7	1.06	1.62
Average value						**3.8**	**1.61**	**1.01**	**1.53**

Note: V_{pc} is measured peak strength per shear connector; V_{AC495} is an angle nominal shear strength calculated by AC495 (2018) equation; V_{Euro4} is an angle nominal shear strength calculated by Eurocode 4 (2001) equation; V_{AISC} is an angle nominal shear strength calculated by AISC 360-16 (2016) equation; and V_{CAN} is an angle nominal shear strength calculated by CAN/CSA-S16-01 (2001) equation.

4.2.3 Strain measurement

The angle shear connector strain-horizontal slip curves are presented in **Figures 4-13**. The plan of strain gauge measurement is shown in **Appendix B**. In general, the higher strain was measured at gauges attached to the edge of angle shear connectors (AG1, 5, 6, 10). On the other hand, the strain gauges attached to the center of angle shear connector had relatively little deformation. The difference in strain between the upper and lower angle shear connectors was almost nonexistent. The specimens with the inverse direction angle had more gauges that increased over yield strain than specimens with the right direction angle. This means that larger deformation occurred in angle shear connectors in specimens with the inverse direction angle.

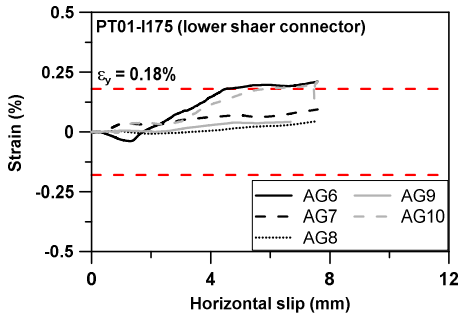

(a) PT01-I175 (lower shear connector)

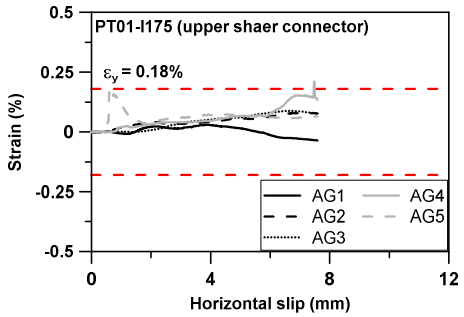

(b) PT01-I175 (upper shear connector)

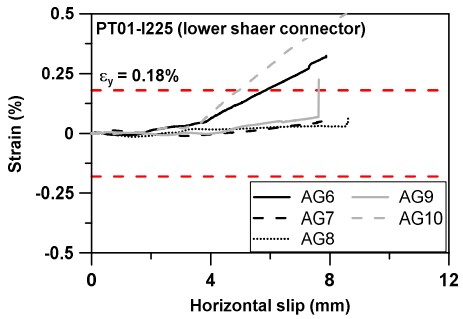

(c) PT01-I225 (lower shear connector)

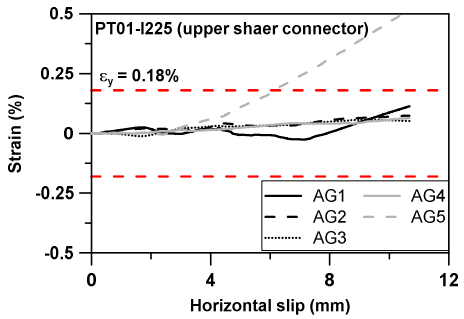

(d) PT01-I225 (upper shear connector)

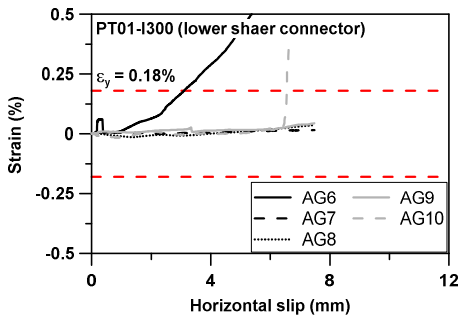

(e) PT01-I300 (lower shear connector)

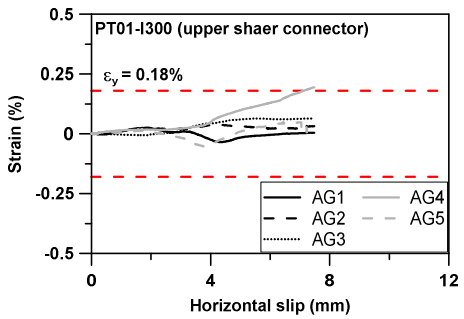

(f) PT01-I300 (upper shear connector)

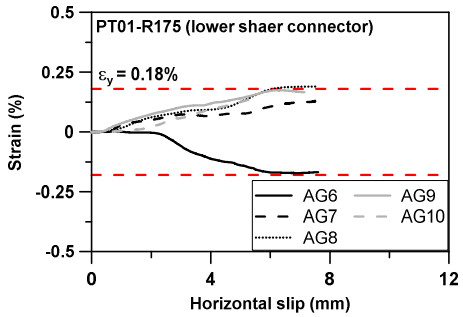

(g) PT01-R175 (lower shear connector)

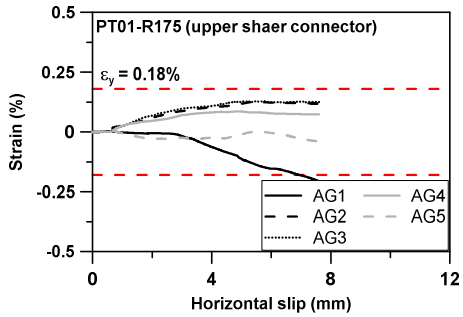

(h) PT01-R175 (upper shear connector)

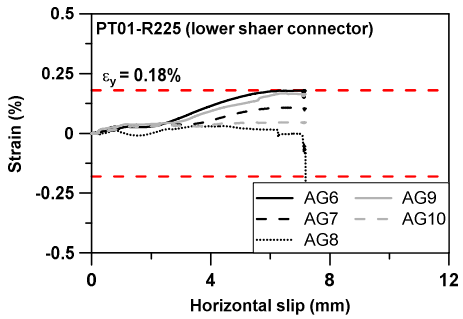

(i) PT01-R225 (lower shear connector)

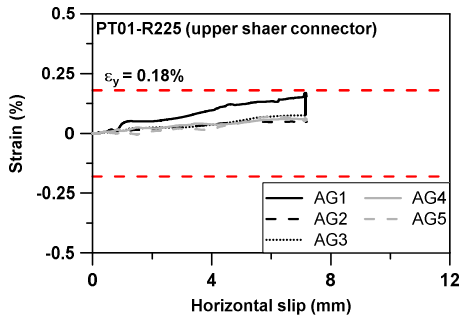

(j) PT01-R225 (upper shear connector)

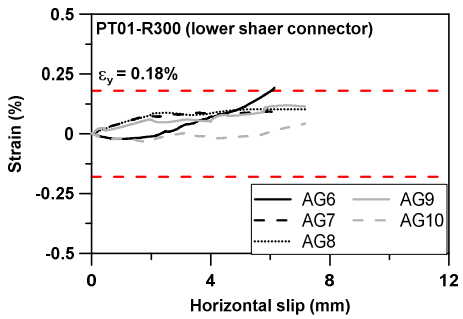

(k) PT01-R300 (lower shear connector)

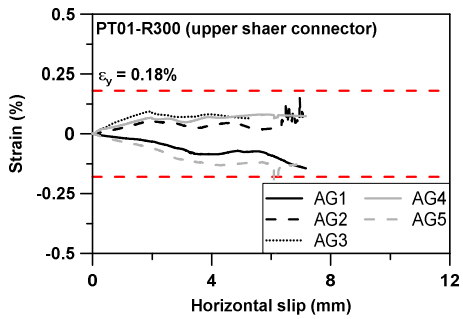

(l) PT01-R300 (upper shear connector)

Figure 4-13 Strain measurements of angle shear connectors in push-out test (phase 1)

4.2.4 Failure mode and deformation

The concrete cracks of PT01-I225 are shown in **Figure 4-14**. For all specimens, the gap between concrete slab and steel beam was first observed in the linear behavior region as load increased, and the gap got larger while displacement and load were increasing. After measured peak strength, concrete cracks began to be observed and intensified as displacement increased. In all push-out specimens, cracks near the angle shear connector were observed as presented in **Figure 4-14(e)**. Therefore, it seems that failure of push-out test specimen was dominated by concrete cracks around angle shear connectors.

(a) North side

(b) South side

(c) East side

(d) West side

(e) Concrete cracks near angle shear connectors (f) The gap between concrete slab and steel beam

Figure 4-14 Concrete cracks and separation gap of PT01-I225

Figure 4-15 shows the deformation of angle shear connectors of push-out test specimens. As shown in **Figure 4-15**, the out-of-plane bending deformation which is the same as behavior of a beam with fixed ends under uniformly distributed loads is almost negligible. However, the angles of phase 1 push-out test showed in-plane bending deformation which is the same as deformation in the transverse direction by folding inward or outward. It means that in-plane bending deformation is dominant in the angle shear connector. Furthermore, the dominant behavior of in-plane bending deformation in push-out test can explain the result of **Table 4-4**. The design equations of Eurocode 4 (2001), AISC 360-16 (2016), and CAN/CSA-S16-01 (2001) are based on that whole flange area of the shear connector is connected with the steel beam. In this connection, the shear connectors are likely to show in-plane bending deformation. Therefore, the shear strength of an angle shear connector in the push-out test was measured similarly to nominal strength calculated by design equation of Eurocode 4 (2001), AISC 360-16 (2016), and CAN/CSA-S16-01 (2001) rather than AC495 (2018).

(a) Deformation of angle shear connectors in PT01-I225

(a) Deformation of angle shear connectors in PT01-R175

Figure 4-15 Deformation of angle shear connectors (phase 1)

4.3 Discussion

In this chapter, flexural test with three specimens and push-out test with six specimens for phase 1 were conducted. In flexural test, the presence of transverse reinforcement in the concrete slab and the direction of angle shear connectors were considered as the main variables. The interval and direction of angles shear connectors were main variables in push-out test. As mentioned in **Chapter 3**, concrete compressive strength and steel yield strength were

measured much lower and higher than specified nominal strength, respectively.

In the flexural test, the higher flexural strength and ductility were measured in the order of FT01-I175, FT01-R175, and FT01-R175-N. Specimen FT01-I175 was the only specimen of which measured peak moment was higher than nominal flexural strength. However, in FT01-R175-N, severe concrete failure occurred near lateral supports due to frictional force between lateral supports and the concrete slab, and it led to flexural strength degradation of the composite beam. Therefore, it is difficult to examine the effect of transverse reinforcement on flexural strength. Consequently, it was more advantageous to place angle shear connectors in the inverse direction for flexural strength and ductility. In FT01-R175, the neutral axis was located almost bottom of the concrete slab, which made the upper flange of steel beam difficult to reach the yield and steel beam fail to perform sufficient tensile force. The flexural strength of FT01-R175 decreased due to insufficient tensile force, and it did not exceed the nominal flexural strength. On the other hand, the neutral axis of FT01-R175-N was located near the center of concrete slab. As mentioned above, the measured peak moment of FT01-R175-N also did not reach the nominal flexural strength due to severe concrete failure.

For all flexural test specimens, the failure of concrete slab was dominated by concrete crushing at the center of the beam, and there were no longitudinal shear cracks. No relative slip between the concrete slab and steel beam was observed. It is judged that composite behavior of the composite beam was excellent. After the test, steel beam and angle shear connectors were observable with the naked eye by demolishing the concrete slab. The deformation of the angles was negligible and there was no local bucking in steel beam.

In the push-out test, the higher shear strength was measured in the specimens with the angle shear connector in the right direction and wider interval of angles. Considering the relation between the interval of angles and measured

peak strength of specimens, it is assumed that the portion of concrete account for shear strength of the specimens is not ignorable. Because according to AC495 (2018) which provides design criteria for the push-out test specimen, widening the interval of angle shear connectors increases the cross section area of concrete slabs integrated with concrete in the steel beam. As the interval of angles increases, shear resistance of concrete that is proportional to the cross section area of concrete also increases.

Compared to various shear connector design equations, the measured peak strength of specimens showed more than 3 times the nominal shear strength calculated by AC495 (2018) design equation. However, in comparison with the other design equations (AISC 360-16, 2016; CAN/CSA-S16-01, 2001; and Eurocode 4, 2001), the measured peak strength was 1 to 1.6 times the nominal shear strength. The design equation of AC495 (2018) is based on that angles behave like a beam with fixed ends under uniformly distributed loads while design equations of the other criteria are based on that shear connectors are likely to show in-plane bending deformation. After the comparison with four design equations, it could be assumed that in-plane bending deformation is dominant in angle shear connectors. The failure mode and deformation of angle shear connectors were observed after the test. There was no weld-zone fracture, and in-plane bending deformation was dominant in angle shear connectors. Thus, the deformation of angles observed after the test explains the result of comparison between measured shear strength and nominal strength calculated by various shear connector design equations.

Chapter 5. Phase 2 Test Results

In this chapter, results of phase 2 test are demonstrated. Flexural tests with three specimens and push-out tests with ten specimens were conducted in phase 2. Through the tests, flexural and interface shear performance of the composite beam were investigated.

5.1 Flexural test

5.1.1 Flexural strength and ductility

The phase 2 flexural test results of flexural strength and ductility are summarized in **Tables 5-1** and **5-2**, respectively. Before the test, it was expected that the increase in angle interval will decrease the flexural strength of specimens by reducing the composite ratio. However, the measured peak moment (M_p) of specimens was measured higher in the order of FT02-I175, FT02-I550, and FT02-I400. Moreover, the strength difference between FT02-I400 and FT02-I550 was almost nonexistent. The nominal flexural strength (M_n) calculated by plastic stress distribution method predicted the actual strength of specimens almost precisely by reflecting the decrease of flexural strength of the composite beam according to the increase of the angle interval.

The comparison of values in which measured peak moment is divided by nominal flexural strength (M_p / M_n) was conducted because measured concrete strength was different between flexural specimens. The value of FT02-I550 was 1.071, which means the measured peak moment exceeded nominal flexural strength. In FT02-I175 and FT02-I400, the values were 0.984 and 0.983, respectively. It means that FT02-I175 and FT02-I400 did not derive sufficient flexural strength. In all specimens, the longitudinal shear cracks

near the angles and slip between concrete slab and steel beam were not observed. Thus, it seems that the reason for insufficient flexural strength is low quality of concrete. In phase 2, measured average concrete strength was 19.78 MPa, which is considerably lower than specified concrete strength, 24 MPa. Considering that concrete curing was conducted in summer and steam curing was accompanied, it can be judged that quality of the concrete is very low and it is not reliable. In addition, the gap between concrete slab and cross head of UTM was observed at only one side in FT02-I400, as presented in **Figure 5-1**. Therefore, it is assumed that eccentric load was applied to FT02-I400, which resulted in insufficient flexural strength. Ductility was inversely proportional to the interval of the angles. Consequently, it was more advantageous to place the angle shear connectors narrower for flexural strength and ductility.

Table 5-1 Flexural test results of specimen flexural strength (phase 2)

Specimen	Measured peak load, P_p (kN)	Measured peak moment, M_p (kN-m)	Nominal peak load, P_n (kN)	Nominal flexural strength, M_n (kN-m)	M_p / M_n
FT02-I175	629.4	1,609.09	640.83	1,635.94	0.984
FT02-I400	532	1,380.2	540.94	1,404.22	0.983
FT02-I550	536.32	1,390.35	497.21	1,298.45	1.071

Table 5-2 Flexural test results of specimen ductility (phase 2)

Specimen	Yield beam-end rotation, θ_y (rad)		Ultimate beam-end rotation, θ_u (rad)		Ductility	
	North end	South end	North end	South end	North end	South end
FT02-I175	0.00821	0.01514	0.0437	0.0551	5.32	3.64
FT02-I400	0.0112	0.01223	0.03907	0.03782	3.49	3.09
FT02-I550	0.0117	0.01497	0.04096	0.04267	3.5	2.85

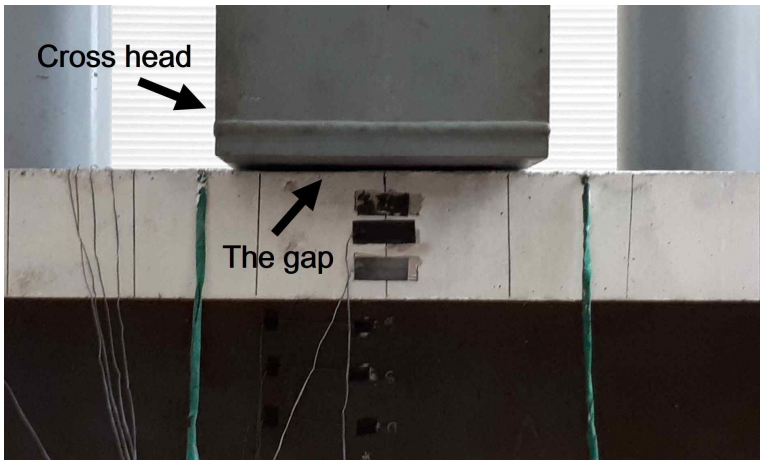

Figure 5-1 Gap between UTM cross head and concrete slab in FT02-I400

Figures 5-2 and **5-3** show load-deflection curves and beam-end rotation curves of flexural test specimens, respectively. In all specimens, load-deflection curves showed elastic behavior until 2/3 of the measured peak load, and after that point the stiffness started to decrease. After reaching the measured peak load, the load-deflection curve was maintained nearly horizontal in FT02-I400 and FT02-I550. For FT02-I175, the curve started to decline gradually. The beam-end rotation curves showed almost the same behavior as load-deflection curves in all specimens. In beam-end rotation curves, there was almost no difference between two ends in FT02-I400 and FT02-I550. For FT02-I175, a large discrepancy existed between two ends. It means that eccentric load was applied to FT02-I175.

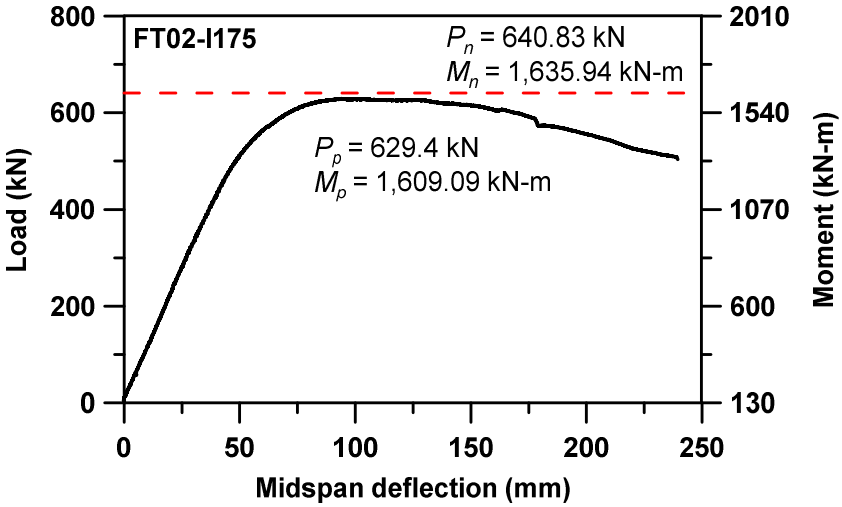

(a) FT02-I175

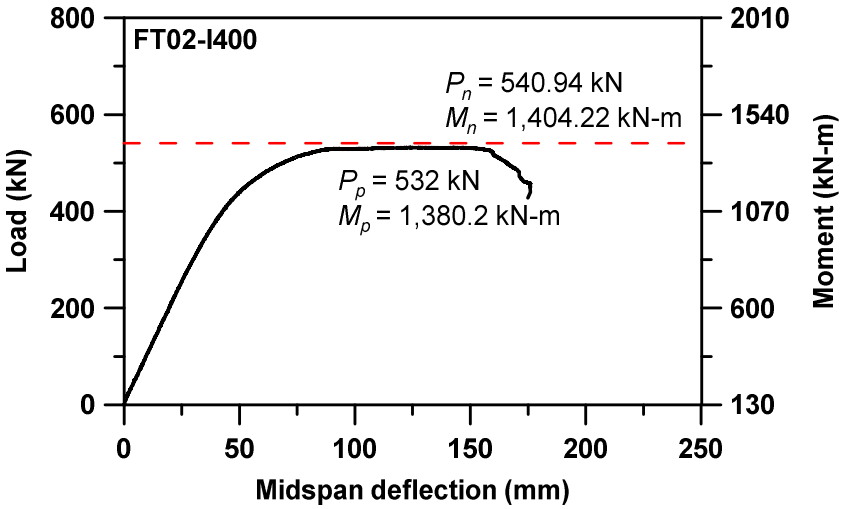

(b) FT02-I400

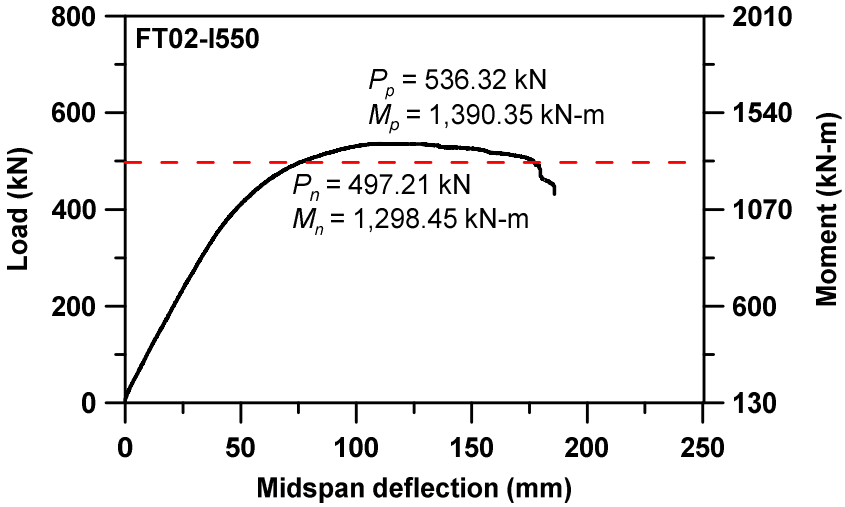

(c) FT02-I550

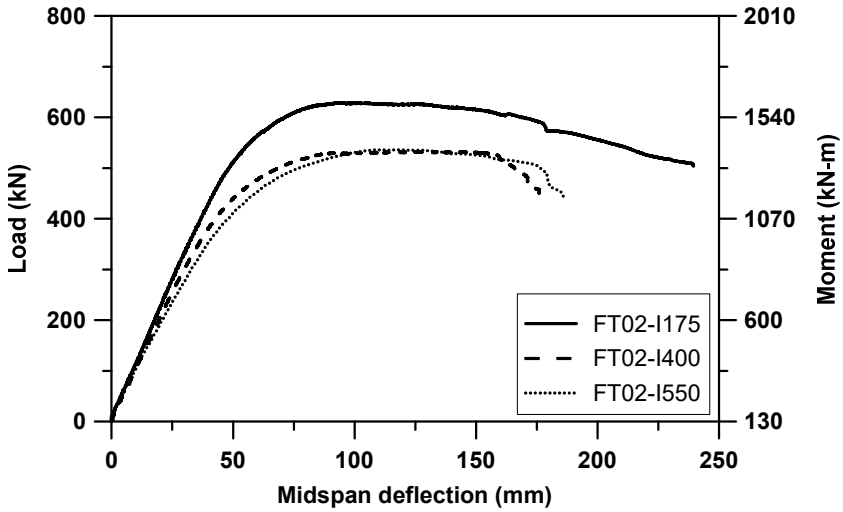

(d) All flexural test specimens

Figure 5-2 Load-deflection curves in flexural test (phase 2)

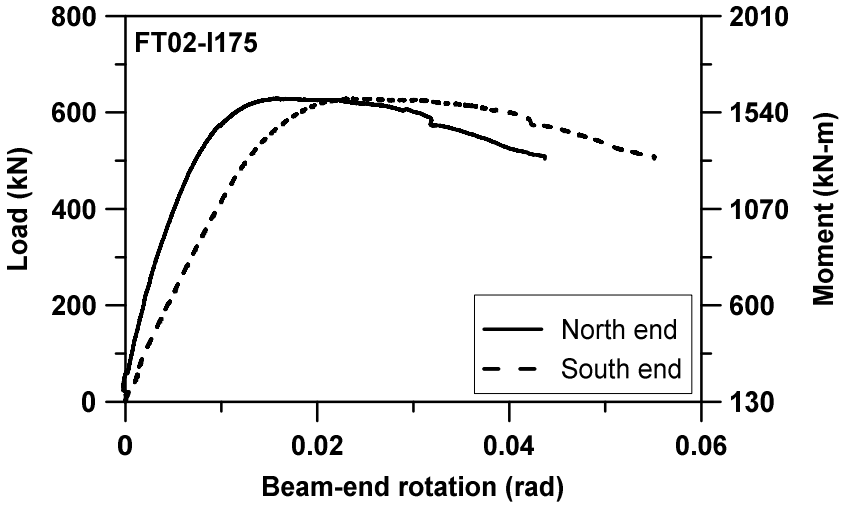

(a) FT02-I175

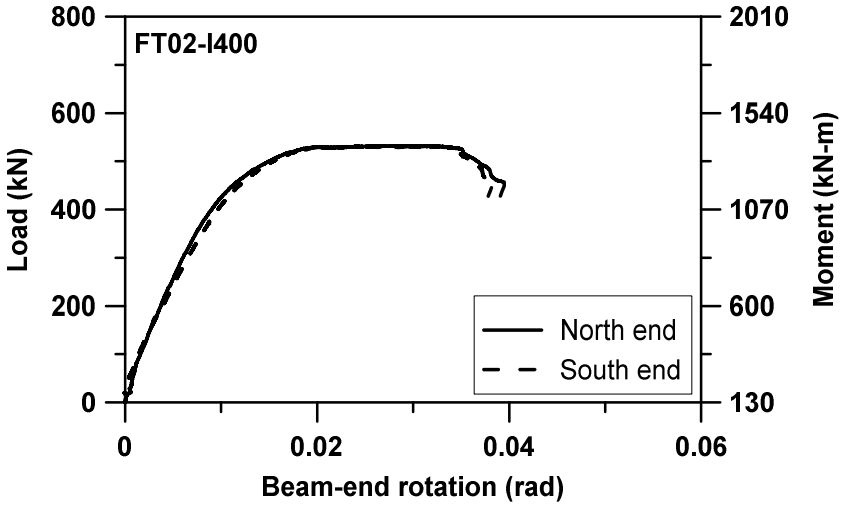

(b) FT02-I400

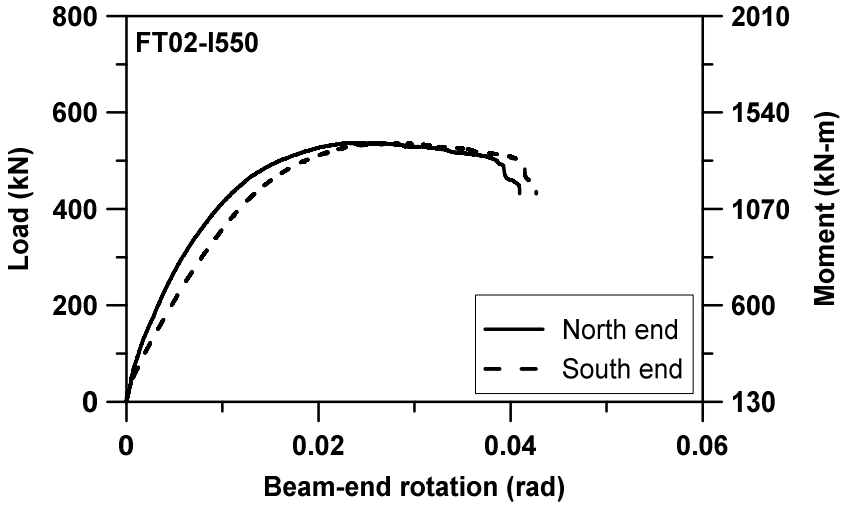

(c) FT02-I550

Figure 5-3 Beam-end rotation curves in flexural test (phase 2)

5.1.2 Concrete slab and U-shaped steel beam strain measurement

The concrete slab and steel beam strain measurement results of the flexural test specimens are shown in **Figures 5-4** to **5-6**. As conducted in phase 1, the composite beam side strains were measured at the loading stages of $0.2P_p$, $0.4P_p$, $0.6P_p$, P_y, and P_p, respectively. The strains of U-shaped steel beam (SG6 to SG9) showed linear behavior before the specimen reached yield load (P_y) for all specimens. However, the upper part of steel beam web (SG9) did not reach the yield until the end of test. In FT02-I175, the neutral axis was placed within the concrete slab in all loading stages. For FT02-I550, the neutral axis was located at almost the bottom of concrete slab throughout the test. In FT02-I400, the location of neutral axis was near the upper flange of steel beam until the yield load stage (P_y). At the peak load stage (P_p), it appears on the graph (**Figure 5-4(c)**) as if the neutral axis is located in the middle of the concrete slab. But considering that the upper part of U-shaped steel beam web (SG9) still did not reach the yield at the peak load stage (P_p) and the sudden increase of CG7 strain which is not reliable, it is assumed that neutral axis existed near the bottom of concrete slab or upper flange of steel

beam. The reason for low neutral axis of FT02-I400 and FT02-I550 is that the two specimens are partially composite beams.

The measurement result of strain gauges attached to the bottom of steel beam lower flange (SG1 to SG5) is shown in **Figure 5-5**. In all specimens, most strain gauges yielded when deflection was around 50 mm, and continued to increase after that point. When the specimens reached the yield load stage, all strain gauges had yielded. Similarly to phase 1, there was no particular correlation of the strain according to the location of strain gauges.

Figure 5-6 shows strain measurements of the top surface of the concrete slab (CG1 to CG5). All specimens showed similar behavior that compressive strain of the top surface of concrete slab increased as load increased. After deflection reached around 100 mm, the compressive strain began to decrease. The average compressive strain of FT02-I550 was measured higher than the other specimens, and especially SG5 strain gauge showed a maximum 0.4% compressive strain.

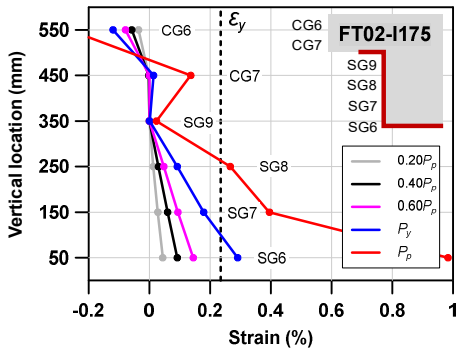

(a) Strains according to loading stage (FT02-I175)

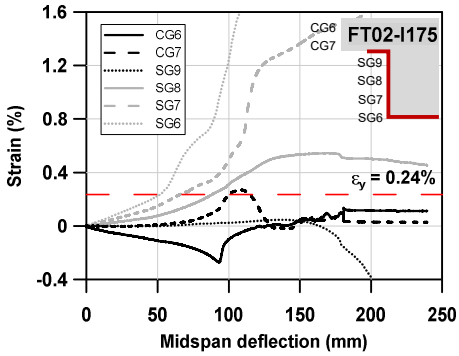

(b) Strain-deflection curve (FT02-I175)

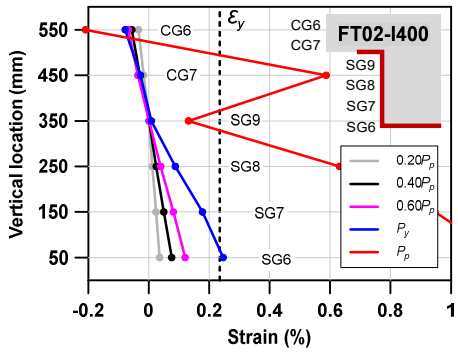

(c) Strains according to loading stage (FT02-I400)

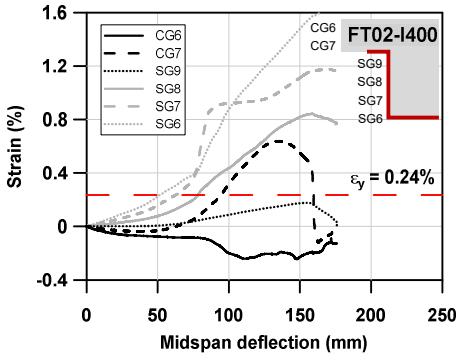

(d) Strain-deflection curve (FT02-I400)

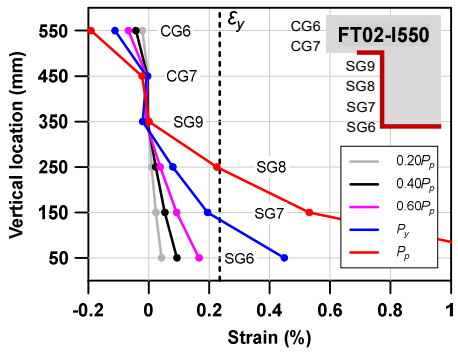

(e) Strains according to loading stage (FT02-I550)

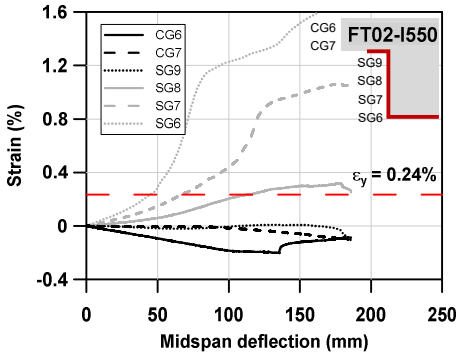

(f) Strain-deflection curve (FT02-I550)

Figure 5-4 Strain measurements of the composite beam side surface (phase 2)

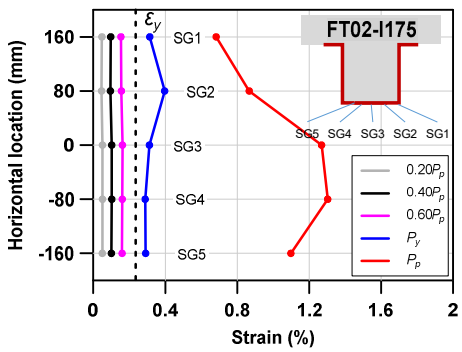

(a) Strains according to loading stage (FT02-I175)

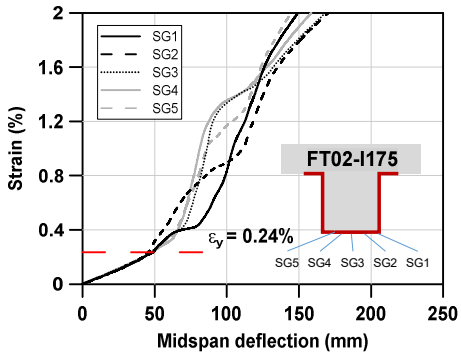

(b) Strain-deflection curve (FT02-I175)

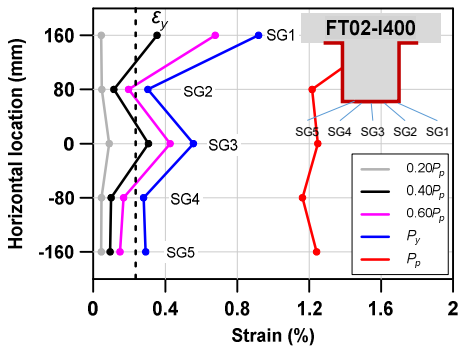

(c) Strains according to loading stage (FT02-I400)

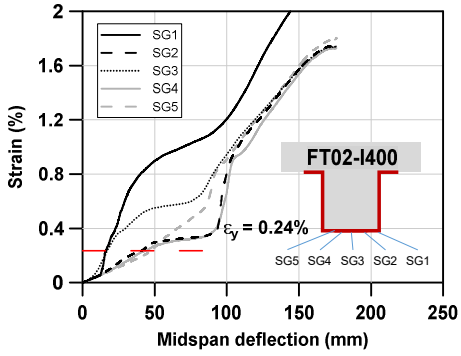

(d) Strain-deflection curve (FT02-I400)

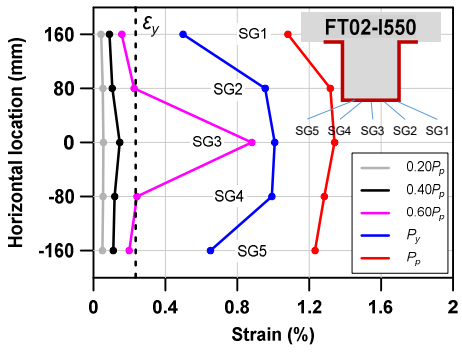

(e) Strains according to loading stage (FT02-I550)

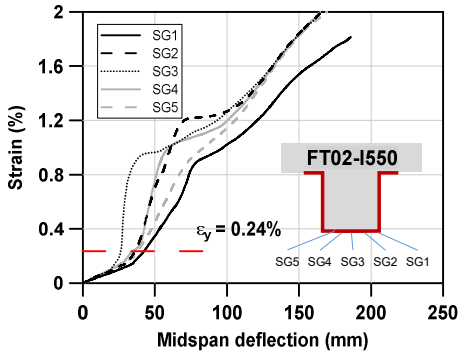

(f) Strain-deflection curve (FT02-I550)

Figure 5-5 Strain measurements of steel beam lower flange bottom surface (phase 2)

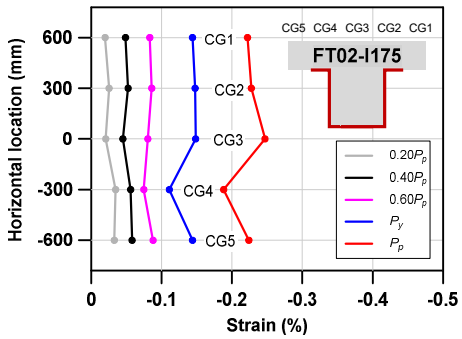

(a) Strains according to loading stage (FT02-I175)

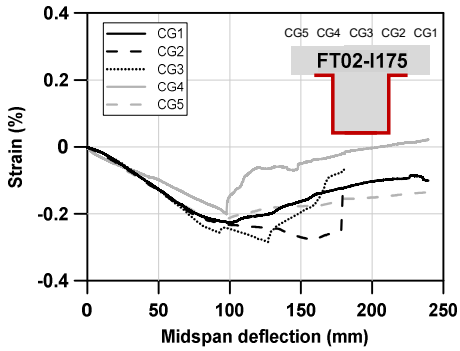

(b) Strain-deflection curve (FT02-I175)

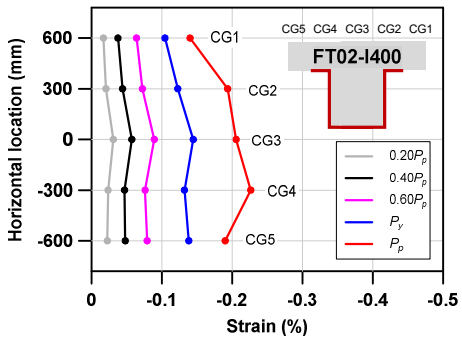

(c) Strains according to loading stage (FT02-I400)

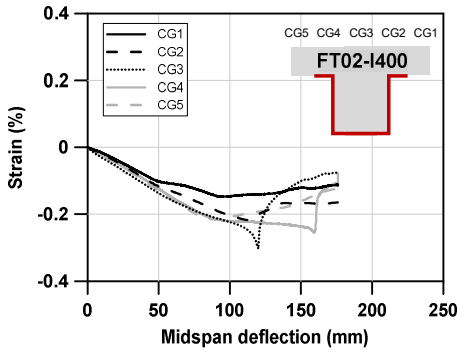

(d) Strain-deflection curve (FT02-I400)

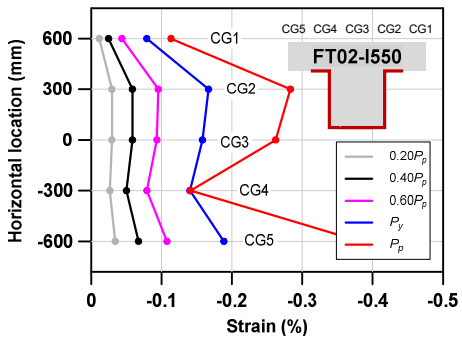

(e) Strains according to loading stage (FT02-I550)

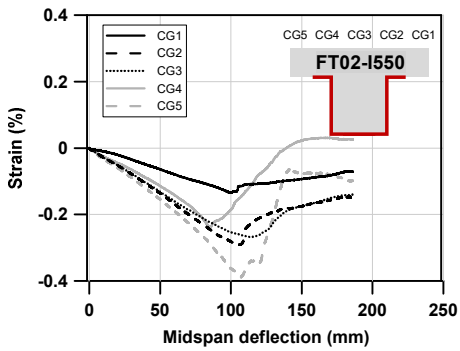

(f) Strain-deflection curve (FT02-I550)

Figure 5-6 Strain measurements of the top surface of concrete slab (phase 2)

5.1.3 Angle shear connector strain measurement

The strain measurement result of angle shear connectors is presented in **Figure 5-7**. The detailed plan of angle shear connector strain measurement is illustrated in **Appendix B**. In all specimens, the largest strain was measured at the edge of angle shear connectors. There were more yielded strain gauges in transverse direction (AG4 to AG6) than longitudinal direction (AG1 to AG 3). For strain gauges installed in the longitudinal direction, difference of strain-deflection curve according to strain gauge location was nearly nonexistent. However, in strain gauges installed in the transverse direction, the difference was prominent. In FT02-I175 and FT02-I550, the average strain of transverse direction was larger than longitudinal direction, but the difference was not large. Therefore, it seems difficult to determine the dominant deformation behavior of angle shear connectors by this strain measurement.

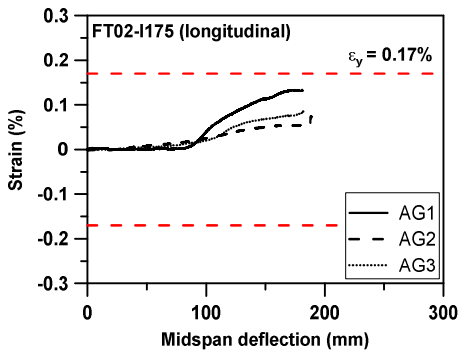

(a) FT02-I175 (longitudinal strain)

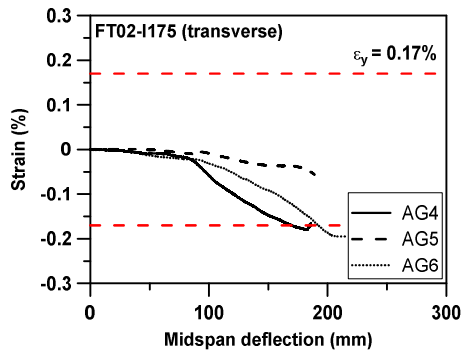

(b) FT02-I175 (transverse strain)

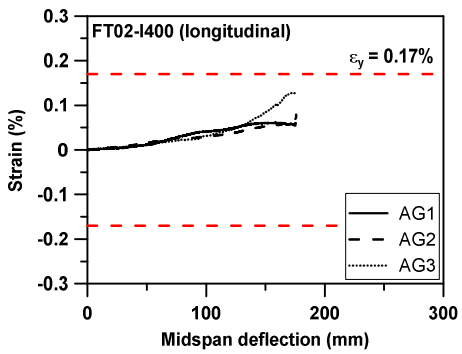

(c) FT02-I400 (longitudinal strain)

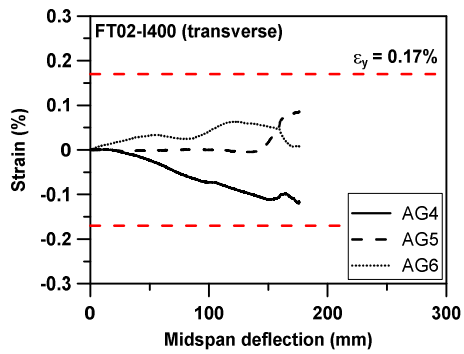

(d) FT02-I400 (transverse strain)

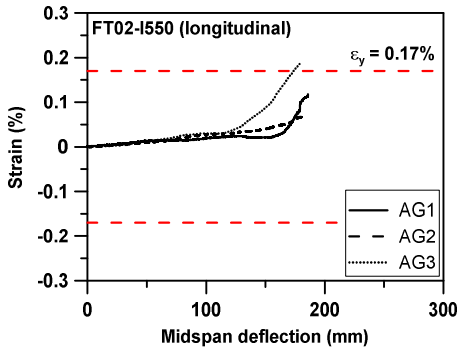

(e) FT02-I550 (longitudinal strain)

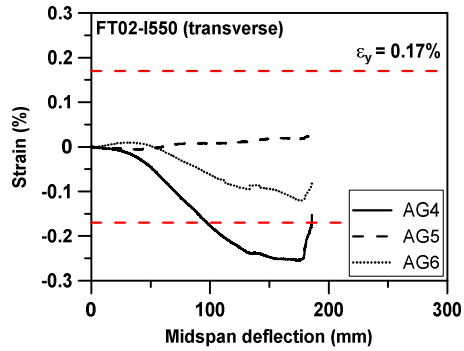

(f) FT02-I550 (transverse strain)

Figure 5-7 Strain measurements of angle shear connectors in flexural test

5.1.4 Failure mode and deformation

Figures 5-8 to **5-10** show failure mode and concrete cracks of phase 2 flexural test specimens. In phase 2, the concrete slab crack pattern and failure mode of the beam were similar to phase 1 flexural test. For all specimens, there was no crack in concrete slab while the beam was in elastic behavior region. But after peak load (P_p), thin longitudinal cracks caused by concrete crushing started to be observed on the side of the concrete slab. The concrete cracks got severe as the deflection increased, and cracks occurred in the bottom of concrete slab either. In FT02-I175 and FT02-I400, the concrete spalling was generated by severe cracks. There was no longitudinal shear crack in the concrete slab and slip between steel beam and concrete slab was not observed. The thin diagonal cracks in **Figures 5-10(e)** and **(f)** were not generated during test but existed from the beginning of the test.

Deformation of angle shear connectors and steel beam is shown in **Figure 5-11**. As similar to phase 1, steel beam local bucking and weld-zone failure were not observed. In addition, the deformation of angle shear connectors was negligible. It means that shear resistance of angle shear connectors was very proper in flexural test.

(a) Concrete cracks on concrete slab east side

(b) Concrete cracks on concrete slab west side

(c) Concrete cracks on concrete slab bottom surface (east)

(d) Concrete cracks and spalling on concrete slab bottom surface (west)

(e) North end of the specimen

(f) South end of the specimen

Figure 5-8 Concrete cracks and failure mode of FT02-I175 after the test

(a) Concrete cracks on concrete slab east side

(b) Concrete cracks on concrete slab west side

(c) Concrete cracks on concrete slab bottom surface (east)

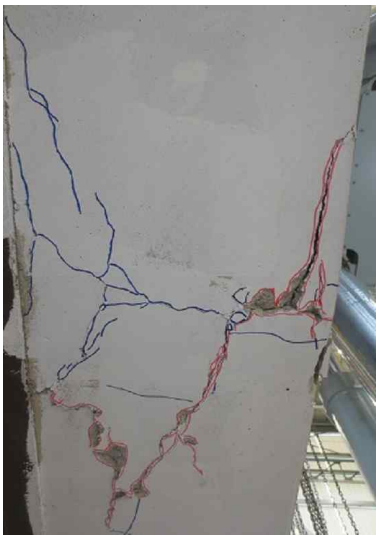

(d) Concrete cracks and spalling on concrete slab bottom surface (west)

(e) North end of the specimen

(f) South end of the specimen

Figure 5-9 Concrete cracks and failure mode of FT02-I400 after the test

(a) Concrete cracks on concrete slab east side

(b) Concrete cracks on concrete slab west side

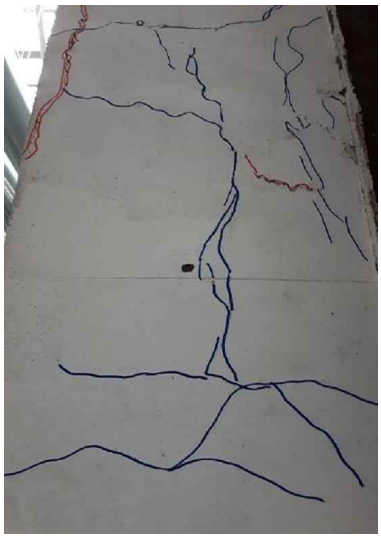

(c) Concrete cracks on concrete slab bottom surface (east)

(d) Concrete cracks and spalling on concrete slab bottom surface (west)

(e) North end of the specimen

(f) South end of the specimen

Figure 5-10 Concrete cracks and failure mode of FT02-I550 after the test

(a) Angle deformation at mid span – top view (FT02-I175)

(b) Angle deformation at mid span – elevation view (FT02-I175)

(c) Angle deformation at mid span – top view (FT02-I400)

(d) Angle deformation at mid span – elevation view (FT02-I400)

(e) Angle deformation at mid span – top view (FT02-I550)

(f) Angle deformation at mid span – elevation view (FT02-I550)

Figure 5-11 Deformation of angle shear connectors in flexural test (phase 2)

5.2 Push-out test

5.2.1 Shear strength and load-horizontal slip curve

The phase 2 load-horizontal slip curves of push-out test specimens are illustrated in **Figure 5-12** and phase 2 push-out test result is summarized in **Table 5-3**. In specimens without shear connectors (PT02-0-1 and PT02-0-2), load-horizontal slip curves increased linearly and then decreased after reaching peak shear strength in general. But unlike the specimens with shear connectors, they experienced the repeated sudden decrease and increase in the curves due to the failure at many sections. In particular, this phenomenon occurred predominantly in PT02-0-2. It is assumed that the phenomenon was observed because of internal concrete cracks which caused an instantaneous decline of shear strength. The specimens with shear connectors showed similar behavior in load-deflection curves to phase 1 push-out test specimens.

For all specimens, the separation gap between the concrete slab and steel beam was measured. Detailed plan of measurement is presented in **Appendix B**. The larger displacement was measured from the upper LVDT for all specimens. In specimens without shear connectors, the separation gap was almost constant in elastic behavior region, and it started to increase sharply at around the peak shear strength. For specimens with shear connectors excluding FT02-I175 and FT02-I400, the separation gap curve remained nearly horizontal during linear behavior region, and the gap at the top began to increase rapidly. The separation gap at the bottom almost did not increase. In FT02-I175 and FT02-I400, the point of sudden increase of the gap was nearly in the middle of elastic behavior region. In addition, the separation gap measured from the lower LVDT also increased.

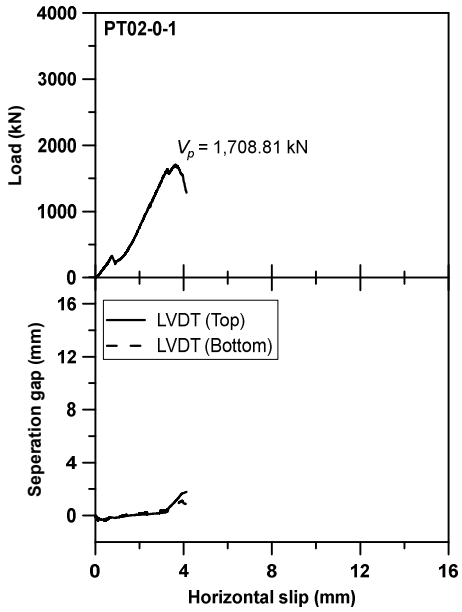

(a) PT02-0-1

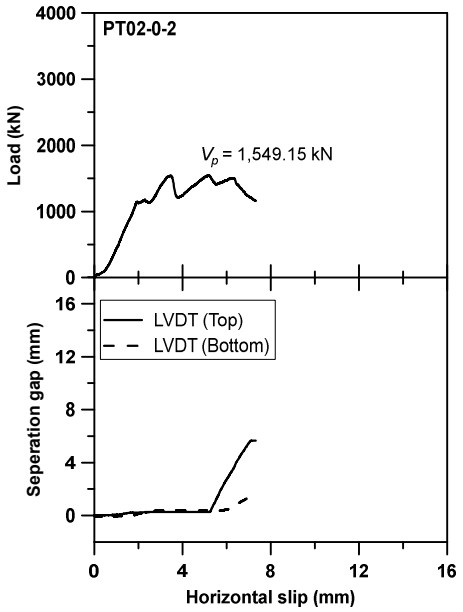

(b) PT02-0-2

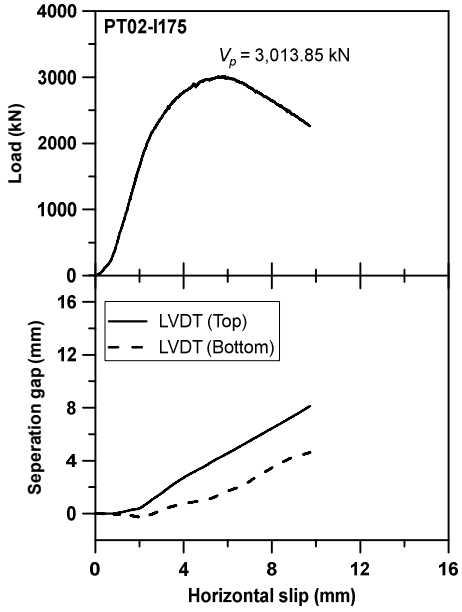

(c) PT02-I175

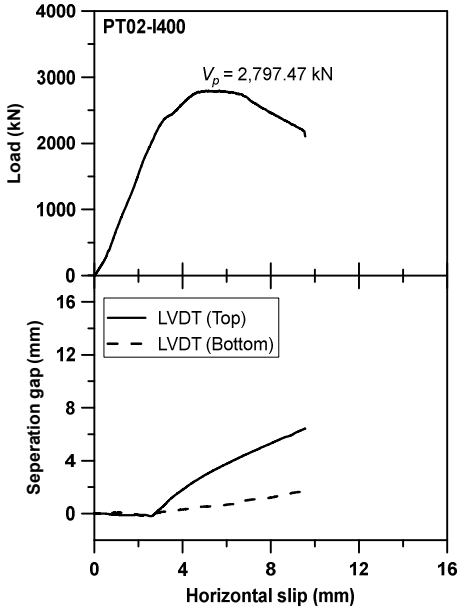

(d) PT02-I400

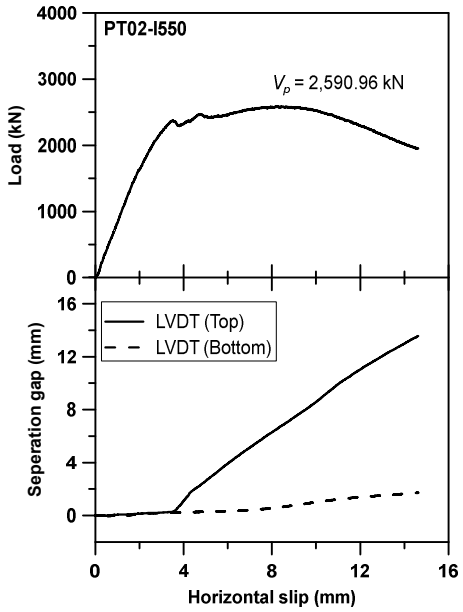

(e) PT02-I550

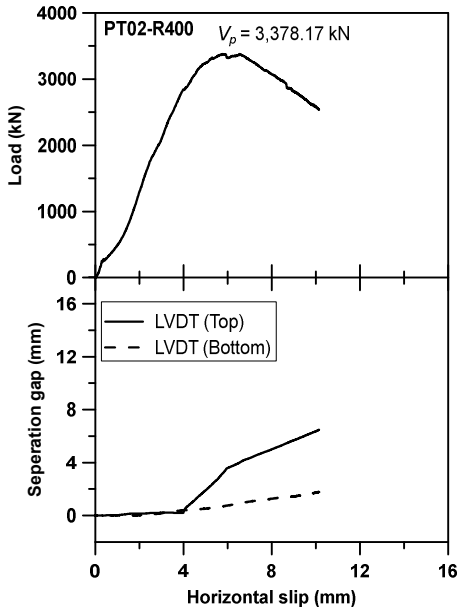

(f) PT02-R400

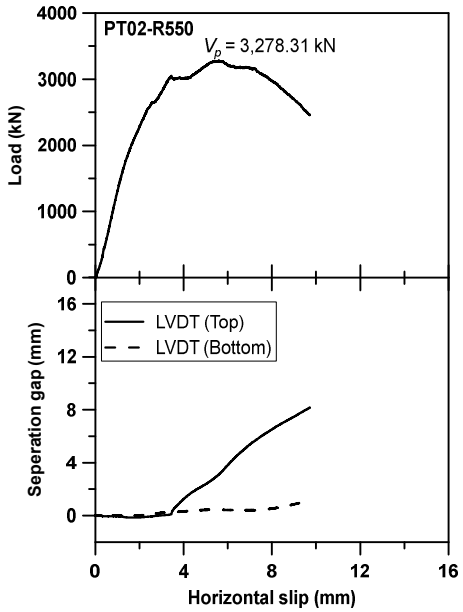

(g) PT02-R550

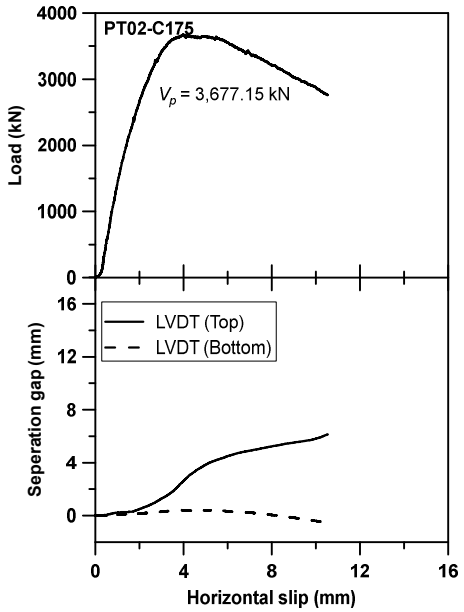

(h) PT02-C175

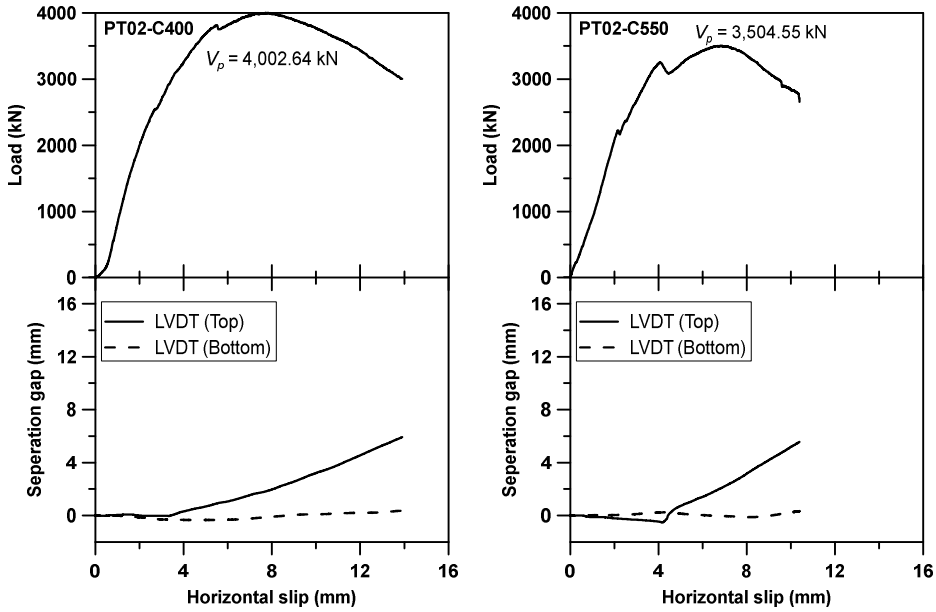

(i) PT02-C400 (j) PT02-C550

Figure 5-12 Load-horizontal slip curves of the push-out test (phase 2)

Table 5-3 Push-out test results of specimen shear strength (phase 2)

Specimen	Shear connector direction	Measured peak strength, V_p (kN)	Measured peak strength per shear connector, V_{pc} (kN)	Measured ultimate horizontal slip, Δ_u (mm)
PT02-0-1	No shear connector	1,708.81	No shear connector	4.12
PT02-0-2		1,549.15		7.31
PT02-I175	⌟ ⌞ (The inverse direction)	3,013.85	502.38	9.73
PT02-I400		2,797.47	699.37	9.56
PT02-I550		2,590.96	647.74	14.63
PT02-R400	⌝ ⌜ (The right direction)	3,378.17	844.54	10.14
PT02-R550		3,278.31	819.58	9.73
PT02-C175	⊓ ⊓ (The right direction)	3,677.15	612.86	10.53
PT02-C400		4,002.64	1,000.66	13.91
PT02-C550		3,504.55	876.14	10.39

Table 5-4 shows the comparison between the specimen without shear connectors (PT02-0-1 and PT02-0-2) and the specimen with shear connectors. The comparison was conducted between the specimens having the same size of concrete slab and steel beam. The measured peak shear strength of the specimen without shear connectors was 38.7 ~ 56.7% of the maximum shear strength of specimen with shear connectors. It cannot be concluded that the ratio calculated by comparison is the same as the actual portion of concrete which contributes to the shear strength of push-out test specimens. However, considering that ratio, it can be seen that shear resistance by concrete is not negligible. The measured peak strength of PT02-0-2 was lower than that of PT02-0-1 despite the size of concrete was larger. As shown in the load-horizontal slip curves, PT02-0-2 curve showed more sections that repeated sudden decrease and increase than PT02-0-1, which means many cracks occurred in PT02-0-2. Therefore, it seems that the shear strength of PT02-0-2 is lower than PT02-0-1 due to relatively more concrete cracks.

Table 5-4 Comparison between specimens with and without shear connectors

	$V_{0\text{-}1} / V_{I175}$	$V_{0\text{-}1} / V_{C175}$	$V_{0\text{-}2} / V_{I400}$	$V_{0\text{-}2} / V_{R400}$	$V_{0\text{-}2} / V_{C400}$
Ratio	56.7%	46.5%	55.4%	45.6%	38.7%

Note: $V_{0\text{-}1}$ is measured peak strength of PT02-0-1; $V_{0\text{-}2}$ is measured peak strength of PT02-0-2; V_{I175} is measured peak strength of PT02-I175; V_{C175} is measured peak strength of PT02-C175; V_{I400} is measured peak strength of PT02-I400; V_{R400} is measured peak strength of PT02-R400; and V_{C400} is measured peak strength of PT02-C400.

In specimens with shear connectors, the higher peak shear strength was measured in the order of the right direction channel, the right direction angle, and the inverse direction angle. The measured peak strength of specimens with 550 mm interval was lower than that of specimens with 400 mm. It contradicts the phase 1 push-out test result in which peak shear strength is proportional to the interval of shear connectors. It indicates that shear strength of push-out test specimens is not simply controlled by the area of concrete resisting shear force. It seems to be due to the change in force flow as the

concrete area of shear resistance increases more than a certain level. To find out the exact reason for this phenomenon, more precise analysis and further research should be conducted.

5.2.2 Comparison with shear connector design equations

Table 5-5 summarizes the comparison between measured peak shear strength per shear connector and nominal shear strength of shear connector calculated by four shear connector design equations which are mentioned in phase 1. For all specimens, the measured peak strength per shear connector was 3 to 4 times the nominal shear strength calculated by AC495 (2018) angle shear connector design equation, while the values were 1 to 1.7 on average in the other design equations. Like in phase 1, AC495 (2018) design equation estimated the strength of shear connector conservative. The equation of AISC 360-16 (2016) predicted the shear strength of shear connector most closely to the actual strength of both angle and channel. In specimens with angle shear connector, CAN/CSA-S16-01 (2001) equation estimated actual strength better than Eurocode 4 (2001) equation, but it was opposite in specimens with channel shear connector. In light of the comparison results, it can be judged that phase 2 shear connectors showed in-plane bending deformation rather than the behavior of a beam with fixed ends under uniformly distributed loads, which is the same as out-of-plane bending deformation.

Table 5-5 Comparison with shear connector design equations (phase 2)

Specimen	V_{pc} (kN)	V_{AC495} (kN)	V_{Euro4} (kN)	V_{AISC} (kN)	V_{CAN} (kN)	V_{pc} / V_{AC495}	V_{pc} / V_{Euro4}	V_{pc} / V_{AISC}	V_{pc} / V_{CAN}
PT02-I175	502.38	183.98	435.48	692.21	459.14	2.73	1.15	0.73	1.09
PT02-I400	699.37					3.8	1.61	1.01	1.52
PT02-I550	647.74					3.52	1.49	0.94	1.41
PT02-R400	844.54					4.59	1.94	1.22	1.84
PT02-R550	819.58					4.45	1.88	1.18	1.79
Average value						**3.82**	**1.61**	**1.02**	**1.53**
PT02-C175	612.86	194.2	590.24	730.67	484.65	3.16	1.04	0.84	1.26
PT02-C400	1,000.66					5.15	1.7	1.37	2.06
PT02-C550	876.14					4.51	1.48	1.2	1.81
Average value						**4.27**	**1.41**	**1.14**	**1.71**

Note: V_{pc} is measured peak strength per shear connector; V_{AC495} is an angle nominal shear strength calculated by AC495 (2018) equation; V_{Euro4} is an angle nominal shear strength calculated by Eurocode 4 (2001) equation; V_{AISC} is an angle nominal shear strength calculated by AISC 360-16 (2016) equation; and V_{CAN} is an angle nominal shear strength calculated by CAN/CSA-S16-01 (2001) equation.

5.2.3 Strain measurement

The strain measurement of shear connectors is presented in **Figure 5-13**. The strain gauges AG1 ~ AG5 were attached to shear connectors in longitudinal direction, and strain gauges AG6 ~ AG10 were attached in transverse direction. The detailed plan of shear connector strain measurement is shown in **Appendix B**. There was no special tendency in the longitudinal strain gauge measurement, while the AG1 strain gauge showed yield strain in most specimens. For transverse strain gauges, the yielding was intensively measured at gauges installed at the edge of angle shear connectors (AG6 and AG10). The measured strain changes were larger in transverse strain gauges than longitudinal strain gauges. Also, more yielding of strain gauges was observed in the transverse direction strain gauges. Thus, it indicates that in-plane bending deformation is more dominant in shear connectors.

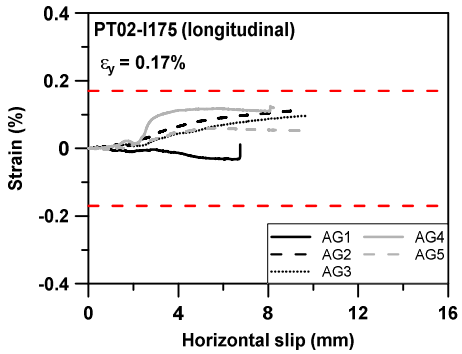

(a) PT02-I175 (longitudinal strain)

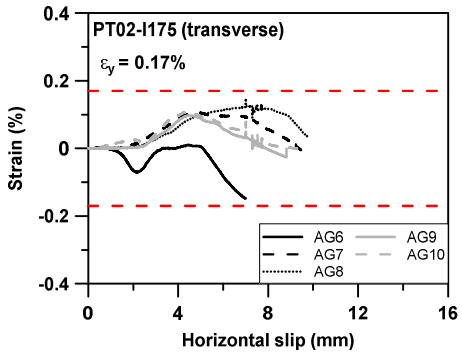

(b) PT02-I175 (transverse strain)

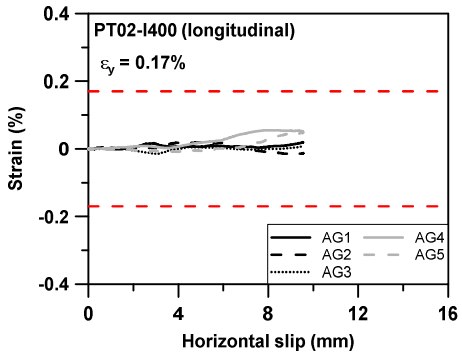

(c) PT02-I400 (longitudinal strain)

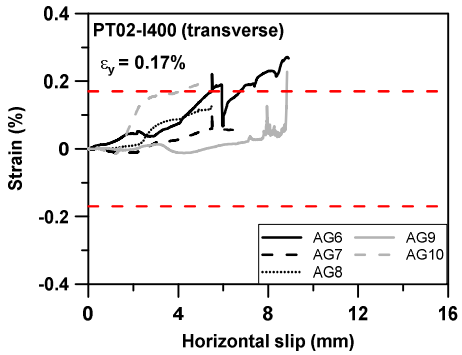

(d) PT02-I400 (transverse strain)

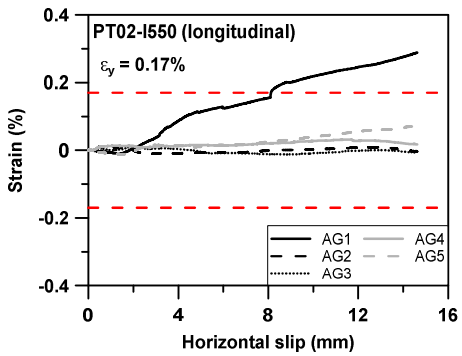

(e) PT02-I550 (longitudinal strain)

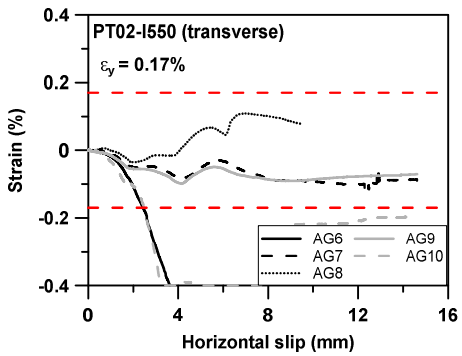

(f) PT02-I550 (transverse strain)

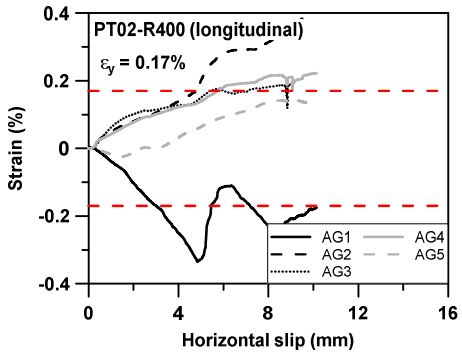

(g) PT02-R400 (longitudinal strain)

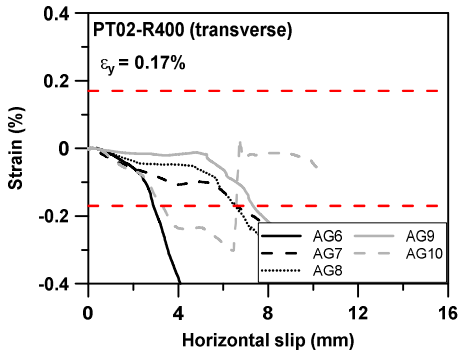

(h) PT02-R400 (transverse strain)

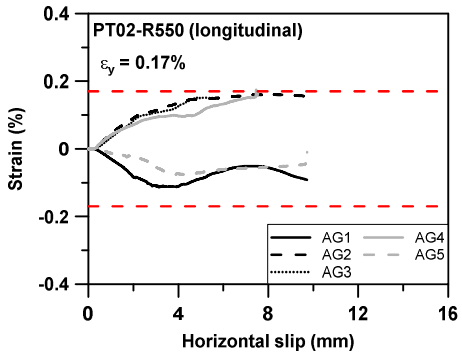

(i) PT02-R550 (longitudinal strain)

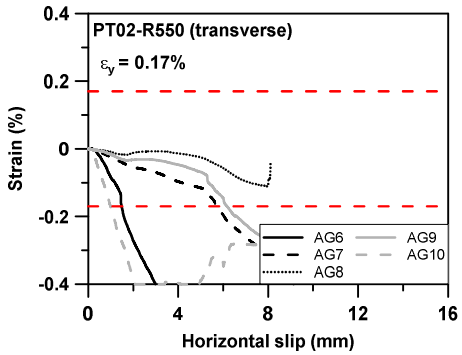

(j) PT02-R550 (transverse strain)

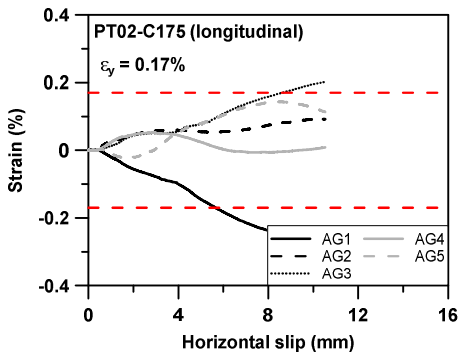

(k) PT02-C175 (longitudinal strain)

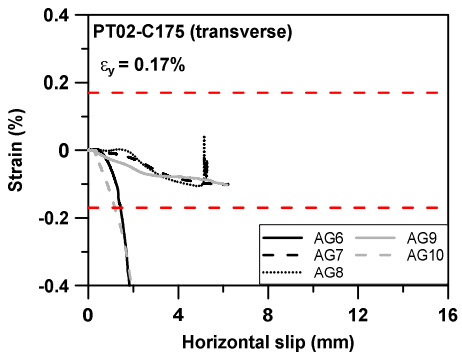

(l) PT02-C175 (transverse strain)

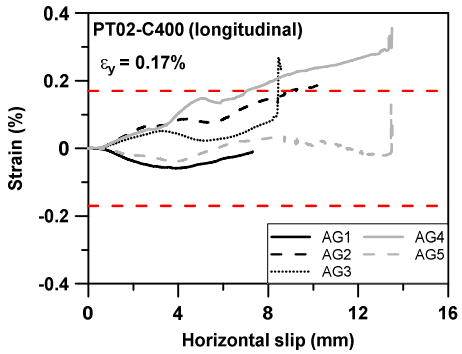

(m) PT02-C400 (longitudinal strain)

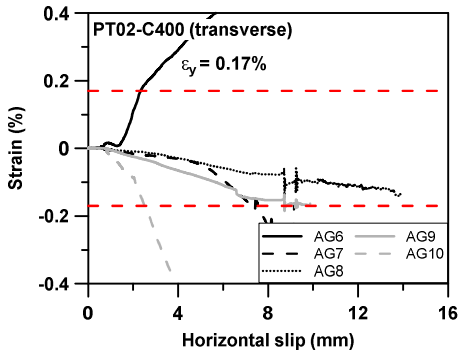

(n) PT02-C400 (transverse strain)

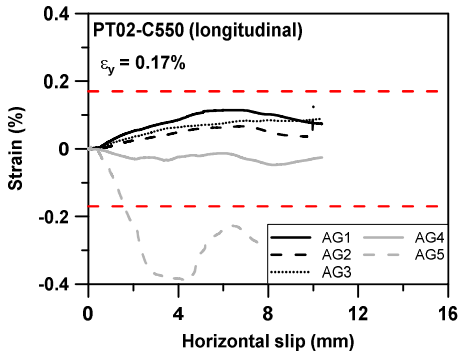

(o) PT02-C550 (longitudinal strain)

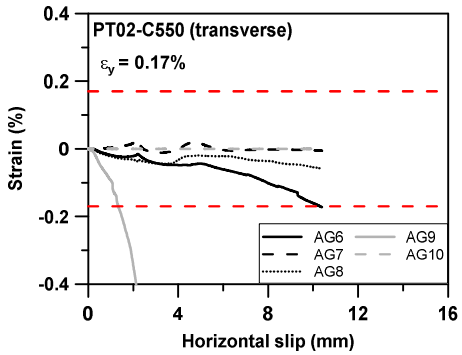

(p) PT02-C550 (transverse strain)

Figure 5-13 Strain measurements of shear connectors in push-out test (phase 2)

5.2.4 Failure mode and deformation

Figures 5-14 and **5-15** show concrete crack pattern of push-out test specimens after the test. In specimens without shear connectors, concrete cracks were barely observed except for the concrete just below the loading plate. It seems that cracks occurred inside of concrete near the concrete slab-steel beam interfaces. In specimens with 175 mm shear connector interval, long diagonal cracks were observed on the side surface of concrete slabs as presented in **Figure 5-14**. For specimens with 400 mm and 550 mm interval, no long diagonal cracks were observed. In all specimens with shear connectors, concrete cracks occurred near shear connectors. Separation was also observed between concrete slabs and steel beam in all specimens. The separation gap

and concrete cracks according to the increase of horizontal slip was similar to that of phase 1 push-out test.

(a) PT02-C175

(b) PT02-I175

Figure 5-14 Diagonal cracks on the side surface of concrete slab

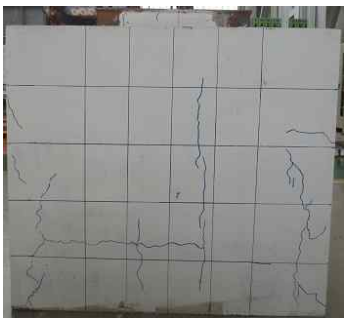

(a) North side

(b) South side

(c) East side

(d) West side

(e) Concrete cracks near channel shear connectors (f) The gap between concrete slab and steel beam

Figure 5-15 Concrete cracks and separation gap of PT02-C400

After the push-out test, the deformation pattern of the shear connectors was observed by demolishing concrete slabs. The deformed shape of shear connectors is shown in **Figure 5-16**. In all specimens, in-plane bending deformation was dominant and weld-zone fracture was not observed. Whereas, out-of-plane bending deformation did not occur in all shear connectors.

(a) PT02-I550 (b) PT02-R550 (c) PT02-C550

Figure 5-16 Deformation of angle and channel shear connectors (phase 2)

5.3 Discussion

In the phase 2 experiment, three flexural tests and ten push-out tests were conducted. In flexural tests, the interval of shear connectors was considered as the main variable. The interval, sectional shape, and direction of shear connectors were main variables in the push-out tests. Similar to the phase 1, measured concrete compressive strength and steel yield strength were much lower and higher than specified nominal strength, respectively.

In the flexural test, the 175 mm interval of shear connectors was determined to be the value for satisfying fully composite behavior, as calculated in **Section 3.1.1**. Specimen FT02-I175 was supposed to be a fully composite beam and the others were partially composite beams. The higher peak moment was measured in the order of FT02-I175, FT02-I550, and FT02-I400. The difference between measured peak moments of FT02-I400 and FT02-I550 was almost negligible, whereas the peak moment of FT02-I175 was much higher than that of the others. The nominal flexural strength was inversely proportional to the interval of angles. And the nominal flexural strength predicted measured peak moment almost precisely. Only the measured peak moment of FT02-I550 exceeded its nominal flexural strength. The ductility was inversely proportional to the interval of angle shear connectors.

It is presumed that the low strength concrete and eccentrically applied load caused deficient flexural strengths in FT02-I175 and FT02-I400. The measured concrete compressive strengths of FT02-I175 and FT02-I400 were 17.7 MPa and 18.7 MPa, respectively, which are far lower than the specified strength, 24 MPa. In FT02-I175, the difference between ductilites measured at both ends was large. It indicates that eccentric load was applied to FT02-I175 in longitudinal direction. Considering that a gap between UTM cross head and concrete slab occurred on one side of FT02-I400, it can be assumed that eccentric load was applied to FT02-I400 in transverse direction. Also, for all

specimens, the upper part of steel beam did not yield due to deep neutral axis caused by low concrete strength. For that reason, the FT02-I175 could not reach its plastic moment (i.e. nominal flexural strength).

Similar to the phase 1, the failure of the beam was dominated by concrete crushing. There were no longitudinal shear cracks and slip between concrete slab and steel beam even in partially composite beams (FT02-I400 and FT02-I550). Although the slip was not measured at the end of the beam, it can be assumed that a slight slip occurred in the middle of the beam for partially composite beams. Deformation of angle shear connectors was almost negligible and there was no weld-zone fracture. Also, no local buckling occurred in steel beam.

In the push-out test, shear strength of specimen without shear connectors was investigated. Compared to the specimen with shear connectors which has the same concrete slab size, the shear strength of specimen without shear connectors was 38.7 ~ 56.7%. It indicates that the concrete itself significantly contributes to the shear strength of push-out test specimens. For the specimens with shear connectors, the higher peak shear strength was measured in order of the right direction channel, the right direction angle, and the inverse direction angle. In contrast with the phase 1, the interval of shear connectors was inversely proportional to the maximum shear strength of push-out test specimen. It means that the shear strength of push-out test specimen is not linearly proportional to the cross section area of concrete slabs contacted with concrete enclosed by U-shaped steel beam. It is presumed that change of force flow in specimen according to increase of shear connector interval caused this phenomenon.

Compared to four shear connector design equations (AC495, 2018; Eurocode 4, 2001; AISC 360-16, 2016; and CAN/CSA-S16-01, 2001), the measured shear strength of angle and channel was much closer to the equations based on in-plane bending deformation (Eurocode 4, 2001; AISC 360-16, 2016; and

CAN/CSA-S16-01, 2001) rather than the equation based on out-of-plane bending deformation (AC495, 2018). In strain measurement of shear connectors, strains in transverse direction were higher than strains in longitudinal direction. After the push-out test, the deformed shape of angle and channel was observed with the naked eye by demolishing concrete slabs. There was no perceptible weld-zone fracture between steel beam and shear connectors. The in-plane bending deformation was dominant in all shear connectors, whereas out-of-plane bending deformation was negligible. Based on the three test results mentioned above, it can be concluded that in-plane bending is dominant in angle and channel shear connectors in the composite beam.

Chapter 6. Conclusion

In this study, the flexural and interface shear behaviors of the composite beam using U-shaped steel beam and angle shear connectors were analyzed by a series of flexural and push-out tests. The whole test was conducted in two distinct phases. For flexural test, the presence of transverse reinforcement in the concrete slab, the direction of angles, and the interval of angles were considered as the main variables. In push-out test, the direction and interval of shear connectors, the sectional shape of shear connector, and the presence of shear connector were set as the main variables. The results can be summarized as follows:

1) In the material test of phase 1 and 2, the measured average compressive strengths of concrete were 20.84 MPa and 19.43 MPa, respectively, which are much lower than the specified concrete strength of 24 MPa. In contrast, in the steel material test, the yield strength of steel was measured to be 28.5% ~ 45.9% higher than the specified yield strength.

2) In the flexural test, it was more advantageous for flexural strength and ductility to arrange angle shear connectors in the inverse direction. The measured peak moment of specimen with the inverse direction angles exceeded the nominal flexural strength. However, the specimen with the right direction angles did not reach its nominal moment capacity.

3) Due to unexpected concrete failure, the effect of transverse reinforcement on the flexural strength of the beam was not confirmed. In specimen FT01-R175-N, which did not have transverse reinforcement, severe concrete failure occurred because of friction between the concrete slab and lateral supports, and this led to the degradation of flexural

strength. Thus, the pure effect of the presence of transverse reinforcement in concrete slab could not be evaluated.

4) In general, as the interval of angles widened, the flexural strength of the composite beam decreased. The increase in shear connector spacing (i.e. decrease in composite ratio) seems to have caused the degradation of flexural strength. The nominal flexural strength that was calculated by the plastic stress distribution method predicted the measured strength of specimens almost precisely by using the relation between the composite ratio and flexural strength. The measured strength of specimens with 175 mm and 400 mm intervals did not reach their nominal strength. This is resulted from low strength concrete and unintended eccentric load.

5) The observed crack pattern after the flexural tests indicated that concrete crushing which occurred at the mid-span caused the failure of flexural specimen. In the flexural specimens, no longitudinal shear crack near angle shear connectors was observed, nor was slip between the concrete slab and steel beam. It indicates that the beams showed fully composite behavior during the test. After the test, the deformation of angle shear connectors was negligible. Also, no local buckling in the steel beam or weld-zone fracture between the angles and steel beam occurred.

6) In the push-out test, as the interval of shear connectors increased, the measured strength of specimen also increased. However, as the interval of shear connectors exceeded a certain limit, the measured strength decreased. Further research and analysis are needed to determine the reasons for this phenomenon.

7) The higher shear strength of push-out specimens was measured in order of the right direction channel, the right direction angle, and the inverse direction angle. The shear strength of specimens with the right direction channel increased by 6.9% ~ 18.5% compared to that of specimens with

the right direction angle. The specimens with the right direction angle showed 9.7% ~ 26.5% increased shear strength, compared to specimens with the inverse direction angle. The shear strength of specimens without shear connectors was measured to be 38.7% ~ 56.7% of that of the specimens with shear connectors.

8) In the push-out test, the shear connectors showed in-plane bending deformation, in which shear connectors deformed by folding inward or outward. No out-of-plane bending deformation, which is similar to the behavior of a beam with fixed ends under uniformly distributed loads, was observed in any of the shear connectors. Verifying strain measurement result, comparison with the nominal strength by design equations and visual inspection after the test confirmed that in angle and channel shear connectors, in-plane bending deformation was dominant. However, in all specimens, the web-to-web clear distance of U-shaped steel beam was 384 mm, and the dominance of in-plane bending deformation is valid only in this condition.

References

1. ACI Committee 318 (2019), "Building Code Requirements for Structural Concrete and Commentary (ACI 318-19)," American Concrete Institute, Farmington Hills, MI.

2. Ahn, H. J., Jung, I. Y., Kim, Y. J., and Hwang, J. S. (2015), "Shear Resistance of BESTOBEAM Shear Connector According to the Length," *Journal of Korean Society of Steel Construction*, V. 27, No. 5, 483-491 (in Korean).

3. AISC (2010), "Specification for Structural Steel Buildings (ANSI/AISC 360-10)," American Institute of Steel Construction, Chicago, IL.

4. AISC (2016), "Specification for Structural Steel Buildings (ANSI/AISC 360-16)," American Institute of Steel Construction, Chicago, IL.

5. ASTM International (2014), "Standard Specification for Carbon Structural Steel (ASTM A36/A36M-14)," ASTM International, West Conshohocken, PA.

6. ASTM International (2015), "Standard Specification for High-Strength Low-Alloy Columbium-Vanadium Structural Steel (ASTM A572/A572M-15)," ASTM International, West Conshohocken, PA.

7. ASTM International (2018), "Standard Practice for Making and Curing Concrete Test Specimens in the Field (ASTM C31/C31M-18a)," ASTM International, West Conshohocken, PA.

8. ASTM International (2018), "Standard Test Methods for Compressive Strength of Cylindrical Concrete Specimens (ASTM C39/C39M-18)," ASTM International, West Conshohocken, PA.

9. ASTM International (2018), "Standard Test Methods and Definitions for Mechanical Testing of Steel Products (ASTM A370-18)," ASTM International, West Conshohocken, PA.

10. Baran, E. and Topkaya, C. (2012), "An Experimental Study on Channel Type Shear Connectors," *Journal of Constructional Steel Research*, V. 74, No. 12, 108-117.

11. Canadian Standards Association (2001), "Limit States Design of Steel Structures (CAN/CSA-S16-01)," Canadian Standards Association, Mississauga, Canada.

12. European Committee for Standardization (2001), “Eurocode 4: Design of Composite Steel and Concrete Structures - Part 1-1: General Rules and Rules for Buildings, Draft No. 2 (prEN 1994-1-1: 2001),” European Committee for Standardization, Brussels, Belgium.

13. Hosain, M. U. and Pashan A. (2006), “Channel Shear Connectors in Composite Beams: Push-Out Tests,” Fifth International Conference on Composite Construction in Steel and Concrete, Mpumalanga, South Africa.

14. ICC-ES (2018), “Cold Formed Steel Structural Beams with Steel Angle Anchors Acting Compositely with Cast-In-Place Concrete Slabs (AC495),” ICC Evaluation Service, LLC, Brea, CA.

15. Jun, S.-C., Lee, C.-H., Han, K.-H., and Kim, J.-W. (2018), “Flexural Behavior of High-Strength Steel Hybrid Composite Beams,” *Journal of Constructional Steel Research*, V. 149, No. 21, 269-281.

16. Kang, T. H.-K., Kim, K., Kim, S., Jung, I.-Y., and Kim, J.-W. (2017), “Development of Design Equation for Steel Angle Anchors Welded to Hat-Shaped Cold-Formed Steel Section,” The 2017 World Congress on Advances in Structural Engineering and Mechanics (ASEM17), Ilsan, Korea.

17. Kim J. T. (2018), “Flexural Capacity of the Composite Beam Using Angle as a Shear Connector,” Seoul National University of Science and Technology, (Master thesis) (in Korean).

18. Kim, Y. J., Bae, J. H., Ahn, T. S., and Jang, D. W. (2014), “Push-Out Test on Welded Angle Shear Connectors Used in Composite Beams” *Journal of Korean Society of Steel Construction*, V. 26, No. 3, 155-167.

19. Lasheen, M. R. M. (2017), “Effective Width for Steel-Light Weight Concrete Composite Girders,” Ain Shams University, (Ph.D. thesis).

20. Lee, M.-K., Shin, K.-J., Lee, J.-S., and Chae, I.-S. (2019), “Push-Out Test on Evaluation of Shear Strength Using Angle Shear Connectors,” *Journal of Korean Society of Steel Construction*, V. 31, No. 6, 413-421 (in Korean).

21. Maleki, S. and Bagheri, S. (2008), “Behavior of Channel Shear Connectors, Part 1: Experimental Study,” *Journal of Constructional Steel Research*, V. 64, No. 12, 1333-1340.

22. Maleki, S. and Mehrdad, M. (2009), “Experimental and Analytical Study on Channel Shear Connectors in Fiber-Reinforced Concrete,” *Journal of Constructional Steel Research*, V. 65, No. 8, 1787-1793.

23. Pashan, A. (2006), “Behavior of Channel Shear Connectors: Push-Out Tests,” University of Saskatchewan, (Master thesis).

24. Shariati, A., Shariati, M., Sulong, N. H. R., Suhatril, M., Khanouki, M. M. A., and Mahoutian, M. (2014), "Experimental Assessment of Angle Shear Connectors under Monotonic and Fully Reversed Cyclic Loading in High Strength Concrete," *Construction and Building Materials*, V. 52, No. 33, 276-283.

25. Slutter, R. G. and Driscoll, G. C. (1965), "Flexural Strength of Steel-Concrete Composite Beams," *Journal of the Structural Division*, V. 91, No. ST2, 71-99.

26. Tahmasbi, F., Shervin, M., Shariati, M., Sulong, N. M. R., and Tahir, M. M. (2016), "Shear Capacity of C-Shaped and L-Shaped Angle Shear Connectors," *PLoS ONE 11(8): e0156989*, https://doi.org/10.1371/journal.pone.0156989.

27. Viest I. M., Siess, C. P., Appleton, J. H., and Newmark, N. M. (1952), "Full-Scale Tests of Channel Shear Connectors and Composite T-Beams," University of Illinois at Urbana-Champaign, Urbana, IL.

Appendix A : Specimen drawings

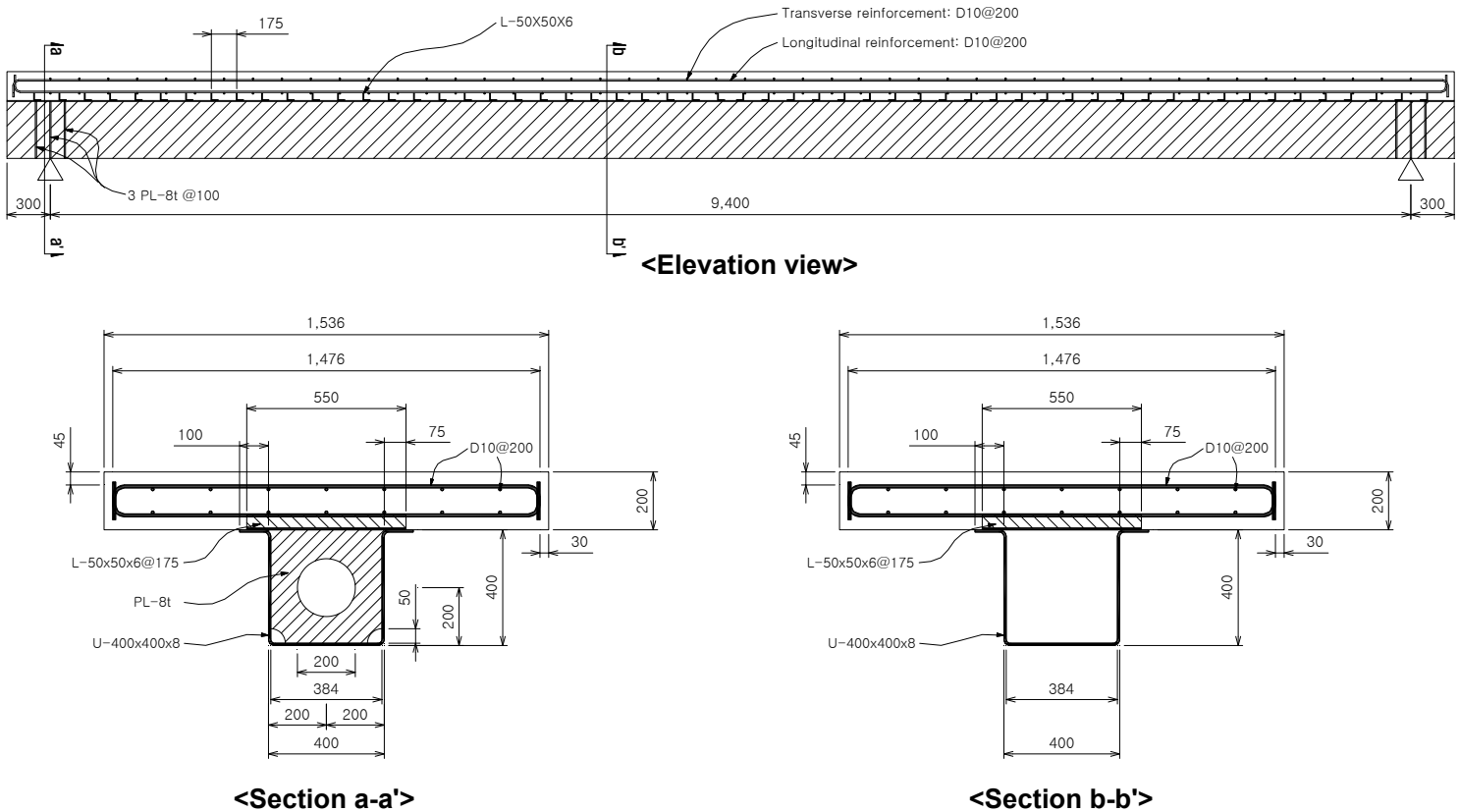

Figure A-1 Details of FT01-R175 (Unit: mm)

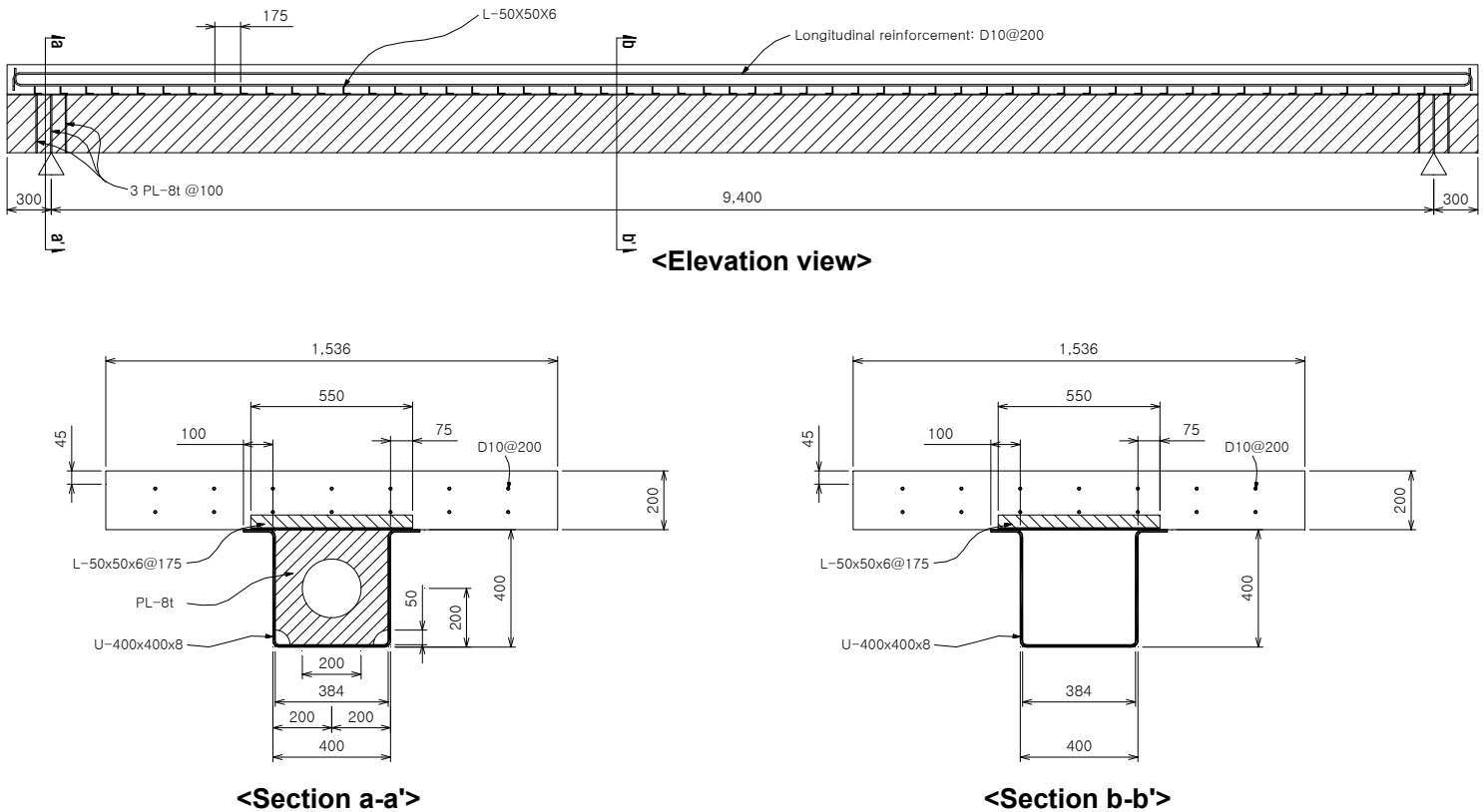

Figure A-2 Details of FT01-R175-N (Unit: mm)

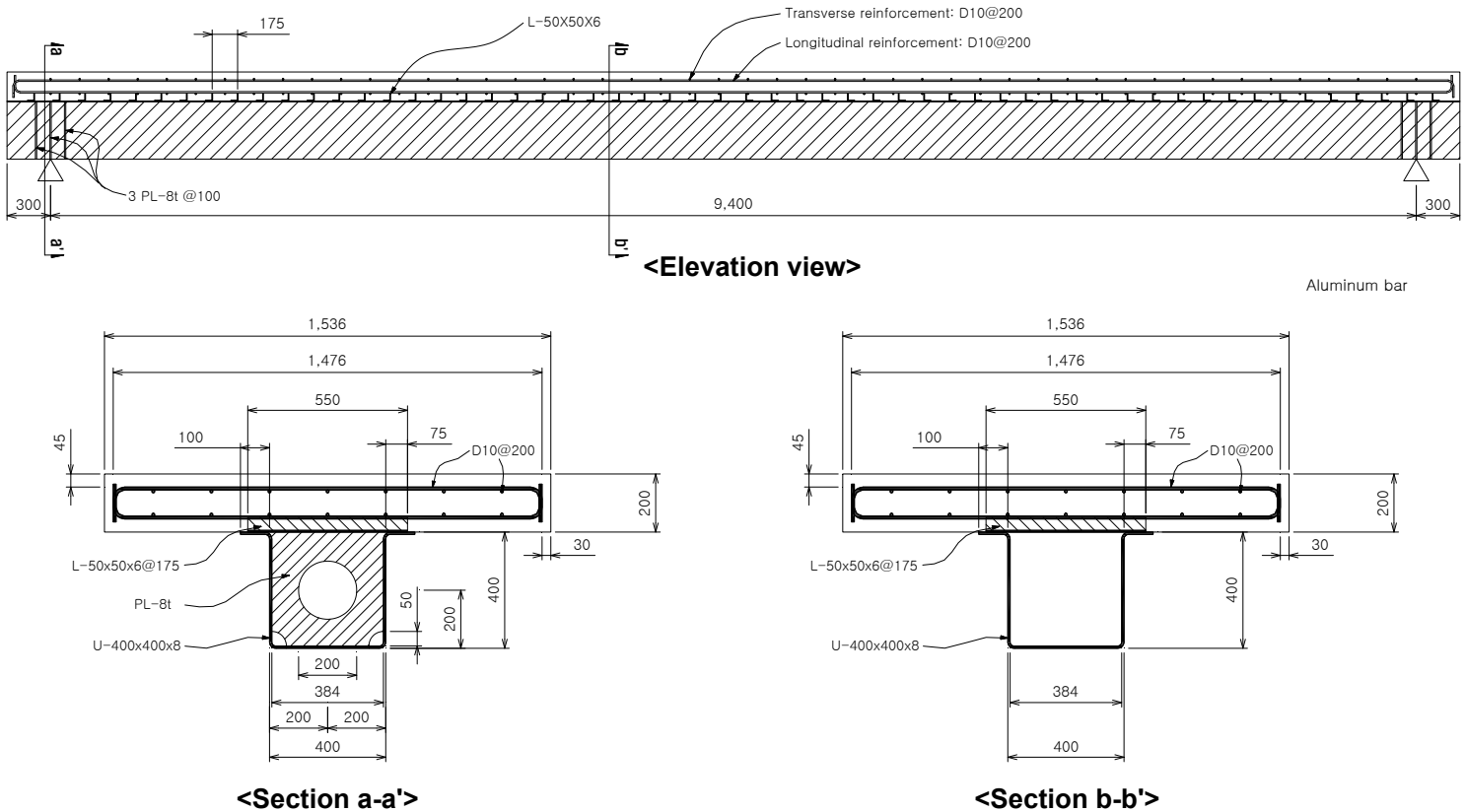

Figure A-3 Details of FT01-I175 (Unit: mm)

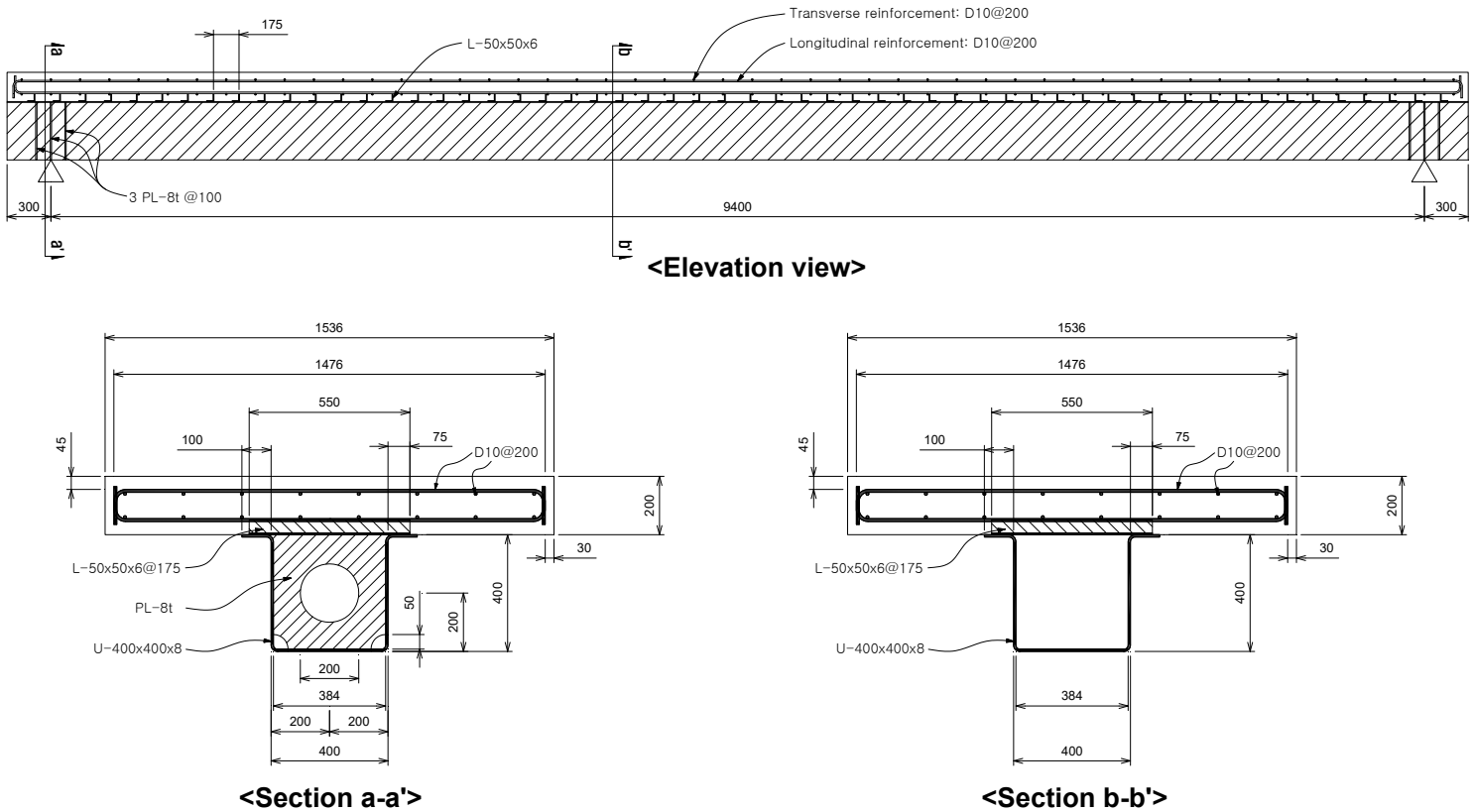

Figure A-4 Details of FT02-I175 (Unit: mm)

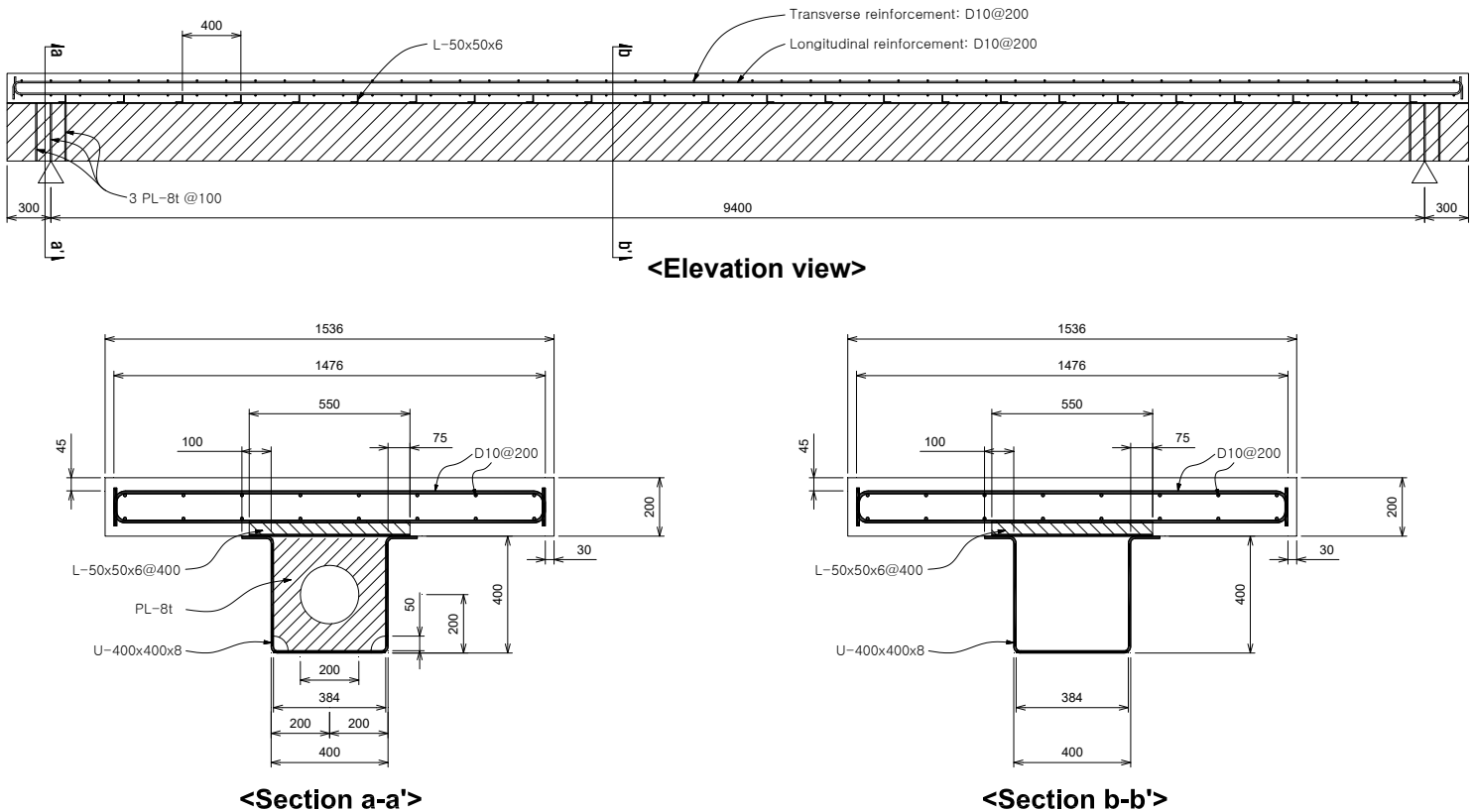

Figure A-5 Details of FT02-I400 (Unit: mm)

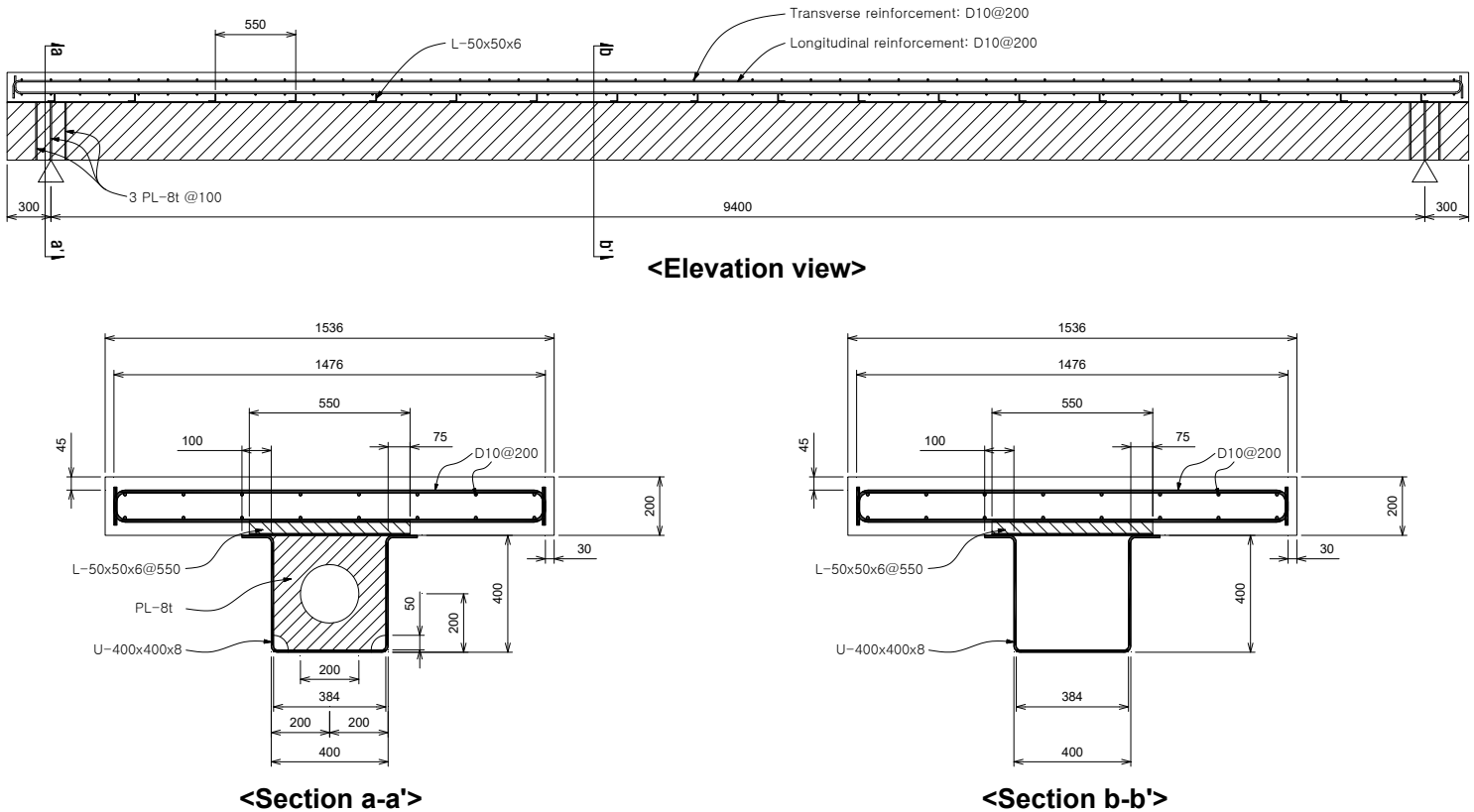

Figure A-6 Details of FT02-I550 (Unit: mm)

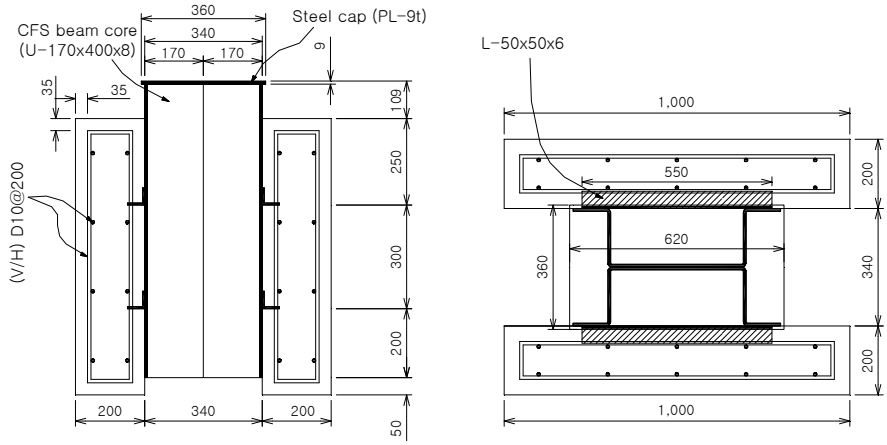

< Side view > < Top view >

(a) PT01-I300

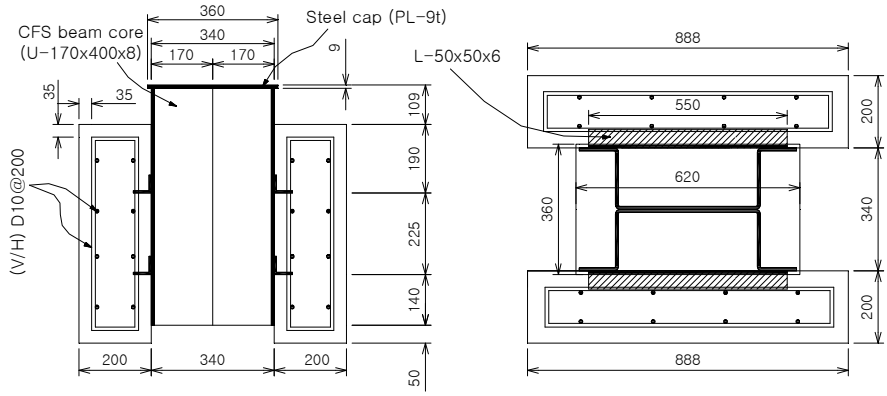

< Side view > < Top view >

(b) PT01-I225

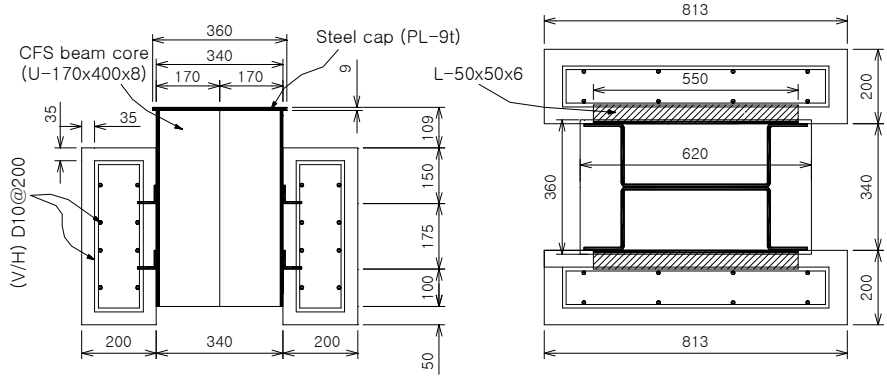

< Side view > < Top view >

(c) PT01-I175

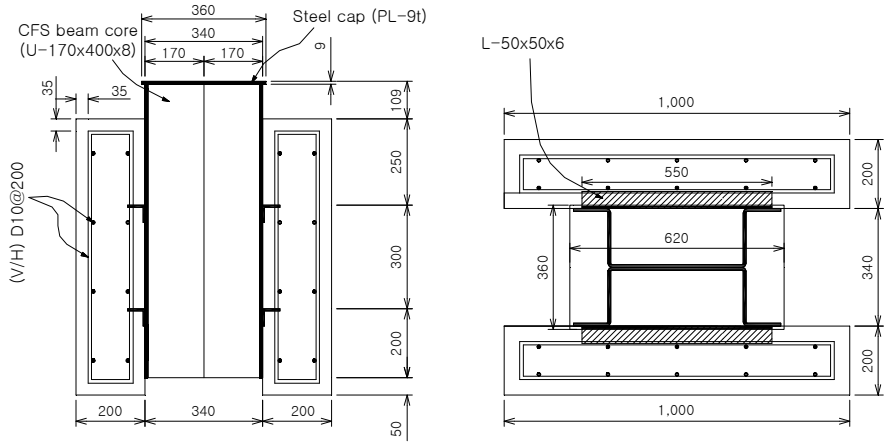

< Side view > < Top view >

(d) PT01-R300

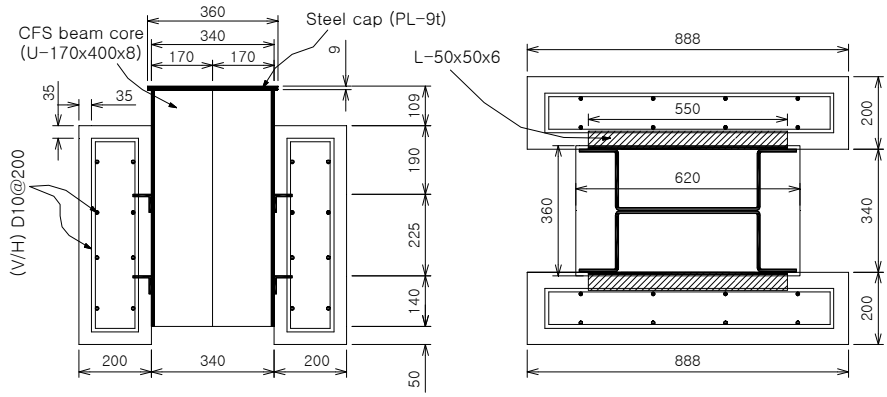

< Side view > < Top view >

(e) PT01-R225

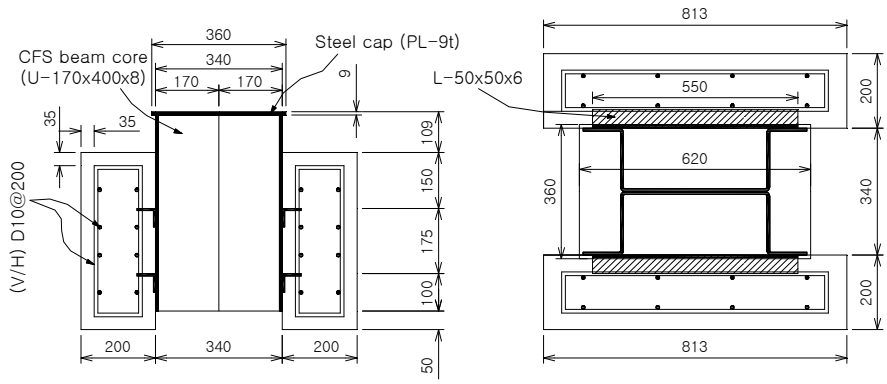

< Side view > < Top view >

(f) PT01-R175

Figure A-7 Details of push-out test specimens of phase 1 (Unit: mm)

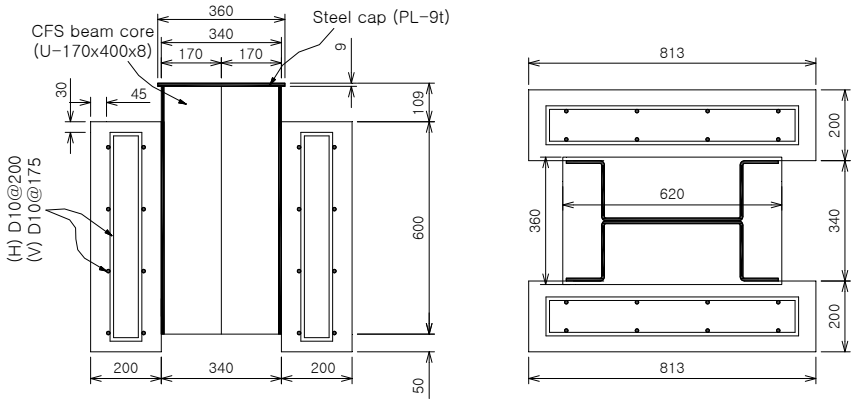

< Side view > < Top view >

(a) PT02-0-1

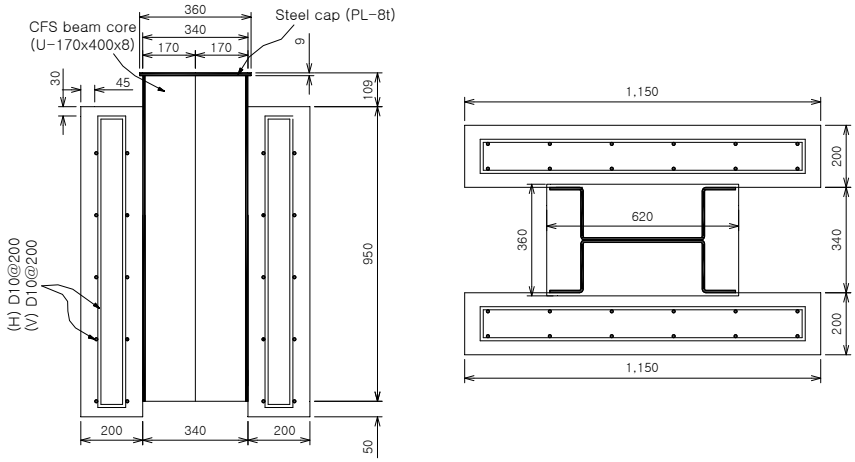

< Side view > < Top view >

(b) PT02-0-2

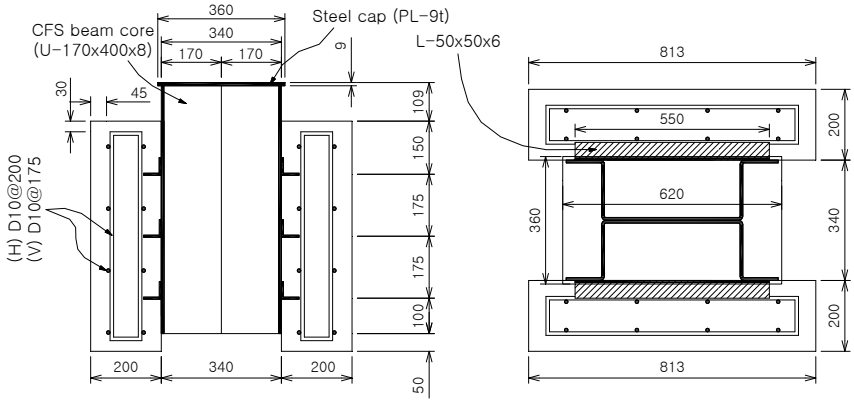

< Side view > < Top view >

(c) PT02-I175

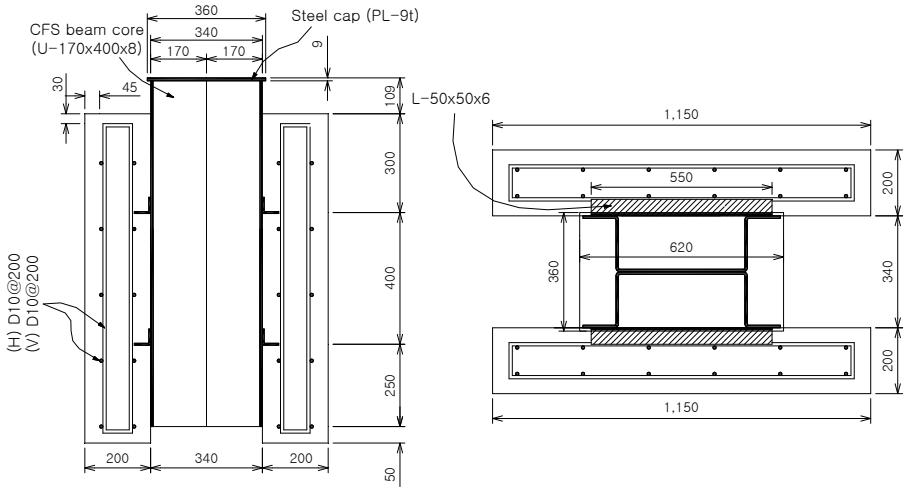

< Side view > < Top view >

(d) PT02-I400

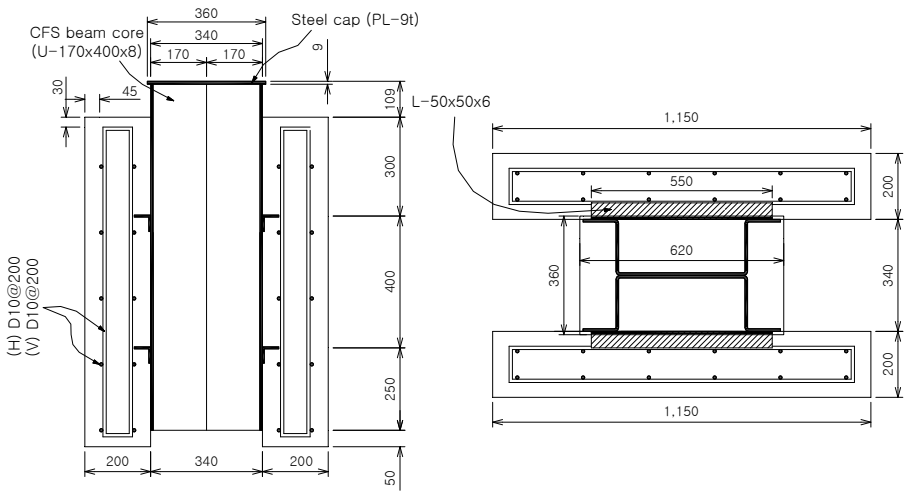

< Side view > < Top view >

(e) PT02-R400

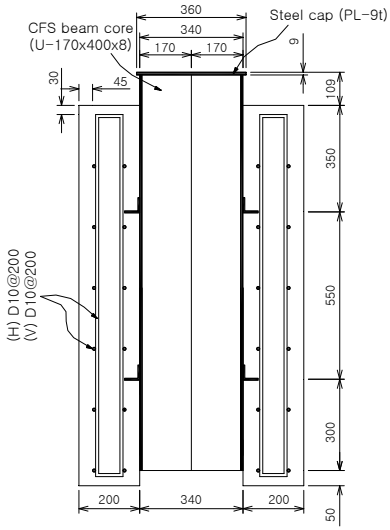

< Side view >

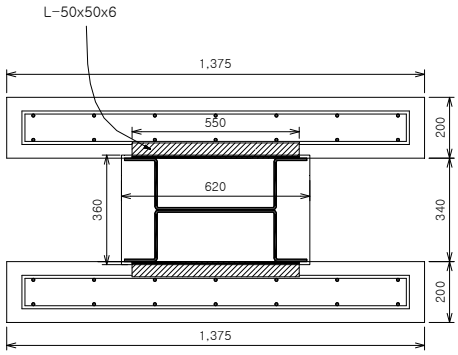

< Top view >

(f) PT02-I550

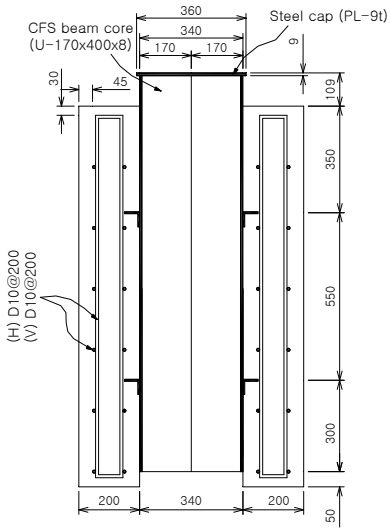

< Side view >

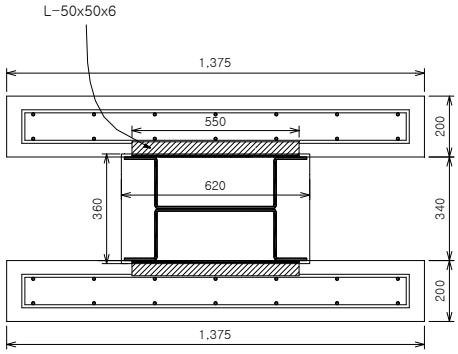

< Top view >

(g) PT02-R550

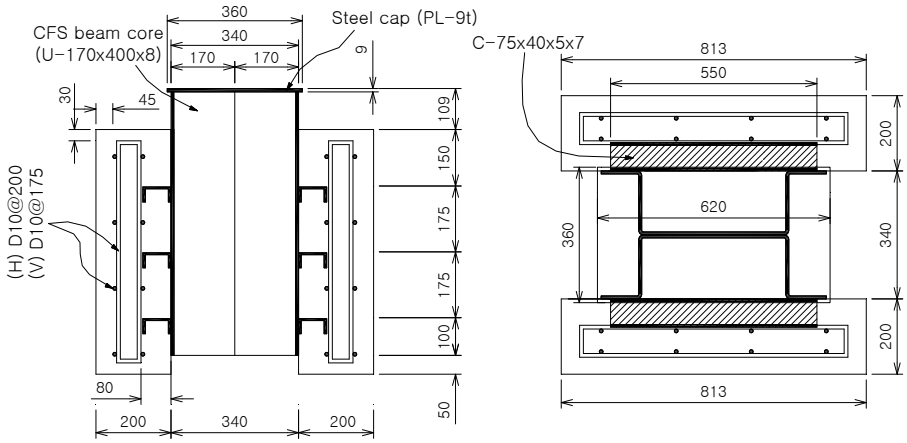

< Side view > < Top view >

(h) PT02-C175

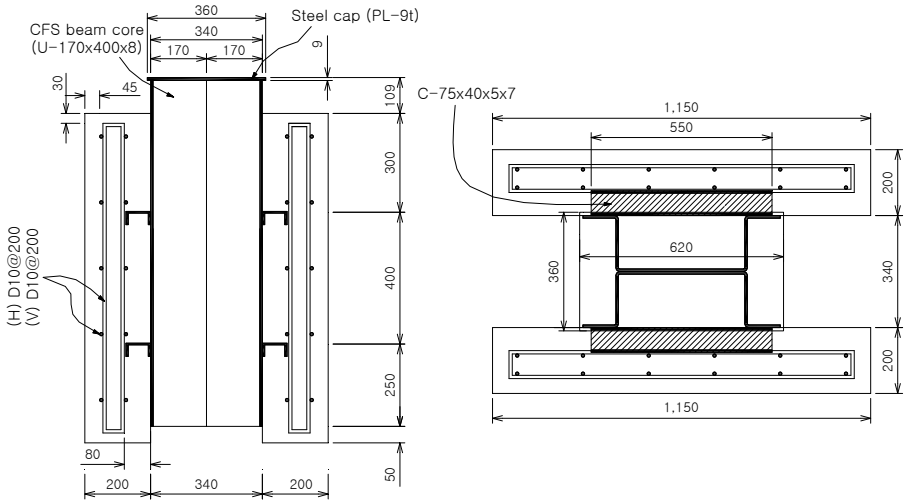

< Side view > < Top view >

(i) PT02-C400

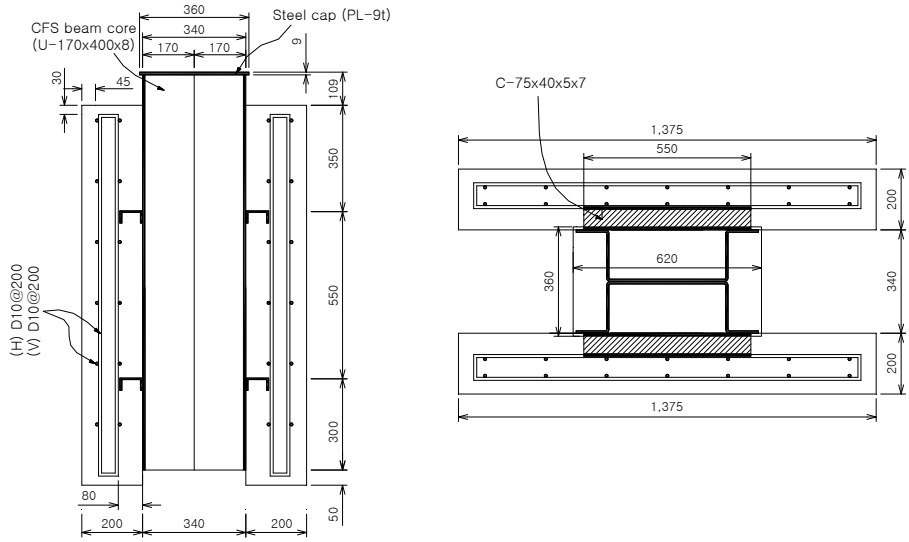

< Side view > < Top view >

(j) PT02-C550

Figure A-8 Details of push-out test specimens of phase 2 (Unit: mm)

Appendix B: Strain gauge and LVDT setup

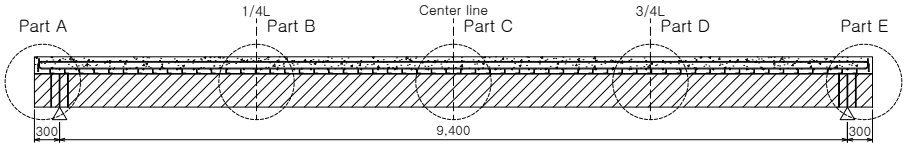

(a) Elevation view

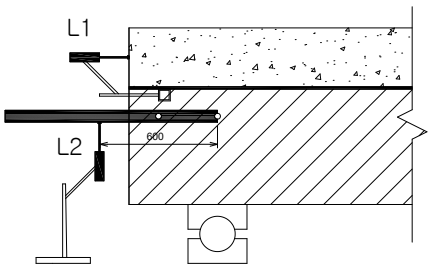

(b) Section at Part A

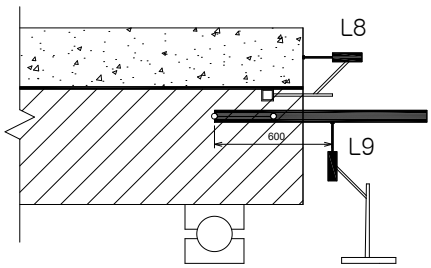

(c) Section at Part E

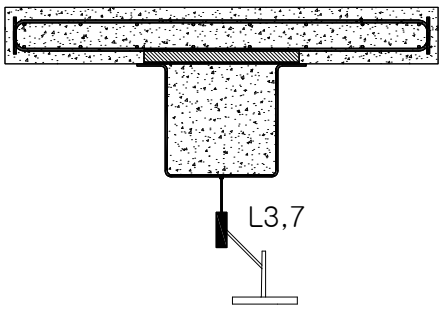

(d) Section at Part B, D

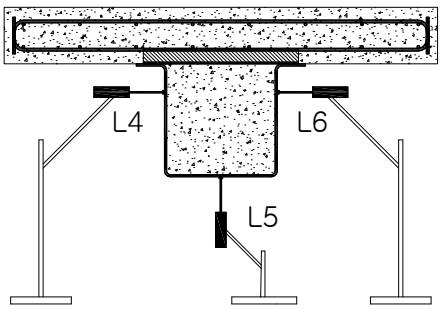

(e) Section at Part C

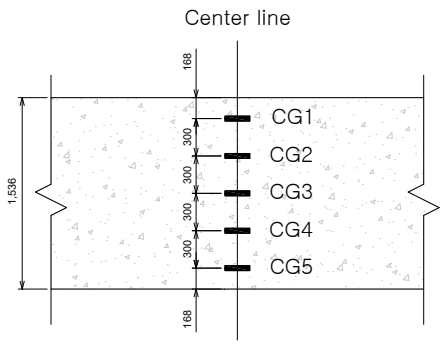

(f) Concrete slab top surface strain measurement at Part C

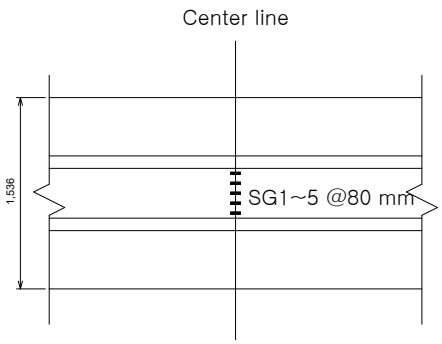

(g) U-shaped CFS beam bottom surface strain measurement at Part C

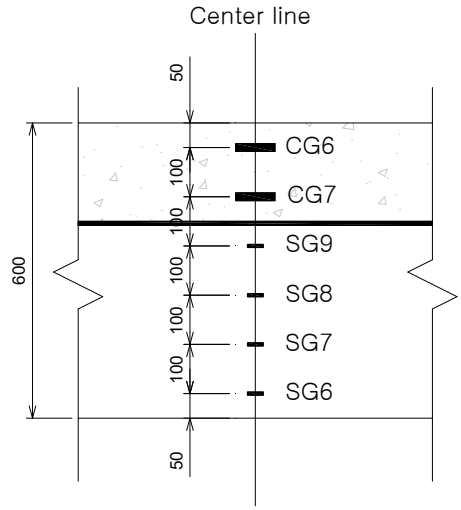

(h) Side surface strain measurement at Part C

Figure B-1 Strain gauge and LVDT setup of phase 1 flexural test (Unit: mm)

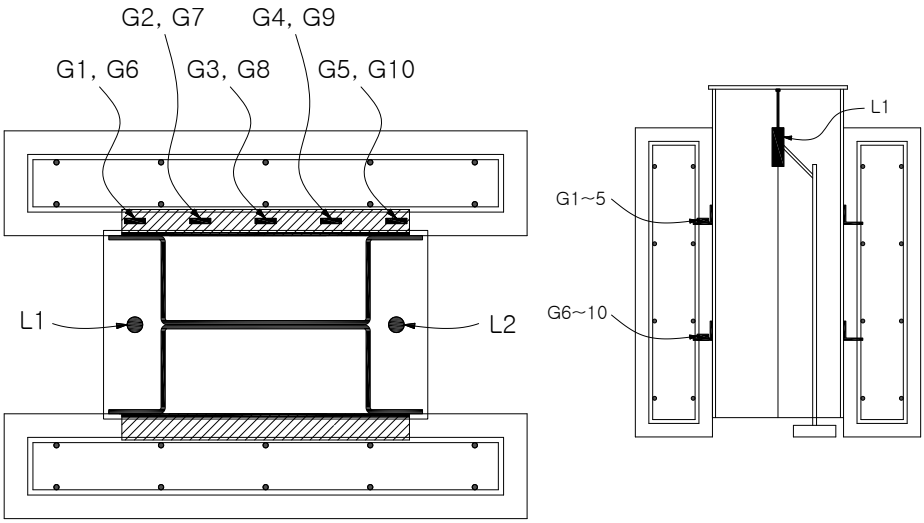

(a) Top view (b) Side view

Figure B-2 Strain gauge and LVDT setup of phase 1 push-out test

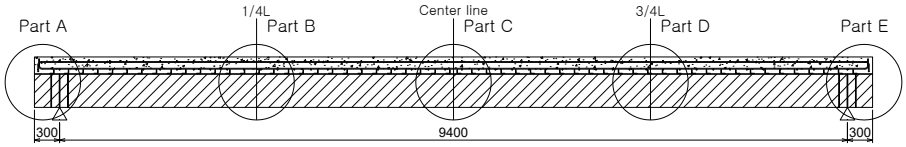

(a) Elevation view

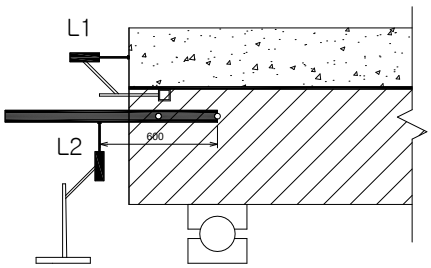

(b) Section at Part A

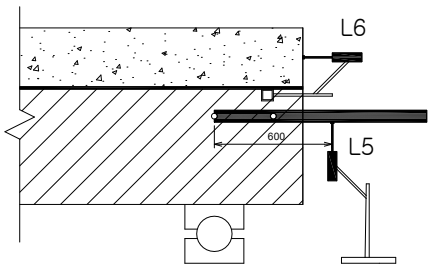

(c) Section at Part E

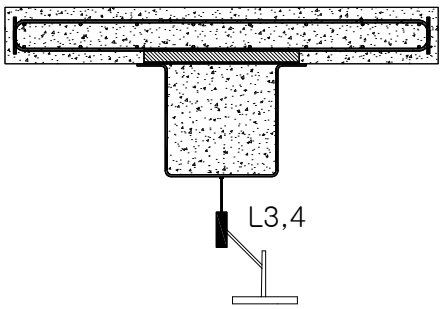

(d) Section at Part B, D

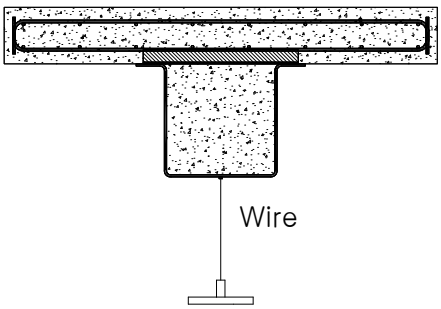

(e) Section at Part C

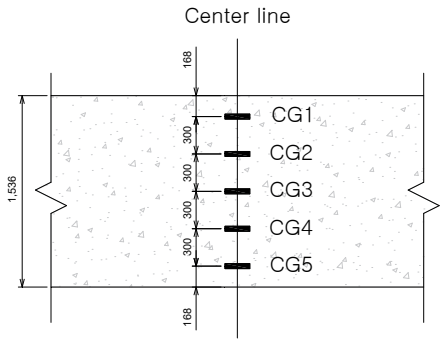

(f) Concrete slab top surface strain measurement at Part C

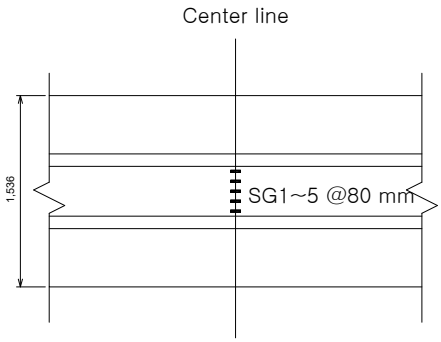

(g) U-shaped CFS beam bottom surface strain measurement at Part C

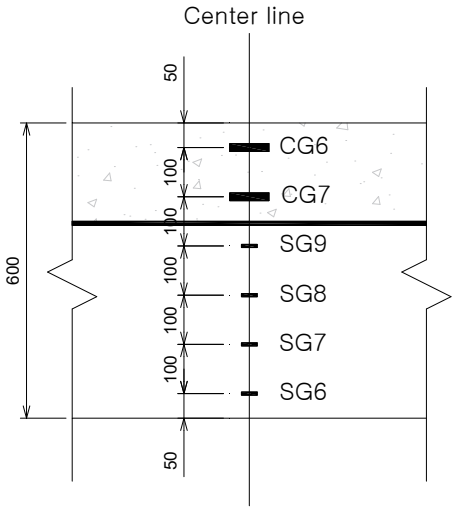

(h) Side surface strain measurement at Part C

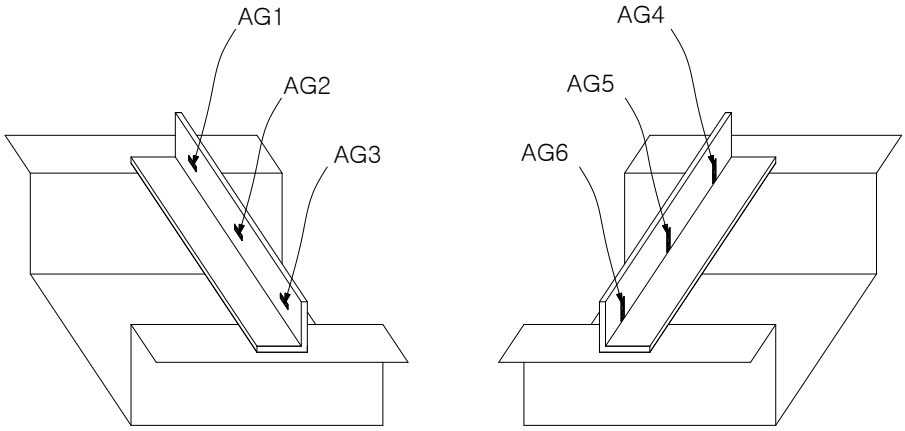

(i) Angle shear connector strain gauge measurement at Part C

Figure B-3 Strain gauge and LVDT setup of phase 2 flexural test (Unit: mm)

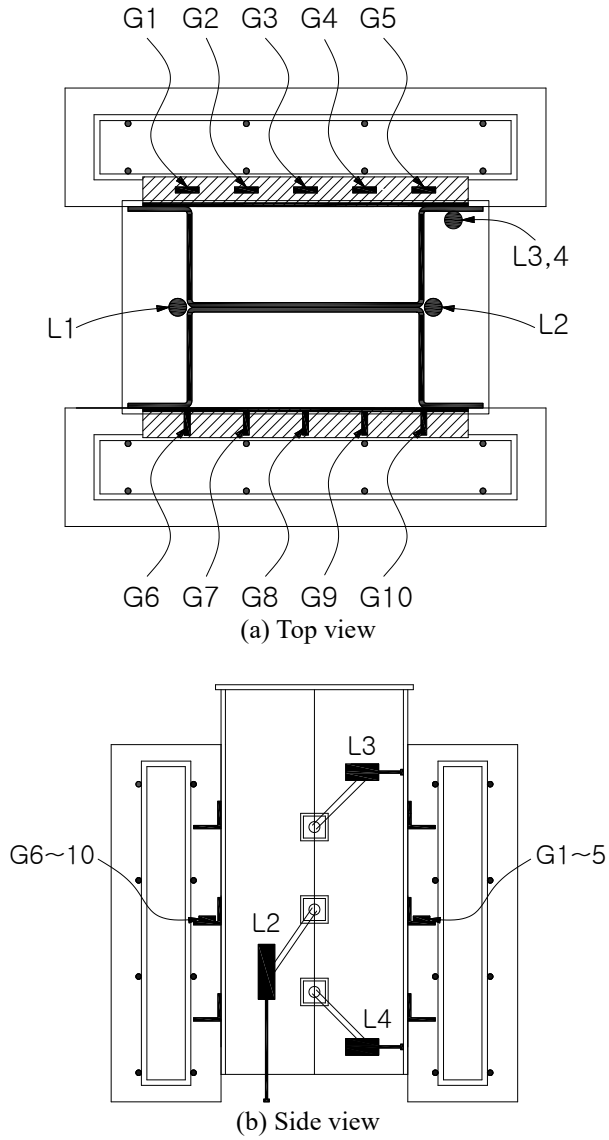

Figure B-4 Strain gauge and LVDT setup of phase 2 push-out test

국 문 초 록

전단연결 앵글과 U자형 강재보를 활용한 합성보의 실험적 연구

최근 한국에서는 산업의 발달과 지가 상승으로 인한 높은 용적률에 대한 요구로 건물들에 대해 고층화, 장스팬화, 층고절감, 경제성과 같은 사항들이 요구되고 있다. 이에 다양한 종류의 합성보의 건설현장 적용이 늘고 있으며, 그 중 하나가 전단연결 앵글과 U자형 강재보를 활용하는 합성보이다. 그러나 이 합성보는 공기단축과 층고절감이 가능하다는 장점에도 불구하고 아직 관련 기준 및 연구가 부족한 실정이다. 따라서 본 연구에서는 전단연결 앵글의 방향 및 간격, 콘크리트 슬래브의 횡 방향 철근의 유무를 휨 실험의 변수로, 전단연결재의 방향, 간격, 단면모양을 푸쉬아웃 실험의 변수로 설정하여 실험을 진행하였다.

실험은 총 2개의 단계로 계획되었으며 1년 간격으로 수행되었다. 재료 실험 결과, 콘크리트의 실제 압축강도가 공칭강도인 24MPa에 크게 못 미치는 것으로 나타났다. 이는 실험에 사용된 콘크리트의 질이 낮고 신뢰성이 부족하였기 때문인 것으로 보인다. 휨 실험 결과, 전단연결 앵글을 역방향으로 배치하고 앵글간 간격이 감소할수록 높은 휨 강도가 측정되는 경향을 보였다. 푸쉬아웃

실험에서는 전단연결재의 단면모양과 방향에 대해서는 정방향채널, 정방향앵글, 역방향앵글 순으로 높은 전단강도가 측정되었다. 기존 선행연구들에서는 푸쉬아웃 시편에 부착된 전단연결재들이 양단이 고정된 보처럼 휘어지는 변형을 보여주었으나, 본 연구에서는 전단연결재의 길이방향의 수직방향으로 내측으로 접히거나 외측으로 벌어지는 거동이 지배적으로 나타났다. 그러나 푸쉬아웃 시편의 U자형 보의 웨브간 거리가 모두 384mm로 동일하였기에 이러한 조건 내에서만 앞에서 언급한 변형거동이 유효하다고 할 수 있다. 본 연구는 전단연결 앵글과 U자형 강재보를 활용한 합성보의 휨 성능과 전단연결재의 성능에 관한 기초연구자료를 제시함으로써 관련기준의 개정 및 추후 관련연구에 있어 유용한 자료가 될 것으로 기대된다.

핵심용어: 전단연결 앵글, 전단연결재, U자형 강재보, 합성보, 휨 실험, 푸쉬아웃 실험
학번: 2019-24377